REPUBLIC OF TURKEY
ACIBADEM MEHMET ALİ AYDINLAR UNIVERSITY
INSTITUTE OF NATURAL AND APPLIED SCIENCES

GENOME ENGINEERING IN THE *TP53* GENE LOCUS IN HUMAN GLIOBLASTOMA CELL MODEL

BAŞAK KAVAKLIOĞLU
MASTER THESIS

DEPARTMENT of MOLECULAR and TRANSLATIONAL BIOMEDICINE

SUPERVISOR
Asst. Prof. Dr. Nazlı Keskin Toklu

ISTANBUL-2023

REPUBLIC OF TURKEY
ACIBADEM MEHMET ALİ AYDINLAR UNIVERSITY
INSTITUTE OF NATURAL AND APPLIED SCIENCES

GENOME ENGINEERING IN THE *TP53* GENE LOCUS IN HUMAN GLIOBLASTOMA CELL MODEL

BAŞAK KAVAKLIOĞLU

MASTER THESIS

DEPARTMENT of MOLECULAR and TRANSLATIONAL BIOMEDICINE

SUPERVISOR
Assist. Prof. Dr. Nazlı Keskin Toklu

ISTANBUL-2023

Department:	Molecular and Translational Biomedicine
Program:	Molecular and Translational Biomedicine
Thesis Title:	Genome Engineering in the *TP53* Gene Locus in Human Glioblastoma Cell Model
Student's name and Surname:	Başak KAVAKLIOĞLU
Date of Defense:	19/06/2023

This is to certify that I have examined this copy of master thesis. I have found that she prepared after fulfilling the specified requirements in the associated legislations before the final examining committee whose signatures are below.

Jury President	Assist. Prof. Dr. Zeynep TOKCAER KESKİN Acıbadem Mehmet Ali Aydınlar University
Jury Member (Thesis Supervisor)	Assist. Prof. Dr. Nazlı KESKİN TOKLU Acıbadem Mehmet Ali Aydınlar University
Jury Member	Assist. Prof. Dr. Esma Nur OKATAN İstinye University

DECLARATION

I hereby declare that; this thesis has been written by me based on the data obtained in line with the scientific rules and ethical principles of responsible conduct of research. All information, data, comments, analyses have been collected and processed through scientific, academic writing style, and literature used have been duly shown by giving reference to the original sources in accordance with the publication ethics. I also announce and emphasize that I have not violated any rules secured by patent and copyrights whilst the conduct and writing of this research.

22.05.2023
Başak KAVAKLIOĞLU

ACKNOWLEDGEMENT

I would like to thank to my supervisor Asst. Prof Dr. Nazlı Keskin Toklu. I am sincerely grateful to her because she accepted me as master student in her young group. She supported me, helped me, believed me and encouraged me for my scientific endeavours even I did not believe in myself to succeed. I expand my scientific knowledges, gain a lot of experience, learn so many laboratory techniques and literature views in her laboratory group. I am also sincerely appreciated to Dr. Emre Deniz. He supported me, believed me and trusted me even I am so young inexperienced undergrad scientist. I would like to thank to Asst. Prof Dr. Zeynep Tokcaer Keskin and Asst. Prof Dr. Erkan Mozioğlu for their kindness, supports, trusts and helps.

Secondly, I would like to thank to Gizem Gençay, İrem Çongur, Merve Gündoğdu, Dilanur Kamalı, Şebnem Özköse, Gülin Baran, Utku Ertetik, Deniz Nalbant, İrfan Baki Kılıç, Ayşegül Ekmekçioğlu, Ece Aksoy, Gizem Kılıç, Beyza Gürler, Berkcan Koç and for all A5- A6. I am appreciated them for their trusts, helps, supports and their friendships. We shared good times and good memories in laboratory together all the time. Gülin, Deniz, Gizem and Baki are special for me. They are best lab-mates ever for me. I would like to special thank to Menar Ekizce, Muazzez Gökalp, Sıla Sığırlı and Rabia Rümeysa Ünal. I never do anything without their love, trusts, helps and supports.

I would like to thank my sister, mum and dad who have supported me all my life and made me stronger with their love. I am happy that you are my family, I love you more than anything and I wish to be with you all my life.

I thank to the The Scientific and Technological Research Council of Türkiye (TÜBİTAK) for supporting me and this Master thesis. This project was funded by TÜBİTAK 3501 Career Development Program Project entitled with “Comparison Of Hot Spot Mutant p53 Proteins’ Effects On Glioblastoma” (Project Number: 120Z817).

TABLE OF CONTENTS

DECLARATION iii

ACKNOWLEDGEMENT iv

TABLE OF CONTENTS v

LIST OF ABBREVIATIONS viii

LIST OF FIGURES xii

LIST OF TABLES xv

ABSTRACT 1

ÖZET 2

1. AIM OF THE STUDY 3
2. INTRODUCTION 4
2.1.Cancer 4
2.2. Glioblastoma 6
2.3. p53 as the "Guardian of the Genome" 10
2.4. Mutant p53 and Cancer 14
2.5. Genome Editing 16
2.6. CRISPR/Cas9 System and its Applications 17

3. MATERIALS AND METHODS 22

3.1. Materials 22
3.1.1. Chemicals 22
3.1.2. Growth Media 22
3.1.3. Buffers and Solutions 23
3.1.4. Commercial Kits 27
3.1.5. Enzymes 27
3.1.6. Plasmids Maps 27
3.1.7. Oligonucleotides and Primers 28
3.1.8. DNA and Protein Molecular Weight Markers 30
3.1.9. Softwares and Programs 30
3.1.10. Equipments 31
3.2. Methods 32
3.2.1. gRNA Design 32
3.2.2.1. Oligo Annealing 34
3.2.2.2. Diagnostic Digestion of pSp-Cas9(BB)-2A-Puro (PX459) V2.0 Plasmid 35
3.2.2.3. Ligation of Annealed Oligonucleotides into pSp-Cas9(BB)-2A-Puro (PX459) V2.0 Plasmid 36

3.2.2.4. Exonuclease V Treatment 37
3.2.2.5. Preparation of Chemically Competent DH5α Bacterial Cells 38
3.2.2.6. Transformation of the CRISPR Plasmid Constructs into *E. coli* DH5α Competent Cells 39
3.2.2.7. Miniprep DNA Isolation with Alkaline Lysis Protocol 39
3.2.2.8. Confirmation of CRISPR Cloning with PCR 40
3.2.2.9. Sanger Sequencing of the Cloned CRISPR Plasmids 42
3.2.2.10. Midiprep Plasmid DNA Isolation for Cloned CRISPR Plasmids 42
3.2.3. Mammalian Cell Culture 42
3.2.3.1. U87-MG Cell Line Thawing, Maintenance and Cryopreservation 42
3.2.3.2. Puromycin Concentration Determination 43
3.2.4. Small-Scale Transfections 44
3.2.4.1. Microscopy and Flow Cytometry Analyses of Small-Scale Transfection Optimization 44
3.2.4.2. Small-Scale Transfections of CRISPR Plasmids 44
3.2.4.3. Genomic DNA (gDNA) Isolation 45
3.2.4.4. PCR Amplification of the CRISPR Target Regions 46
3.2.4.5. Restriction Fragment Length Polymorphism (RFLP) Assay 47
3.2.4.6. T7 Endonuclease I (T7EI) Assay 48
3.2.5. Large- Scale Transfections 50
3.2.5.1. Microscopy and Flow Cytometry Analyses of Large-Scale Transfection Optimization 50
3.2.5.2. Large-Scale Transfection of CRISPR Plasmids 51
3.2.5.3. Genotyping of U87-MG Cell Pools Co-Transfected with CRISPR Pairs…….. 51

3.2.5.4. Single Cell Cloning of CRISPR A + CRISPR C Co-Transfected Cell Pool……. 53

3.2.5.5. Genotyping of the Single Cell Colonies Derived from CRISPR A + CRISPR C Co-transfected U87-MG Cell Pool 53

3.2.6. Sanger Sequencing of the Single Cell Colonies Showing $p53^{-/-}$ Profile 54
3.2.7. Control of Off-Target Effect in Single Cell Colonies Showing $p53^{-/-}$ Profile ……..54
3.2.8. Western Blot 56
3.2.9. Trypan Blue Exclusion Assay 57
3.2.10. Wound Healing Assay (Scratch Assay) 57
3.2.11. Colony Formation Assay 58

4. RESULTS 59

4.1. Cloning gRNA Candidates into pSp-Cas9(BB)-2A-Puro (PX459) V2.0 Plasmid 59
4.1.1. Diagnostic Digestion of the pSp-Cas9(BB)-2A-Puro (PX459) V2.0 Plasmid ……59
4.1.2. Oligonucleotide Annealing and Cloning into pSp-Cas9(BB)-2A-Puro (PX459) V2.0 Plasmid 61
4.1.3. Confirmation of the Cloned CRISPR Plasmids with Sanger Sequencing 66

4.2. Determination of Puromycin Concentration for Enrichment of the Transfected Population 70
4.3. Small-Scale Transfection Optimization 71
4.3.1. Microscopy Results of Small - Scale Transfection Optimization 72
4.3.2. Flow Cytometry Results of Small- Scale Transfection Optimization 73
4.4. Comparison of Individual Gene Editing Performances of CRISPR Candidates by RFLP and T7E1 Assays 75
4.5. Large-Scale Transfection Optimization 84
4.5.1. Microscopy Results of Large - Scale Transfection Optimization 85
4.5.2. Flow Cytometry Results of Large -Scale Transfection Optimization 86
4.6. Gene Editing Results of Co-transfected CRISPR Pairs 88
4.7. Genotyping of The Single Cell Colonies Derived from CRISPR A and CRISPR C Co-transfected Cells 94
4.8. Confirmation of the Single-Cell Colonies Showing $p53^{-/-}$ Profile with Sanger Sequencing 97

4.9. Off-Target Analysis of the Single-Cell Colonies Showing $p53^{-/-}$ Profile 101

4.10. Western Blot Results of Single Cell Colonies Showing $p53^{-/-}$ Profile 103
4.11. Characterization of U87-MG $p53^{-/-}$ Cell Line 104

4.11.1. Characterization of U87-MG $p53^{-/-}$ Cells: Cell Proliferation 105

4.11.2. Characterization of U87-MG $p53^{-/-}$ Cells: Migration 106
4.11.3. Characterization of U87-MG $p53^{-/-}$ Cells: Colony Formation 108

5. DISCUSSION AND COCLUSION 110

6. REFERENCES 123

7.APPENDIX 136

APPENDIX A: Chemicals Used in This Project 136

APPENDIX B: DNA and Protein Molecular Weight Markers 139
APPENDIX C: Equipment Used in This Project 140

APPENDIX D: Other Components Used in This Project 142

8.CURRICULUM VITAE 143

LIST OF ABBREVIATIONS

α	Alpha
β	Beta
γ	Gamma
Acryl:Bis	Acrylamide: Bisacrylamide
ATP	Adenosine 5'-Triphosphate
BD	Basic Region Domain
$CaCl_2$	Calcium Chloride
Cas9	CRISPR Associated Protein 9
cDMEM	Complete Dulbecco's Modified Eagle Medium
CO_2	Carbon dioxide
CRISPR	Clustered Regularly Interspaced Short Palindromic Repeats
crRNA	CRISPR RNA
DBD	DNA Binding Domain
dCas9	dead-Cas9
ddH_2O	Double Distilled Water
DMSO	Dimethyl Sulfoxide
DNA	Deoxyribonucleic Acid
DSB	Double Strand Break
E.coli	*Escherichia Coli*
EDTA	Ethylenediamine Tetraacetic Acid
EGF	Epidermal Growth Factor
EGFR	Epidermal Growth Factor Receptor
EtBr	Etidium Bromide

EtOH	Ethanol
FACS	Fluorescence-based Cell Sorting
FBS	Fetal Bovine Serum
FITC	Fluorescein Isothiocyanate
FLp53	Full- Length p53
FM	Freezing Medium
GBM	Glioblastoma Multiforme
gDNA	Genomic DNA
GFP	Green Fluorescent Protein
GOF	Gain of Function Mutation
gRNA	Guide RNA
h	Hour
HDR	Homolog Directed Repair
HR	Homologous Recombination
HRP	Horseradish Peroxidase
IN-DEL	Insertion-Deletion
IRES	Internal Ribosome Entry Site
KRAB	Krüppel Associated Box
LB	Luria Broth
LOF	Loss of Function Mutation
MDM2	Mouse Double Minute Protein 2
MDR	Multi Drug Resistance
MGMT	Methylguanine-DNAMethyltransferase
min	Minute
MRE11	Mitotic Recombination 11

NaOH	Sodium Hydroxide
nCas9	Cas9 Nickase
NHEJ	Non-Homologous End Joining
NLS	Nuclear Localization Signal
NT-C1	Non-Targeting Control 1
NT-C2	Non-Targeting Control 2
OD	Optical Density
PAM	Protospacer Adjacent Motif
PBS	Phosphate Buffered Saline
PCR	Polymerase Chain Reaction
pegRNA	Prime Editing RNA
Pen-Strep	Penicillin-Streptomycin
PIPES	1,4-Piperazinediethanesulfonic acid
Pin1	Prolyl Isomerizes
PML	Promyelocytic Leukemia
PR	Proline-Rich Domain
pre-crRNA	Precursor CRISPR RNA
Rb	Retinoblastoma
REPAIR	RNA Editing for Programmable A to I Replacement
RESCUE	RNA Editing for Specific C to U Exchange
RFLP	Restriction Fragment Length Polymorphism
RNA	Ribonucleic Acid
RT	Room Temperature
s	Second
SDS	Sodium Dodecyl Sulfate

SH3	Sarc-3-Homology Domain
SNV	Single Nucleotide Variations
T4 PNK	T4 Polynucleotide Kinase
T7EI	T7 Endonuclease I Assay
TAD	Trans-Activation Domain
TAE	Tris-Acetate EDTA
TALEN	Transcription Activator-like Effector nuclease
TCGA	The Cancer Genome Atlas
TET	Tetramerization Domain
TMD	Transmembrane Domains
TMZ	Temozolomide
tracrRNA	Transactivating CRSIPR RNA
U87-MG	Uppsala 87 Malignant Glioma
WHO	World Health Organization
WT	Wild-Type
WA	Wound Area
ZFN	Zinc Finger Nucleases

LIST OF FIGURES

Figure 2.1 *TP53* gene structure……..…..…..13

Figure 2.2 Domains of the p53 protein……...……...14

Figure 3.1 Schematic representation of the upstream and downstream target regions in the *TP53* gene locus……33

Figure 4.1 Diagnostic digestion of pSp-Cas9(BB)-2A-Puro (PX459) V2.0 plasmid with different restriction enzymes…….…….60

Figure 4.2 The results of top and bottom oligonucleotide annealing of each gRNA candidates and non-targeting gRNA……...62

Figure 4.3 PCR screening of CRISPR cloning for candidate A……63

Figure 4.4 PCR screening of CRISPR cloning for candidate B…….64

Figure 4.5 PCR screening of CRISPR cloning for candidate C…….64

Figure 4.6 PCR screening of CRISPR cloning for candidate D……65

Figure 4.7 PCR screening of CRISPR cloning for candidate NT-C1……65

Figure 4.8 PCR screening of CRISPR cloning for NT-C2……66

Figure 4.9 Sanger sequencing result of candidate A colony 3…….……..67

Figure 4.10 Sanger sequencing result of candidate B colony 5…….67

Figure 4.11 Sanger sequencing result of candidate C colony 9…….68

Figure 4.12 Sanger sequencing result of candidate D colony 4…….68

Figure 4.13 Sanger sequencing result of candidate NT-C1 colony 8……69

Figure 4.14 Sanger sequencing result of candidate NT-C2 colony 8……....69

Figure 4.15 Cell Viability % vs Puromycin concentration graph……..…71

Figure 4.16 Microscopy images of GFP expressing cells that are transfected with different pcDNAGFP:Lipofectamine 3000 ratios for small-scale transfection experiments…….....72

Figure 4.17 Flow cytometry results of cells that are transfected with different pcDNAGFP:Lipofectamine 3000 ratios for small-scale transfection experiments ……74

Figure 4.18 RFLP assay results of CRISPR A ……76

Figure 4.19 T7EI assay results of CRISPR A …….…..78

Figure 4.20 RFLP assay results of CRISPR B ……..…79

Figure 4.21 T7EI assay results of CRISPR B……...…….80

Figure 4.22 RFLP assay results of CRISPR C…….....81

Figure 4.23 T7EI assay results of CRISPR C and CRISPR D ……..82

Figure 4.24 RFLP assay results of CRISPR D……..……..…..83

Figure 4.25 Microscopy images of GFP expressing cells that are transfected with different pcDNAGFP:Lipofectamine 3000 ratios for large-scale transfection experiments…….85

Figure 4.26 Flow cytometry results of cells that are transfected with different pcDNAGFP:Lipofectamine 3000 ratios for large-scale transfection experiments …….87

Figure 4.27 Result of CRISPR activities of co-transfected CRISPR candidates…...89

Figure 4.28 Results of gene editing due to CRISPR A + CRISPR C pairs activity in U87-MG cells……..90

Figure 4.29 Results of gene editing due to CRISPR A + CRISPR D pairs activity in U87-MG cells……..91

Figure 4.30 Results of gene editing due to CRISPR B + CRISPR C pairs activity in U87-MG cells……..92

Figure 4.31 Results of gene editing due to CRISPR B + CRISPR D pairs activity in U87-MG cells……..93

Figure 4.32 Genotyping of single-cell colonies derived from CRISPR A + CRISPR C co-transfected cell pool……...96

Figure 4.33 Sanger sequencing result of single cell colony 2……....98

Figure 4.34 Sanger sequencing result of single cell colony 16……..…99

Figure 4.35 Sanger sequencing result of single cell colony 17……...….100

Figure 4.36 Off-target analysis of CRISPR A…….102

Figure 4.37 Off-target analysis of CRISPR C …….103

Figure 4.38 Confirmation of p53 expression loss in single cell colonies ……...……104

Figure 4.39 The results of trypan blue exclusion assay…….……..105

Figure 4.40 Microscopy images of the wound healing assay……..…107

Figure 4.41 Results of the wound healing assay…….……...…….……108

Figure 4.42 Results of the colony formation assay ……..…109

LIST OF TABLES

Table 3.1 Plasmids used in this thesis……..…….28

Table 3.2 Oligonucleotides used in this thesis……...29

Table 3.3 Upstream target region and downstream target region primers used in this thesis……...29

Table 3.4 Off-target primers used in this thesis…….30

Table 3.5 Softwares used in this thesis……..31

Table 3.6 gRNA candidates and non-targeting control gRNAs used in this thesis……...33

Table 3.7 Oligo annealing reaction components……34

Table 3.8 Oligo annealing reaction conditions…….…..34

Table 3.9 Diagnostic digestion reaction components……..……..…35

Table 3.10 Diagnostic digestion reaction conditions…….....……...35

Table 3.11 Ligation reaction components…….….36

Table 3.12 Ligation reaction conditions…….…36

Table 3.13 Exonuclase V treatment components……...37

Table 3.14 Exonuclase V treatment conditions……..37

Table 3.15 Exonuclase V reaction inhibition components…….…38

Table 3.16 Exonuclase V reaction inhibition conditions……...38

Table 3.17 PCR components for confirmation of CRISPR cloning …….……41

Table 3.18 PCR conditions for confirmation of CRISPR cloning …..……...…...41

Table 3.19 PCR components for amplification of the target regions…….…46

Table 3.20 PCR conditions for amplification of the target regions …..……46

Table 3.21 Digestion components of RFLP assay……...…..48

Table 3.22 Digestion conditions of RFLP assay ……..……48

Table 3.23 Components and conditions of denaturation and re-annealing steps of T7EI assay …….……..…..49

Table 3.24 Components and conditions of T7EI digestion……..……...……..49

Table 3.25 PCR components for genotyping……. ……...…52

Table 3.26 PCR conditions for genotyping…….……...……52

Table 3.27 Off-target PCR components…….…..……...55

Table 3.28 Off-target PCR conditions……..…..55

ABSTRACT

The p53 tumor suppressor protein, known as the guardian of the genome, is a transcription factor that regulates many biological activities such as cell survival, apoptosis, autophagy, senescence, cell cycle, metastasis, invasion, DNA repair and cell metabolism. p53 is found to be mutant in more that 50% of cancer cases. Glioblastoma is one of the most difficult type of cancer to treat due to not only the location of the tumor but also its heterogeneous structure and 85% of the glioblastoma tumors have deregulated p53 pathway. However, the specific effects of mutant p53 proteins have not been comprehensively investigated in glioblastoma, yet. In order to study mutant p53 proteins in glioblastoma, a cell line model that lacks p53 expression is needed. Therefore, in this study, the aim is to create a p53 knockout glioblastoma cell line via targeting the *TP53* gene locus by CRISPR/Cas9 with a novel approach. Two different regions in the *TP53* gene locus were targeted with CRISPR/Cas9 simultaneously and the region in between was deleted. The single cell colonies derived from the gene edited cell pool were screened to find the $p53^{-/-}$ cell clone. In this newly created U87-MG $p53^{-/-}$ cell line, biallelic deletion in the *TP53* gene locus was confirmed by performing Sanger Sequencing and the loss of p53 protein expression was confirmed by performing western blot. In addition, it was shown that there were no off-target effects in this cell line. For further characterization, proliferation, migration and colony formation abilities of U87-MG $p53^{-/-}$ cells were investigated.

Keywords: Cancer, Glioblastoma, U87-MG Cell Line, p53, CRISPR/Cas9

ÖZET

İNSAN GLİOBLASTOMA HÜCRE MODELİNDE *TP53* GEN BÖLGESİNDE GENOM MÜHENDİSLİĞİ YAPILMASI

"Genomun Koruyucusu" olarak bilinen, tümör baskılayıcı p53 proteini, hücre sağ kalımı, apoptoz, otofaji, senesans, hücre döngüsü, metastaz, invazyon, DNA tamiri ve hücre metabolizması gibi birçok biyolojik faaliyeti regüle eden bir transkripsiyon faktördür. İnsan kanser vakalarının %50'sinden daha fazlasında p53 mutant olarak bulunmaktadır. Glioblastoma sadece tümörün lokasyonu nedeniyle değil aynı zamanda heterojen yapısı nedeniyle tedavi edilmesi en zor kanser türlerinden biridir ve glioblastoma tümörlerinin %85'inde deregüle olmuş p53 yolağı bulunmaktadır. Ancak, mutant p53 proteinlerinin spesifik etkileri glioblastomada henüz kapsamlı olarak araştırılmamıştır. Mutant p53 proteinlerinin glioblastomadaki etkilerinin çalışılabilmesi için p53 protein ifadesinin olmadığı bir glioblastoma hücre hattı modeline ihtiyaç, duyulmaktadır. Bu nedenle bu çalışmanın amacı, *TP53* gen lokusunu CRISPR/Cas9 sistemi ile özgün bir yaklaşımla hedefleyerek p53 nakavt glioblastoma hücre hattı oluşturmaktır. *TP53* gen lokusundaki iki farklı bölge CRISPR/Cas9 ile eş zamanlı olarak hedeflendi ve aradaki bölge silindi. Gen düzenlemesi yapılan hücre havuzundan elde edilen tek hücre kolonileri taranarak $p53^{-/-}$ hücre klonu bulundu. Bu yeni yaratılan U87-MG $p53^{-/-}$ hücre hattında, *TP53* gen lokusundaki bialelik silinme Sanger dizileme ile teyit edildi ve p53 proteinin ifade edilmediği western blot ile gösterildi. Bu hücre hattında hedef dışı etkilerin olmadığı da gösterildi. Bunlara ek olarak, daha ileri karakterizasyon için U87-MG $p53^{-/-}$ hücrelerinin, çoğalma, migrasyon ve koloni oluşturma becerileri incelendi.

Anahtar Sözcükler: Kanser, Glioblastoma, U87-MG Hücre Hattı, p53, CRISPR/Cas9

1. AIM OF THE STUDY

p53 tumor suppressor protein is found to be mutant in 50% of cancer cases (1). While some of these mutations cause the p53 protein to lose its function, some of these mutations cause the p53 protein to gain new oncogenic functions (2). p53 protein is a tetrameric protein and in case of co-expression of WT and mutant p53 proteins in the cell, heterotetramer of WT and mutant p53, inhibit tumor suppression function of p53 and the complex is incapable of DNA binding. In addition, some hotspot mutations of p53 protein might cause gain of new oncogenic functions when WT p53 is not present (3). The specific effects of mutant p53 proteins have not been comprehensively investigated in glioblastoma, yet. In order to study the roles of mutant p53 proteins in glioblastoma, a cell line model that lacks p53 expression is needed. The aim of this thesis is to create U87-MG $p53^{-/-}$ cell line model for further hotspot mutant p53 studies in glioblastoma. The novelty of this thesis is the creation of U87-MG $p53^{-/-}$ cell line with a pair of gRNA/Cas9 targeting two different regions in the *TP53* gene locus in order not to express any isoforms of p53 protein. Mostly, in knockout studies, lentiviral delivery methods are preferred due to having high efficiency (4,5,6). However, as a result of lentiviral delivery, gRNA/Cas9 are stably expressed due to genomic incorporation into the host cell. Therefore, in this thesis, transient transfection of gRNA/Cas9 was selected as the delivery method, in order not to limit the potentiality to study the roles of mutant p53 proteins in this newly created cell line. Since WT and mutant p53 have only one nucleotide difference in the DNA sequence, in case of stable expression of gRNA/Cas9, there would be the risk of modification of the mutant p53 proteins in case of their overexpression in this cell line. In this thesis, U87-MG $p53^{-/-}$ cell line is created as a result of biallelic deletion in the *TP53* gene locus of U87-MG cells and is characterized from the perspectives of cell proliferation, migration and colony formation abilities. Therefore, this $p53^{-/-}$ genotype and phenotype bearing cell line can be used safely to overexpress mutant p53 proteins for further studies.

2. INTRODUCTION

2.1. Cancer

Cancer, followed by cardiovascular disease, is the second most serious major group of diseases threatening human health (7). Mutations, copy number increases, chromosomal rearrangements and changes in epigenetic regulation may drive cancer. Lifestyle, environmental conditions, exposure to chemicals and behavioural factors have an indirect effect on the progression of cancer. Proto-oncogenes and tumor suppressor genes are two groups of genes associated with cancer. Mutations and/or gene expression changes in proto-oncogenes and tumor suppressors lead to the acquisition of the hallmarks of cancer (8,9,10).

Proto-oncogenes encode proteins that regulate cell growth, proliferation, apoptosis, metabolism and genomic stability. Proto-oncogenes are converted into oncogenes as a result of different changes in the genome which drive cancer development. These changes are deletions or point mutations in the coding sequence, gene amplifications and chromosomal rearrangements. *RAS*, *MYC*, *ABL* and *EGFR* are the well-known proto-oncogenes (11,12,13,14,15,16). The point mutations such as base pair substitutions that occur in the reading frame of the *RAS* proto-oncogene family cause the conversion of the *RAS* family to become oncogenes. Upon conversion to oncogenes, RAS-related proteins lead to cancer development through an increase in invasion and metastasis and a decrease in apoptosis. *HRAS*, *KRAS* and *NRAS* proto-oncogenes belong to the *RAS* proto-oncogene family. Point mutations in *HRAS* gene, *KRAS* gene and *NRAS* gene are most commonly seen in head&neck cancers, pancreas cancers and melanoma (skin cancers), respectively (15,16,17,18,19,20). HRAS oncoprotein has an amino-acid substitution at residue 12. KRAS oncoprotein has an amino-acid substitution at residue 13. NRAS oncoprotein

has an amino-acid substitution at residue 61 (15,16,21). Another proto-oncogene that is well studied is *MYC*. Gene amplification of the *MYC* proto-oncogene causes *MYC* to become an oncogene. Excessive levels of the MYC protein lead to cancer by causing with uncontrolled cell proliferation, inhibition of the apoptosis, uncontrolled cell cycle and altered metabolism. *MYC* gene amplification is most commonly seen in Burkitt Lymphoma (15,16,22,23). The *BCR-ABL* oncogene arises from Philadelphia chromosome (Ph) translocation. In Philadelphia chromosome (Ph) translocation, *BCR* gene fuses with the *ABL* gene. BCR-ABL oncoprotein induces cell proliferation and haematopoietic malignancies. lt is known that ABL tyrosine kinase activity is elevated in the BCR-ABL oncoprotein. This increase is a major reason for the transformation of haematopoietic cells. Formation of the *BCR-ABL* oncogene is most common in chronic myeloid leukaemia (CML) (15,16,24,25). The *EGFR* (epidermal growth factor receptor) proto-oncogene is a member of the receptor tyrosine kinase family. In normal circumstances, EGFR releases a signal into the cell when it interacts with EGF (epidermal growth factor) ligand. EGFR is mutated, truncated or overexpressed in some cancers such as lung cancer and brain cancer (26). Ligand independent firing takes place due to overexpression and truncations. EGFR sends growth-stimulating signals into the cells so that cell proliferation is enhanced. In some cancers, ligands are also overexpressed. Ligand overexpression increases EGFR dimerization, activation, and tyrosine kinase-mediated signaling so that cell proliferation is enhanced (15,16,27,28).

Tumor suppressor proteins are essential due to the fact that they regulate many cellular functions. The loss or inactivation of functional tumor suppressor genes drive the mechanism of cancer development. The pRB protein which is encoded by the *RB1* gene is the first identified tumor suppressor protein and therefore it is one of the most intensively studied tumor suppressor protein (11,12,13,14,15,16). pRb protein is considered as the master regulator of restriction gate in cell cycle by being the inhibitor of E2F which is a master transcription factor controlling the expression of cell cycle related proteins such as Cyclin E, A, Cdt1. The active, hypo-

phosphorylated form of the pRb protein binds and inhibits the transcription factor E2F. Inhibition of the E2F leads to the downregulation of the necessary DNA replication factors to inhibit the G1 to S transition. E2F induces the G1/S transition when the pRb protein is inactive in its hyperphosphorylated form. Defects in the pRb cause the childhood cancer, bladder cancer and osteogenic sarcoma (15,16,29,30,31). *TP53* gene is another well studied and characterized tumor suppressor gene. *TP53* gene is found to be mutant in 50% of cancer cases (1). p53 tumor suppressor protein is a transcription factor which has roles in regulation of cell for cell cycle, apoptosis, senescence, autophagy, cell metabolism and DNA repair. p53 mutations are categorized into two: loss-of-function (LOFs) and gain-of-function mutations (GOFs). LOFs prevent p53 from transactivating its canonical target genes. Gain of function mutations cause p53 to not only lose its tumor suppressor functions but also gain new oncogenic functions (15,16). Another example of well-known and well-studied tumor suppressor genes are *BRCA1* and *BRCA2* genes. BRCA1 and BRCA2 proteins play roles in DNA repair after double-stranded breaks and assisting in maintenance of genomic integrity. The most common types of mutations are small insertion/deletion mutations that cause frameshifts, non-synonymous truncations and splice site disruptions that result in non-functional BRCA proteins (15,16,32,33). *BRCA1* and *BRCA2* are mostly mutated in breast and ovarian cancers (15,16,32,34).

2.2.Glioblastoma

Gliomas, the general term for brain tumors in adults, are classified according to the origin of the cells, the degree of histological malignancy and the mitotic activity (35,36,37). Gliomas are classified into grades I, II, III and IV by World Health Organization (WHO). Grades I and II are considered as low grade due to the proliferative potential of the tumors. Grades III and IV are considered as high grade because of the aggressiveness and proliferation rate of the tumors (36).

Glioblastoma Multiforme (GBM) which occurs in the central nervous system (CNS) is the most common type of IV grade glioma (37). GBM tumors which arise from oligodendrocytes and astrocytes are most commonly located in the supratentorial brain but rarely located in the cerebellum, the brainstem and the spinal cord (36). Compared to other cancers such as colorectal, lung, prostate and breast, GBM is rare, constituting only 3% of all cancers (38). Among other human brain tumor types, GBM tumors are heterogenous, vascularized, highly invasive and the most malignant type of tumors (39). Despite the recent developments in GBM treatments such as surgery, chemotherapy and radiotherapy, it has poor prognosis (40). The survival of the glioblastoma patients is increased to about 12-15 months with treatment but, without treatment the survival of the glioblastoma patients is only 3 months (41). It has been shown that patients over the age of 40, are more likely to develop glioblastoma (38). Glioblastoma is more common in men than in women (42).

GBMs are classified into two groups: primary and secondary glioblastomas. These two types of glioblastomas arise from different genetic pathways and have different epigenetic profiles. Primary and secondary glioblastomas affect patients of different genders and ages. Deletion of *CDKN2A,* amplification of *EGFR*, loss-of-function mutation of *PTEN* are associated with the formation of primary glioblastomas. Low-grade, diffuse astrocytomas (WHO grade II) or anaplastic astrocytomas (WHO grade III) develop secondary glioblastomas. Secondary glioblastoma is mainly manifested by p53 signaling pathway mutations (43,44).

Alterations in the EGFR-PTEN-Akt-mTOR signaling cascade can cause the development of primary glioblastoma. Overexpression of EGFR enhances cell proliferation and triggers activation of the (PI3K)/Akt pathway which activates mTOR. mTOR activation results in inhibition of apoptosis, increased cell survival and cell proliferation. PTEN is modulated by kinase or kinase domain containing proteins. There are several intracellular proteins that target PTEN to inhibit or

activate its cellular functions. The main mechanism by which PTEN functions are inhibited or activated is through phosphorylation of specific residues in the C-terminal region. Mutant version of the PTEN induces cell migration and invasion in primary glioblastoma. The $p16^{INK4a}$/pRb signaling pathway is an important pathway in both primary and secondary glioblastomas (43,44). *RB1* gene encodes pRb protein which inhibits G1 to S phase transition in cell cycle (45). E2F transactivates the expression of many cell cycle related genes when it is active. Therefore, E2F increases proliferation by inducing the G1 to S transition (46). The cyclin-dependent kinase 4 (CDK4) cyclin D complex is regulator of the transition through the G1 phase of the cell cycle (47). $p16^{INK4a}$ is CDK inhibitor to regulate cell cycle. Increased expression of $p16^{INK4a}$ inhibits proliferation and is dominant to a variety of mitogenic and oncogenic signals (48). $p16^{INK4a}$ binds and inhibits the CDK4/cyclin D1 complex (49). In the absence of mitogens, CDK4/cyclin D1 complex is unable to phosphorylate pRb. Hypophosphorylated pRb interacts with the transcription factor E2F. The interaction with hypophosphorylated pRb blocks E2F activity to inhibit transcription of cell cycle related genes that are required for the transition from G1 to S phase (50). In the presence of mitogens, elevated cyclin D levels in response to mitogenic stimuli form active CDK4/cyclin D1 complexes. After the activation of CDK4/cyclin D1 complex, pRb is hyperphosphorylated. Hyperphosphorylated pRb dissociates from E2F-DP binding sites. E2F transactivates genes involved in the cell cycle for the transition from G1 to S (51,52).

RB1 gene promoter methylation is significantly higher in secondary glioblastomas than primary glioblastomas. Methylation of the *RB1* gene promoter leads to pRb protein inactivation (43,44). The *CDKN2A* gene alterations are more common in primary glioblastomas than in secondary glioblastomas (53). The *CDKN2A* gene is often deleted in GBM, contributing to unchecked pRb phosphorylation and rapid cell division (54). O^6-Methylguanine-DNA methyltransferase (MGMT) is DNA repair enzyme that plays role in maintaining genomic stability. The frequency of promoter methylation of *MGMT* is different in

primary and secondary glioblastomas. Methylation of the gene promoter leads to loss of *MGMT* expression. MGMT removes guanine-alkyl groups from the O^6 position of guanine in DNA and repairs O^6-alkylguanine DNA adducts. Repair of O^6-alkylguanine DNA adducts decreases the cytotoxicity of chemotherapeutic drugs, leading to the development of drug resistance. TMZ is a chemotherapy drug that is used in the treatment of GBM. However, the development of resistance to TMZ limits effective treatment. More than 50% of GBM patients treated with TMZ drugs do not respond to treatment because they develop resistance to TMZ. The epigenetic status of *MGMT* is one of the markers used to identify TMZ resistance in GBM. GBM patients with unmethylated *MGMT* promoter are commonly developing TMZ resistance (43,44,55). According to The Cancer Genome Atlas (TCGA) GBM project results, the p53 pathway (including *MDM2* (Mouse Double Minute Protein 2), *TP53*, *CDKN2A*) was deregulated in 85% percent of the GBM tumors. Mutations in the p53 signaling pathway are more common in secondary glioblastomas than in primary glioblastomas. The most common alterations in glioblastomas are loss of *CDKN2A* expression with homozygous deletion and promoter methylation of the *CDKN2A*. Promoter methylation of *CDKN2A* is frequently seen in secondary than primary glioblastomas. The $p14/p19^{ARF}$ protein, which interacts with MDM2 to increase the level of p53 protein. Point mutations, deletions and/or truncations of the *TP53* gene are seen in secondary glioblastomas (43,44,56). In some types of WHO grade II and IV gliomas, *IDH1* and *IDH2* mutations are common (57,58,59). IDHs (Isocitrate Dehydrogenase) catalyze the oxidative decarboxylation of isocitrate to α-ketoglutarate (α- KG). *IDH1* or *IDH2* mutations cause the conversion of alpha-ketoglutarate (α- KG) to 2-hydroxyglutarate (2-HG), which functions as an oncometabolite. 2-HG is a key driver of gliomagenesis. 2-HG acts as competitive inhibitor of α-KG so that α-KG-dependent histone and DNA demethylation is blocked (60,61,62). One of the classification markers between primary and secondary glioblastoma is *IDH1* mutations. *IDH1* mutations are common in secondary glioblastomas but rare in primary glioblastomas. The mutations of *IDH1* shows heterogeneity between patients with glioblastoma (43,44).

2.3. p53 as the “Guardian of the Genome”

p53 also known as the “Guardian of the Genome” is a stress responsive tumor suppressor transcription factor (63). The p53 protein has crucial roles in cell cycle, apoptosis, senescence, autophagy, cell metabolism and DNA repair (1). Under normal circumstances, p53 protein levels are kept under control by p53-binding proteins, which directly and/or indirectly cause p53 to be polyubiquitinated and degraded. MDM2 plays the most crucial role in controlling p53 protein levels. MDM2 which is an E3 ubiquitin ligase is one of the master negative regulators by causing polyubiquitination of p53 and targeting the protein for proteasomal degradation (64,65). The level of p53 is also controlled by several regulators and mechanisms other than MDM2. MDMX, also known as MDM4, is another partner that interacts with p53. MDMX and MDM2 have close homology due to their evolutionarily conserved RING domains. MDMX does not polyubiquitinate and degrade p53 as MDM2 does. MDMX heterodimerizes with MDM2. After heterodimerization, the RING domain of MDMX triggers the ubiquitin ligase activity of MDM2. Therefore, the prolonged interaction of MDMX with the E2 ubiquitin-conjugating domain of MDM2 is critical to activate MDM2 to polyubiquitinate p53 for proteasomal degradation and therefore maintain p53 levels low. (65,66).

Under stress conditions such as DNA damage, oncogenic signaling activation, nutrient deficiency and oxidative stress, p53 is stabilized with post-translational modifications such as methylation, acetylation, phosphorylation, sumoylation and neddylation (67,68). Activation of p53 is initiated by phosphorylation. The N-terminus of the p53 protein is phosphorylated by Chk1/Chk2 kinases from residues S15 and S20 upon ATM/ATR activation (65,69,70). The phosphorylation of p53 inhibits its interaction with MDM2, thereby blocking the ubiquitination of p53 (71,72). This causes p53 to accumulate. Accumulation of p53 and subsequent interaction with sequence-specific DNA activates or represses the expression of

target genes (65,70). p53 is also acetylated from lysine residues (K370, K371, K372, K381, K382) by the CBP (CREB binding protein)/p300 complex (73,74). The ubiquitination of the p53 is blocked by the acetylation of the lysine residues. p53 degradation is inhibited and p53 accumulates. SET7/9 is metyl-transferase that transfers methyl group to K372 residue of p53 for its activation (75). SET8 is also metyl-transferase that transfers methyl group to K382 residue of p53 to inhibit p53 transcriptional activity (76). Oncogenic stress such as oncogene activation and/or tumor suppressor gene inactivation regulates p53 stabilization in addition to post-translational modifications. Ras, E2F-1, MYC, β-catenin and nucleophosmin oncoproteins lead accumulation of p53 in the nucleus. The p14/p19 ARF tumor suppressor proteins are involved in p53 activation with inhibition of MDM2 activity in the presence of the oncogenic stress. Ras, nucleophosmin and MYC oncoproteins increase the p14/p19 ARF proteins levels by inhibiting the degradation of the ARF protein. p14/p19 ARF interact with MDM2 and inhibit MDM2-mediated ubiquitination of p53. As a result, the level of the p53 protein increases. Oncogenic stress regulates IGF-1/AKT pathway. This pathway plays role in the regulation of cell survival and cell proliferation. IGF-1/AKT pathway is negative regulator of p53 protein. AKT mediated phosphorylation of MDM2 induces p53 protein degradation. A number of factors are positively or negatively control the activity of AKT and its regulation of MDM2. AKT and MDM2 activity is inhibited by PTEN and 14-3-3σ to enhance p53 function. Overexpression of Her-2/neu in human cancers activates the AKT pathway. Activation of AKT induces phosphorylation of the MDM2 and inhibits p53 function. PRL-1 and PRL-3 enhance AKT activity. This leads to the phosphorylation of MDM2 (77).

p53-mediated transcription is initiated by p53 binding to its recognition site on DNA. p53 forms a homotetramer consisting of four p53 domains. The consensus sequence of p53 on DNA is RRRCWWGYYY. R indicates for purines, Y indicates pyrimidines. W indicates A or T. Two p53 dimers interact with two half-sites of the DNA so that p53 is tetramerized for its activation and function. Functionally, p53 is a

transcription factor that forms a homotetramer to activate target genes, responsible for cell cycle, apoptosis, senescence, autophagy, cell metabolism and DNA repair (78,79,80,81).

p53 is located in the central region of the signaling network. Under stress circumstances, p53 protein is stabilized. For stabilization of p53, various transcriptional output such as cell cycle arrest, senescence, apoptosis and cell metabolism are regulated depending on the epigenetic landscape, binding partners, post-translational modifications and strength of p53 response element. Activation of p53 in response to stress conditions directs cell cycle inhibition (82). *SFN, CDKN1A* and *GADD45A* genes are induced by p53 activation. 14-3-3σ, p21 and GADD45A proteins are encoded from *SFN, CDKN1A* and *GADD45A* genes, respectively. 14-3-3σ, p21 and GADD45A proteins have roles in cell cycle arrest with inhibition of cell cycle (83,84). p53 activation in response to stress circumstances directs also senescence. p53 increase the expression of *SERPINE1*, and *PML* genes and the proteins encoded by these genes (PAI-1 and TRIM) induce senescence (84,85). p53 activation in response to prolonged stress circumstances directs apoptosis. p53 increases the expression of the *BBC3*, *APAF1* and *PMAIP1* genes and the proteins encoded by these genes (PUMA, AFAF1 and NOXA) induce apoptosis (84,86). p53 activation in response to stress circumstances directs also regulation of autophagy. p53 upregulates *ATG7* and *DRAM2* genes and proteins encoded by these genes (ATG7, DRAM2) regulate autophagy (84). p53 activation in response to stress circumstances also affects regulation of the cell metabolism. p53 upregulates *TIGAR* and *PRKAA1* genes and the proteins encoded by these genes (TIGAR, AMPK) regulate cell metabolism (84,87). p53 activation in response to stress circumstances has effect on regulation of the DNA repair mechanism. *PTF1* and *POLK* genes which encode p48 and DNA polymerase kappa protein regulate DNA repair mechanisms (84).

p53 protein is encoded by the *TP53* gene on chromosome 17p13.1 (88,1). *TP53* has 3 promoters, 11 exons and 10 introns as shown in Figure 2.1 (89,90). There are 12 isoforms of the p53 protein (88,89). Three distinct promoters and alternative splicing pattern of the exon 9 give rise to isoforms of p53. By using the P1 promoter, the full length of the p53 protein is transcribed and is referred to as the full length p53 (FLp53) transcript. The Δ40p53 isoform is transcribed from codon 40 using promoter P1'. The Δ133p53 and Δ160p53 isoforms are transcribed from codon 133 and 160, respectively, using promoter P2. All exons, including exons 10 and 11, are conserved in the α isoform. Alternative splicing of exon 9 produces exon 9β or exon 9γ. These transcripts form p53 β and γ isoforms after translation (90,91).

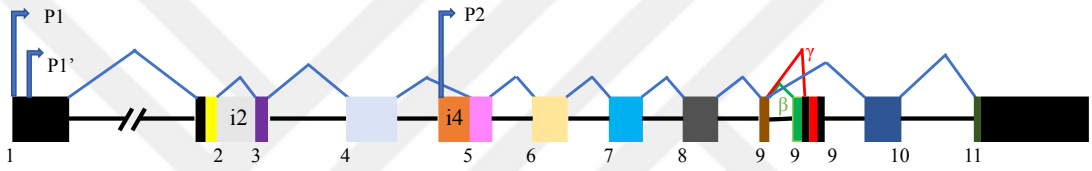

Figure 2.1 *TP53* gene structure. The rectangles illustrate the exons. The region in between rectangles illustrates the introns. P1, P1' and P2 which are indicated with blue arrows illustrate promoters of the *TP53* gene. This figure is adapted from Vieler M. et al. (88).

p53 protein has many domains, as shown in Figure 2.2. Two trans-activation domains (TAD I and TAD II) are encoded in exons 2-4, proline-rich domain (PR) in exon 4, DNA binding domain (DBD) in exons 4-8, nuclear localization sequence (NLS) in exon 9, tetramerization (oligomerization) domain (TET) in exons 9-10 and basic domain (BD) in exons 10-11 (92,93). Each domain has distinct functions. The TAD I and II domains, located at the N-terminus of the p53 protein, play a role in the tumor suppressor function of the p53 protein and the transcriptional activation of p53 target genes (94). PR have a role in linking DBD and TAD. PR contains a PXXP motif to generate SH3 domain binding sites. PXXP motif is important role for p53. In order to presence of PXXP motif, p53 responds to DNA-damaging agents to cause cell death (95,96). The central core region of p53 contains DBD. DBD is crucial role for p53 as a sequence-specific transcription factor. DBD recognizes and binds to the

specific DNA sequences in the gene locus of p53 target genes to regulate their transcription (89). NLS plays role in localization p53 to the nucleus (97). p53 monomers are dimerized then dimers of the p53 are tetramerized with TET to form the correct p53 quaternary structure to recognize and bind DNA. Tetramerized p53 is stabilized through hydrophobic forces BD is located at the C-terminus of the p53 protein. BD regulates the overall functions of the p53 protein both positively and negatively through post-translational modifications (98).

Figure 2.2 Domains of the p53 protein. TAD I and TAD II are represented with red and orange boxes, respectively. PR is represented with yellow box. DBD is represented with green box. NLS is represented with light blue box. TET is represented with purple box. BD is represented with brown box. This figure is adapted from Beckerman R. et. al. (99).

2.4.Mutant p53 and Cancer

p53 is found to be mutant in 50 % of human cancers such as bladder, breast, colon, prostate, liver, bladder and skin (1). Several mechanisms alter the p53 protein and related pathways. The majority of *TP53* mutations is missense mutations. Frameshift deletions and insertions, silent mutations, nonsense mutations and other infrequent changes are other important alterations (100). The p53 residues which are frequently found to be mutant in cancers are R175, G245, R248, R249, R273 and R282 and these residues are corresponding to the DBD domain of p53 (101,102). p53 mutations are categorized into two: LOFs and GOFs (102). In the LOF situation, mutation of one allele of *TP53* results in impaired function of the p53 protein (103). In addition to the acquisition of a *TP53* mutation in one allele, the majority of tumors also lose the second allele through a deletion or a copy neutral loss of heterozygosity (LOH) (102). Mutant p53 is capable of tetramerization, however this tetramer is

unable to bind DNA and transactivate its canonical target genes (104). In addition to the LOF situation, the expression of a mutant p53 protein interferes with the activity of a wild-type p53 tumor suppressor protein in dominant negative (DN) effects (102). Mutant/wild-type heterotetramer form of the p53 interacts with DNA with weaker affinity. Weak interaction with DNA leads to defective binding of mutant p53 to the transcriptional cofactor that is important for p53 activity (105). *TP53* mutations are mostly resulted by LOH during cancer progression. Therefore, heterozygous state of the *TP53* is transient. LOH is generally involved in tumor suppressors. In the case of a heterozygous locus (WT allele and mutant allele presence), the WT allele is either deleted or mutated (102). In GOF situation, mutant p53 is capable of tetramerization, this tetramer is able to bind DNA and transactivate its non-canonical target genes to drive tumor development. In addition, mutant p53 binds DNA indirectly through interaction partners and complexes to transactivate non-canonical target genes (82,92,106,107).

Wild-type p53 and mutant p53 have not only common but also different interacting partners. MRE11 is one of the interacting partners of mutant p53 (p53-R248W and p53-R273H) (108,109,110). PML (Promyelocytic Leukaemia) is an interacting partner of both the wild-type p53 and the mutant p53. PML interacts with mutant p53 to induce proliferation and inhibit apoptosis. PML interacts with wild-type p53 to induce apoptosis (108,109,111). For both wild-type and mutant p53, the other interacting partner is PIN1 (Prolyl Isomerised). PIN1 interacts with mutant p53 to promote migration and invasion of breast cancer. PIN1 interacts with wild-type p53 to cause cell cycle arrest via cyclin dependent kinase inhibitor p21 (108,109,110,112). The mutant p53 protein also interacts with other members of its family, such as p63 and p73. The TAD, DBD and TET domains of p53, p63 and p73 are homologous. p63 and p73 interact with mutant p53 to form heterotetramer but do not bind to wild-type p53. Mutant p53 blocks transcriptional activation of both p63 and p73. Mutant p53–p63 and mutant p53–p73 heterotetramers promote invasion, metastasis and chemoresistance (110,113,114)

2.5.Genome Editing

Genome engineering has started a new era in human genome research. Genome engineering has been evolved since 1970s to diagnose disease, to treat disease and to study the human genome (115). In genome engineering, the genome is manipulated at the DNA level. Genomic modification at the desired region begins with the generation of a double-stranded break (DSB), which is mechanism for triggering the DNA repair machinery. After formation of the DSB, the DNA is repaired via either Homology Directed Repair (HDR) or Non-Homologous End Joining (NHEJ) (116). In HDR mechanism, homologous donor DNA is used as a template to repair DNA damage. HDR is precise repair mechanism. Broken ends of DNA are directly rejoined. This creates a heterogeneous pool with insertions and deletions of the bases. NHEJ is a more error-prone mechanism (116,117). Endonucleases such as I-SceI were first used to edit the mouse genome by DSBs strategy. Then the scientists also used meganucleases, which recognize long sequences of DNA. However, genome editing with meganucleases has a major drawback. Each meganuclease has a unique sequence to recognize the target site, so the probability of finding meganucleases that target the corresponding region is very low (116).

One of the technologies used to edit the genome is Zinc Finger Nucleases (ZFNs). Zinc-finger DNA-binding domain and FokI type II restriction endonuclease are found in ZFNs. The zinc finger DNA binding domain is able to bind DNA with the recognition of the specific sequence. ZFNs are specified in terms of the amino acid sequence of each finger and the number of fingers that interact with the nuclease domain. The FokI endonuclease recognizes and cleaves specific sequences of DNA. FokI works via homodimerization so that ZFNs are designed as two proximal close target sites to activate FokI to create DSB in the target sequence (116,118).

One of the techniques being developed for genome editing is transcription activator-like effector nucleases (TALENs). DBD (transcriptional activating effector) and the restriction endonuclease FokI are found in TALENs. Nuclease and DNA binding domains are linked by a 12-25 bp spacer sequence called linker. FokI endonuclease homodimerization is needed for its activation. Therefore, two TALENs targeting the opposite strand recognize their target regions and a double-strand break is generated by FokI endonucleases. Genome editing with ZFNs and TALENs has played a crucial role in the development of recombinant DNA technology, but there are also some disadvantages such as off-target effects, complexity and cost. As a result, scientists have been working to find a simple, efficient, affordable and reliable method of genome editing until they investigated CRISPR/Cas9 genome editing technology (116,118).

2.6.CRISPR/Cas9 System and lts Applications

CRISPR and Cas are forming an adaptive immune defense system to counteract bacteriophage infection (119,120,121,122). After discovery of CRISPR/Cas in bacteria, the CRISPR/Cas9 system was generated as a tool for genome editing. The CRISPR system has two components; one of the components is the Cas9 endonuclease and the other component is the guide RNA (gRNA). In order to apply easily, scientist developed gRNA. gRNA was chimeric RNA containing tracrRNA and crRNA components. crRNA plays a role in target recognition. tracrRNA is a linker in between crRNA and Cas9. CRISPR/Cas9 system is used to recognize 20 nt or 24 nt target sequences matching engineered gRNA (123). Cas9 undergoes conformational change upon gRNA interaction which causes Cas9 activation (124). Protospacer Adjacent Motif (PAM) sequence on target DNA strands is crucial to mark proper target site. PAM sequence is essential for the endonuclease activity of the Cas9. 5'-NGG-3' sequence is the most commonly used PAM sequence. G indicates guanine nucleotide. N indicates A, T, G or C (125). Cas9 protein has 6

domains. These are Rec I, Rec II, Arginine-rich bridge, PAM interacting, HNH and Ruv C domains. The Rec I and REC II domains have role in the interaction with gRNA. The role of the arginine-rich bridge is critical for gNRA:DNA recognition. The PAM interaction domain recognizes the PAM sequence and binds to the target DNA. From 3-4 base pairs upstream of the PAM sequence, Cas9 generates a DSB with its Ruv C and HNH domains (126). After induced DSB by nucleases is repaired with two DNA repair systems, HDR and NHEJ. HDR mechanism, which uses a homologous donor DNA template, is used to introduce specific sequence into target region or to introduce mutations into target region in the genome. NHEJ is more prone to error when IN-DEL is generated during the repair process. IN-DEL causes frameshift mutation or formation of early stop codon. This is very useful for gene knockout experiments using the CRISPR/Cas9 system (127).

CRISPR/Cas9 system is also used to regulate gene expression. Dead Cas9 (dCas9), which contains inactive RuvC and HNH nuclease domains, is used for gene expression regulation. For epigenetic reprogramming, dCas9 is used to activate or inhibit transcription of the target part of the genome (119,127,128). dCas9 has the ability to bind target site with complementary gRNA to target sequence. Transcriptional repressor protein such as Krüppel Associated Box (KRAB) is fused to dCas9. The dCas9-KRAB fusion has the ability to bind to the target DNA sequence so that inhibition of binding of DNA binding proteins such as transcription factors or DNA polymerase II to the target region causes transcriptional repression. Epigenetic reprogramming of dCas9-KRAB fusion decreases chromatin accessibility and increases H3 lysine 9 trimethylation (H3K9me3) at target gene promoter sites (119,128,129). Fusion of DNMT3A and MQ1, which induces promoter cytosine methylation, with dCas9 plays a role in transcriptional silencing (130,131). Another strategy for epigenetic reprogramming is the activation of the expression of genes. dCas9 is fused to a variety of transcriptional activators, such as Rta (VPR), P65 and VP64. Rta is transactivator of the Epstein-Barr virus. P65 is derived from the transcriptional activation domain of the mammalian transcription factor NF-κB. VP64 is an activator that is derived from the transactivation domain of the herpes

simplex virus. For transcriptional activators, there are many CRISPR activation systems such as SAM, SunTag and VPR. gRNA scaffold is modified with MS2 hairpin aptamers in some of the CRISPR activation system. Activators interact and localize to the target locus to activate gene expression with the gRNA-MS2 scaffold (119,128,132,133). The fusion of p300, which is a component of histone acetylation, with dCas9 induces the expression of genes. Fusion of TET1, which induces promoter cytosine demethylation, with dCas9 is involved in activating genes (134,135).

The CRISPR/Cas9 system is also used for studying base editing. The base editing system is composed of two components: gRNA and Cas9 nickase (nCas9) fused to a deaminase. gRNA directs base editors to a specific locus. Base editors change one base to another within a small editing window near the PAM. Cytidine (C) is converted to uridine (U) by cytosine base editors (CBEs). Base excision repair converts uridine to thymidine (T). On the other hand, A-T base pair is converted to G-C base pair by adenine base editors (ABEs). Therefore, scientists use ABEs and CBEs base editors to convert “C” to “T”, “A” to “G”, “T” to “C” and “G” to “A”. Base editing technology may use to treat genetic diseases associated with single nucleotide changes such as point mutations or single nucleotide polymorphisms (SNPs) (128,136).

Another application of the CRISPR/Cas9 system is prime editing. The reverse transcriptase enzyme is fused to nCas9. gRNA is replaced by prime editing gRNA (pegRNA) which contains desired edits on RT template with primer binding site (PBS). Desired deletions, insertions and possible base-to-base conversions are introduced by transcriptase enzyme using pegRNA. pegRNA recognizes target region and directs the nCas9 to the target sequence. nCas9 generates 3’ flap in the non-target strand. Primer binding site (PBS) of the pegRNA interacts with the 3' flap. The desired modification is incorporated into the DNA by reverse transcription. In

prime editing technology, the desired DNA sequence is placed into the target region without the use of donor DNA template (128,136,137).

Gene editing tools based on RNA-targeting nuclease has been popular for editing RNA rather than permanently editing the DNA. lt is possible to perform RNA editing by using CRISPR/Cas system. RNA-based CRISPR/Cas editing system uses the Cas13 and CRISPR RNA (crRNA), which targets RNA. Cas13 enzymes contains two higher eukaryotes and prokaryotes nucleotide-binding (HEPN) domains. Cas13 enzyme cleaves target RNA by recognizing protospacer flanking sites (PFSs). There are three Cas13 proteins; Cas13a, Cas13b, and Cas13c. Cas13a enzyme is adapted to use for nucleic acid detection, RNA knockdown and transcript tracking in plants and mammals. For Cas13a, the biochemical (PFS) is not required to interference of the RNA (138,139,140). Mutations on the HEPN domains lead to a catalytically inactive Cas13, but the ability of the Cas13 to bind to the target RNA is preserved. There are two types of CRISPR/Cas based RNA base editors: REPAIR and RESCUE. Catalytically inactive dCas13 is fused with adenosine deaminase ADAR2 to form REPAIR (RNA editing for programmable A to I replacement), which converts adenosine to inosine in targeted ssRNA. Inosine is read as guanine (G) during translation and splicing. Therefore, this conversion is crucial for the correction of G-A mutations. In RESCUE, catalytically inactive dCas13 is fused with ADAR2dd cytidine deaminase to form RESCUE (RNA editing for specific C to U exchange) (138,139,141,142). RNA base editors are also used for targeting the sites of post-translational modifications such as methylation, acetylation, phosphorylation and glycosylation. In RNA methylation (TRM) system, dCas13 is fused with methyltransferase such as METTL3 and/or METTL14 for site-specific methylation of transcripts and alteration of alternative splicing patterns. The dCas13-ALKBH5 fusion protein plays a role in the demethylation of RNA from a specific target site. dCas13-based RNA imaging is a useful method that can be developed for cancer research to identify the subcellular localization of RNAs in order to understand RNA function. dCas13-based RNA imaging strategy allows live-cell imaging of RNAs. dCas13 RNA imaging does not cause any genetic alterations. In RNA tracking

methods, dCas9 can be fused with crRNA to detect target RNA and fluorescent tag such as GFP or mCherry for imaging (138,139,143).

3. MATERIALS AND METHODS

3.1. Materials

3.1.1. Chemicals

All the chemicals used in this thesis are listed in Appendix A.

3.1.2. Growth Media

Luria Broth (LB)

20 g LB powder was dissolved in 1L ddH_2O. Solution was autoclaved at 121°C for 15 min and stored at room temperature (RT).

LB Agar

20 g LB powder and 15 g agar powder were dissolved in 1L ddH_2O. Solution was autoclaved at 121°C for 15 min. After cooling down to RT, for Ampicillin containing LB Agar plates were divided into bacterial culture petri dishes and agar plates were stored at + 4 °C.

87% Bacterial Glycerol Stock

885 µL of overnight cultured bacterial suspension was mixed with 115 µL of sterile 87% glycerol and glycerol stock was kept in -80 °C.

Complete High Glucose Commercial Dulbecco's Modified Eagle Medium (cDMEM)

Gibco High Glucose DMEM was mixed with 10 % FBS, Gibco and 1% Penicillin-Streptomycin, Gibco (Pen-Strep). cDMEM was preserved at 4°C.

Freezing Medium for Mammalian Cells

10% DMSO in FBS was prepared and filter sterilized. FM was aliquoted and stored at – 20 °C.

3.1.3. Buffers and Solutions

1X PBS

1X PBS was prepared from 2 tablet in 100 mL ddH_2O.

Ampicillin Stock Solution (100 mg/ mL)

1 g ampicillin salt was dissolved in 10 mL ddH_2O, then solution was filter sterilized and stored at – 20 °C.

$CaCl_2$ Working Solution

86 mL 87% glycerol, 15 mL 2 M $CaCl_2$ and 10 mL 0.5 M PIPES (pH 7.00) were dissolved in ddH_2O and final volume was adjusted up to 500 mL. Prepared solution was filter sterilized and stored at 4 °C.

Alkaline Lysis Solution I

Final concentrations of 50 mM glucose, 25 mM Tris-Cl (pH 8.00) and 10 mM EDTA (pH 8.00) were mixed in 100 mL ddH_2O. Solution was filter sterilized.

Alkaline Lysis Solution II

Final concentrations of 0.2 N NaOH and 1% (w/v) SDS were mixed and final volume was adjusted up to 10 mL with ddH_2O. Solution was stored at RT and freshly used.

Alkaline Lysis Solution III

60 mL 5 M potassium acetate and 11.5 mL glacial acetic acid were mixed. Final volume was adjusted up to 100 mL with ddH_2O and solution was stored at +4 °C.

Tail Lysis Buffer

5 mL 1 M Tris-HCl (pH 8.00), 10 mL 5 M NaCl, 10 mL 0.5 M EDTA (pH 8.00) and 25 mL 10% SDS were mixed in ddH_2O and final volume was adjusted to 500 mL. Solution was kept at RT.

50X TAE Buffer

242 g tris base, 57.1 mL glacial acetic acid and 100 mL of 0.5 M EDTA (pH 8.00) were mixed. Final volume was adjusted with ddH_2O.

Agarose Gel Electrophesis

For 1% w/v agarose gel preparation, 1 g of agarose was dissolved in 100 mL 1X TAE buffer by heating in microwave. 0.002 % ethidium bromide was added to the solution.

SDS Separating Gel (13%)

3 mL ddH_2O, 2.5 mL Tris 1.5 M,pH:8.8, 100 µL 10% SDS, 4.34 mL Acrylamide: Bisacrylamide (30%) ,100 µL 10% APS and 10 µL TEMED were mixed.

SDS Stacking Gel (4%)

2.70 mL ddH_2O, 1.25 mL Tris 0.5 M,pH:6.8 , 50 µL 10% SDS, 1 mL Acrylamide: Bisacrylamide (30%), 15 µL 10% APS and 7.5 µL TEMED were mixed.

3X Laemmli Buffer

For preparation of 3X Laemmli Buffer, 8.75 mL Tris 0.5 M at pH:6.8, 8.62 mL 87% glycerol, 3.75 mL 20% SDS, 3.75 mL β-mercaptoethanol, 0.13 mL ddH_2O and 7.5 mg bromophenol blue was mixed and aliquoted. For long term storage, the aliquots were stored at -20 °C.

10X Tris-Glycine Buffer

40 g tris base and 144 g glycine were dissolved in ddH_2O and then pH was adjusted to 8.3 with 37% HCl. Buffer volume was completed to 1L.

1X Running Buffer

100 mL 10X Tris-Glycine buffer and 5 mL 20% SDS solution were mixed and adjusted to 1L with ddH_2O.

1X Transfer Buffer

100 mL 10x Tris-Glycine buffer, 200 mL methanol and 1.8 mL 20 %SDS were mixed and adjusted to 1L with ddH_2O.

1X PBS-T

A final concentration of 0.05% Tween-20 was prepared in 1X PBS.

Red Solution

0.05 % PBS- T ,15 g 5% BSA, 0.06 gram 0.02 % NaN_3 and 20 mg phenol red were mixed up. Red solution was stored at 4°C.

3.1.4. Commercial Kits

For midiprep plasmid DNA isolation, QIAGEN PureLink® HiPure Plasmid Midi Kit, QIAGEN, Germany was used. For PCR purification, PureLink™ PCR Purification Kit, Invitrogen, #K310001 was used.

3.1.5. Enzymes

The brand of restriction enzymes and their reaction buffers used in this thesis is New England Biolabs (NEB). The brand of polymerase enzyme and their reaction buffer used in this thesis is Meridian Bioscience Bioline.

3.1.6. Plasmids Maps

Plasmids used in this thesis are listed in Table 3.1.

Table 3.1 Plasmids used in this thesis

Plasmid Name	Use	Resistance Marker	Source
pcDNA-GFP	Transfection Control	Ampicillin for *E.coli*	Gift from Prof. Dr. M. Batu Erman
pSp-Cas9(BB)-2A-Puro (PX459) V2.0	CRISPR/Cas9 Cloning	Ampicillin for *E.coli* Puromycin for Mammalian Cells	Addgene plasmid # 62988 (92)

3.1.7. Oligonucleotides and Primers

Oligonuclotides and primers used in this thesis are listed in Table 3.2, Table 3.3 and Table 3.4.

Table 3.2 Oligonucleotides used in this thesis. The sequences of top and bottom oligonucleotides for each gRNA candidate and non-targeting control gRNAs are shown in the following table. The DNA sequences indicated with red color in the top and bottom oligonucleotides are required for cloning.

A top	CACCGCGTCGAGCCCCCTCTGAGTC
A bottom	AAACGACTCAGAGGGGGCTCGACGC
B top	CACCGCCATTGTTCAATATCGTCCG
B bottom	AAACCGGACGATATTGAACAATGGC
C top	CACCGCGCTATCTGAGCAGCGCTCA
C bottom	AAACTGAGCGCTGCTCAGATAGCGC
D top	CACCGGTTGATTCCACACCCCCGCC
D bottom	AAACGGCGGGGGTGTGGAATCAACC
NT-C1 top	CACCGCTGAAAAAGGAAGGAGTTGA
NT-C1 bottom	AAACTCAACTCCTTCCTTTTTCAGC
NT-C2 top	CACCGAAGATGAAAGGAAAGGCGTT
NT-C2 bottom	AAACAACGCCTTTCCTTTCATCTTC

Table 3.3 Upstream target region and downstream target region primers used in this thesis

Primers For Genotyping (5'-3')	
Upstream_Target_Region_A_Fwd	GAAGGGAGTTGGGAATAGGG
Upstream_Target_Region_A_Rev	GGGGACTGTAGATGGGTGAA
Upstream_Target_Region_B_Fwd	ACTTTCTGCTCTTGTCTTTC
Upstream_Target_Region_B_Rev	GGTGTGATGGGATGGATAAA
Downstream_Target_Region_Fwd	TATCCATCCCATCACACCCTC
Downstream_Target_Region_Rev	CCAAATACTCCACACGCAAA

Table 3.4 Off-target primers used in this thesis

Primer Name	Primer Sequences
CRISPR_A_Off_Target_fwd	GAATATTCACAGGATGGGCC
CRISPR_A_Off_Target_rev	CTACGCCTGCCTTAAATACC
CRISPR_C_Off_Target_fwd	AGCAACAGAAAGGAAACGAG
CRISPR_C_Off_Target_rev	AAACCCCACATCCTAACTCA

3.1.8. DNA and Protein Molecular Weight Markers

DNA and protein molecular weight markers used in this thesis are listed in Appendix B.

3.1.9. Softwares and Programs

Softwares and programs used in this thesis are listed in Table 3.5.

Table 3.5 Softwares used in this thesis

Program Name	**Use**
CLC Main Workbench (Qiagen)	Alignments
Image J	Analyze scratch assay
Image Lab Software (BioRad)	Analyze and view agarose gel and membrane images
Zeiss ZEN Microscopy Software	Analyze and view fluorescence microscope image
GraphPad	Bioinformatic and statistics analysis

3.1.10. Equipments

All the equipments used in this thesis are listed in Appendix C.

3.2. Methods

3.2.1. gRNA Design

In order to create *TP53* knockout U87-MG cell line, two target regions were determined as upstream and downstream target regions in the *TP53* gene locus (Figure 3.1) Considering these target regions, four gRNA candidates (gRNA A, B, C and D) were designed by using CRISPOR tefor tool (http://crispor.tefor.net/) (144). gRNA A and B were designed to target the upstream target region whereas gRNA C and D were designed to target the downstream target region as shown in Figure 3.1. In addition, two non-targeting gRNAs (gRNA NT-C1 and NT-C2), which do not target anywhere in the genome, were planned to use as negative controls of the further experiments. The gRNA target sequences, PAM sequences, strand information, restriction site to be expected to be destroyed and the target exon in the *TP53* gene locus were shown in Table 3.6. After determination of individual efficiencies of the gRNA candidates, the best pair was planned to be selected for further deletion of the DNA sequence in between the upstream and downstream target regions. As a result of this deletion in the *TP53* gene locus, p53 protein expression was not expected to be seen.

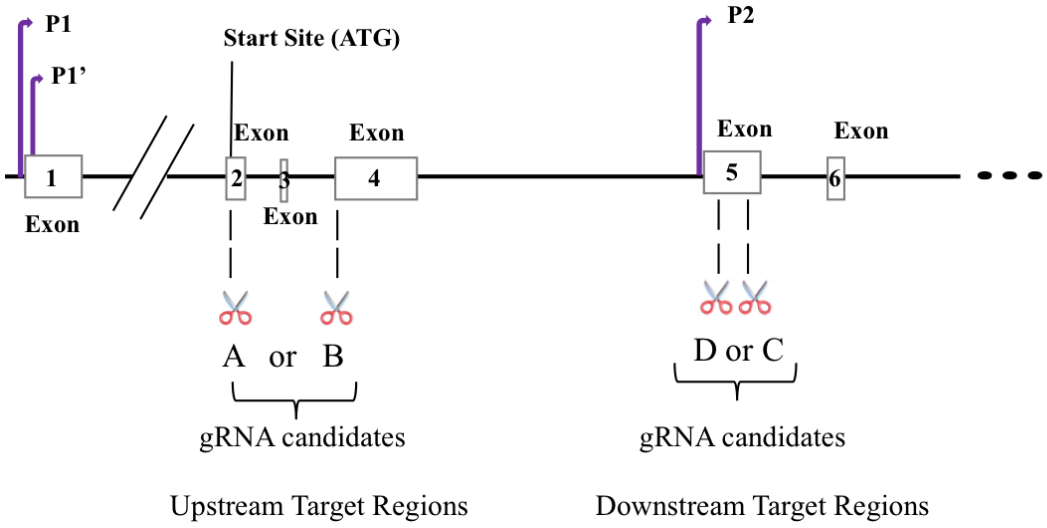

Figure 3.1 Schematic representation of the upstream and downstream target regions in the *TP53* gene locus. The rectangles illustrate the exons, the regions in between the rectangles illustrate the introns and the dashed line at the end illustrates the rest of the genomic locus. The purple arrows represent the promoters.

Table 3.6 gRNA candidates and non-targeting control gRNAs used in this thesis. This table shows gRNA candidates and non-targeting control gRNAs target sequences, target regions, their PAM sequences, their strand positions, their restriction sites expected to be destroyed and their target exons in the *TP53* gene locus.

		gRNA Target Sequence	PAM	+/- Strand	Restriction Site Expected To Be Destroyed	Target Exon In The *TP53* Gene Locus
Upstream Target Region	gRNA A	CGTCGAGCCCCCTCTGAGTC	AGG	+	HinfI	Exon2
	gRNA B	CCATTGTTCAATATCGTCCG	GGG	-	NciI	Exon4
Downstream Target Region	gRNA C	CGCTATCTGAGCAGCGCTCA	TGG	-	Aor51HI	Exon5
	gRNA D	GTTGATTCCACACCCCCGCC	CGG	+	HinfI	Exon5
NT-C1gRNA		CTGAAAAAGGAAGGAGTTGA	Non-targeting Control1			
NT-C2 gRNA		AAGATGAAAGGAAAGGCGTT	Non-targeting Control2			

3.2.2. Construction of CRISPR/Cas9 Plasmids

For construction of CRISPR/Cas9 plasmids, the protocol of Ran et. al. 2013 was followed (145).

3.2.2.1.Oligo Annealing

Top and bottom oligonucleotides of gRNA candidates (A, B, C and D) and non-targeting controls (NT-C1 and NT-C2) were annealed individually. The annealing reaction components and conditions are shown in Table 3.7 and Table 3.8, respectively.

Table 3.7 Oligo annealing reaction components

Components	Amounts
Top Oligo (100 µM)	1 µL
Bottom Oligo (100 µM)	1 µL
T4 DNA Ligase Buffer (10X)	1 µL
T4 PNK (10 U/µL)	1 µL
ddH_2O	6 µL
Total	10 µL

Table 3.8 Oligo annealing reaction conditions

Temperature	Time
37 °C	30 min
95 °C	5 min
95 °C to 25 °C	Ramp down (-5°C/min)
4 °C	∞

3.2.2.2. Diagnostic Digestion of pSp-Cas9(BB)-2A-Puro (PX459) V2.0 Plasmid

pSp-Cas9(BB)-2A-Puro (PX459) V2.0 plasmid was purchased from Addgene as *E.coli* bacterial stab. The bacteria were streaked on LB agar plates. Then, bacteria were incubated for 16 h at 37 °C. One single colony was picked and grown inside of 3 mL LB containing Ampicillin for 16 h at 37 °C for midiprep plasmid isolation. Plasmid was isolated with PureLink® HiPure Midiprep Plasmid DNA Purification Kit using manufacturer's protocol. Isolated plasmid DNA was with PstI, EcoRI, EcoRV, NotI, BgII and SacI restriction enzymes and the protocol is shown in Table 3.9. Digestion reaction conditions are shown in Table 3.10.

Table 3.9 Diagnostic digestion reaction components

Components	**Amounts**
pSp-Cas9(BB)-2A-Puro (PX459) V2.0 plasmid (0.5 µg/ µL)	1 µL
Compatible Buffer (10X)	2 µL
Restriction Enzymes (10 U/mL)	0.5 µL
ddH_2O	16.5 µL
Total	20 µL

Table 3.10 Diagnostic digestion reaction conditions

Temperature	**Time**
37 °C	2 h
4 °C	∞

3.2.2.3.Ligation of Annealed Oligonucleotides into pSp-Cas9(BB)-2A-Puro (PX459) V2.0 Plasmid

Annealed oligonucleotides were cloned into pSp-Cas9(BB)-2A-Puro (PX459) V2.0 plasmid by using BbsI restriction sites. The reaction components are shown in Table 3.11 and the reaction conditions are shown in Table 3.12

Table 3.11 Ligation reaction components

Components	Amounts
pSp-Cas9(BB)-2A-Puro (PX459) V2.0 (100 ng/µL)	1 µL
Annealed oligos (1:200 diluted)	2 µL
ATP (10 mM)	2 µL
BbsI HF (20 U/µL)	1 µL
r-CutSmart Buffer (10X)	2 µL
T4 DNA Ligase (400 U/µL)	0.5 µL
ddH_2O	11.5 µL
Total	20 µL

Table 3.12 Ligation reaction conditions

Temperature	Time	
37°C	5 min	10X Cycles
21°C	5 min	
4 °C	∞	

3.2.2.4.Exonuclease V Treatment

After ligation of the CRISPR constructs, samples were treated with Exonuclease V. The treatment components and conditions are shown in Table 3.13 and 3.14, respectively.

Table 3.13 Exonuclase V treatment components

Components	**Amounts**
Ligation Reaction	11 µL
ATP (10 mM)	1.5 µL
NEB Buffer 4 (10X)	1.5 µL
Exonuclease V (RecBCD) (10U/µL)	1 µL
Total	15 µL

Table 3.14 Exonuclase V treatment conditions

Temperature	**Time**
37°C	30 min
4 °C	∞

To avoid excess degradation, after 30 min of Exonuclease V treatment, the activity of the enzyme was inhibited. The components and the conditions of Exonuclase V enzyme inhibition reaction are shown in Table 3.15 and Table 3.16, respectively.

Table 3.15 Exonuclase V reaction inhibition components

Components	Amounts
ExoV Treated Sample	15 µL
EDTA (110 mM)	2 µL
ddH_2O	3 µL
Total	20 µL

Table 3.16 Exonuclase V reaction inhibition conditions

Temperature	Time
70°C	30 min
4 °C	∞

3.2.2.5.Preparation of Chemically Competent DH5α Bacterial Cells

Competent cell stock was streaked on LB Agar plates and incubated for 16 h at 37 °C. Next day, a single colony was picked and incubated in 50 mL LB at 220 rpm for 16 h at 37 °C. After 16 h, 4 mL of the overnight grown bacterial culture was diluted in 400 mL LB a 2- L flask. Bacterial culture was incubated at 220 rpm for 1.5-2 h at 37 °C until OD590 (Optical Density at 590 nm) was 0.375. Culture was transferred into 50 mL microcentrifuge tubes and leaved on ice for 8-10 min. Then, the culture was centrifuged at 1600 g for 10 min at 4°C. Supernatants were discarded. Pellets were resuspended in 10 mL ice-cold $CaCl_2$ and centrifuged at 1100 g for 5 min at 4°C. Supernatants were discarded and pellets were resuspended in 10 mL ice-cold $CaCl_2$. Resuspended cells were incubated on ice for 30 min. Cells were centrifuged at 1100 g for 5 min at 4°C. Supernatants were discarded and pellets were

resuspended in 2 mL ice-cold $CaCl_2$ solution. All the resuspensions (in total 16 mL) were pooled in a 50 mL microcentrifuge tube. Then, competent cells were aliquoted as 200 µL in of 1.5 mL pre-chilled microcentrifuge tubes and snap frozen in liquid nitrogen. Cells were stored at -80°C.

3.2.2.6.Transformation of the CRISPR Plasmid Constructs into *E. coli* DH5α Competent Cells

Chemically competent *E.coli* DH5α cells were thawed on ice for transformation of ligated CRISPR plasmid constructs that were explained in section 3.2.2.3 and 3.2.2.4. 10 µL of the reaction was mixed with competent cells and incubated on ice for 30 min. Then, cells were heat-shocked for 90 s at 42°C and then incubated on ice for 1 min. 800 µL LB was added and incubated at 37 °C for 45 min. Then, cells were centrifuged at 13.000 rpm for 1 min at RT. 900 µL of the supernatants were discarded and pellets were resuspended with 100 µL leftover LB. Then, 100 µL cell suspension was spread onto pre-warmed LB agar with 100 µg/mL Ampicillin. Plates were incubated at 37 °C for 16 h.

3.2.2.7.Miniprep DNA Isolation with Alkaline Lysis Protocol

After transformation, for each cloning ten single bacterial colonies were picked and inoculated in 3mL LB at 220 rpm for 16 h at 37 °C. The overnight grown bacterial cultures were centrifuged at 13.000 rpm for 5 min at 4 °C. Supernatants were discarded. The pellets were resuspended in 100 µL pre-chilled Alkaline Lysis Solution I. Then, 200 µL freshly prepared Alkaline Lysis Solution II was added and

the mixture was inverted 4-6 times. Samples were incubated for 5 min at RT. 150 µL freshly prepared Alkaline Lysis Solution III was added and the mixture was inverted 4-6 times. Samples were incubated for 5 min on ice then centrifuged at max speed for 5 min at 4°C. After centrifugation, the 450 µL supernatants were transferred to clean tubes and 900 µL absolute EtOH was added. After inverting 4-6 times, the samples were centrifuged at 13.000 rpm for 5 min at 4°C. 1mL 70% EtOH was added and the pellets were washed via inverting the tube 4-6 times. Samples were then centrifuged at 13.000 rpm for 5 min at 4°C. After discarding the supernatants, pellets were air dried. Then, DNA was dissolved in 50 µL TE with 20 µg/mL RNaseA. For long-term storage, the DNA samples were stored at -20 °C.

3.2.2.8.Confirmation of CRISPR Cloning with PCR

In order to confirm the presence of the inserts (annealed oligonucleotides for each gRNA candidates and the non-targeting gRNAs) in the cloned plasmids, the screening of the cloned CRISPR plasmids was performed by performing PCR. For PCR amplification, hU6fwd-[(5'GAGGGCCTATTTCCCATGATT-3')] primer was used as forward primer, and as reverse primer, bottom oligonucleotides specific to each different gRNA candidate and non-targeting control gRNAs were used. Other contents of the PCR reactions are shown in Table 3.17. The optimized PCR reaction conditions for these screens are shown in Table 3.18.

Table 3.17 PCR components for confirmation of CRISPR cloning

Components	Amounts
MyTaq Buffer (5X)	5 µL
Template DNA (1 ng/ µL)	1 µL
hU6 Forward Primer (5 µM)	1 µL
Reverse Primer (5 µM)	1 µL
MyTaq Polymerase (5U/µL)	0.125 µL
ddH_2O	16.875 µL
Total	25 µL

Table 3.18 PCR conditions for confirmation of CRISPR cloning

	Temperature	Time	
Initial Denaturation	95 °C	1 min	
Denaturation	95 °C	15 s	30X Cycles
Annealing	55 °C	15 s	
Extension	72 °C	6 s	
Hold	4 °C	∞	

The PCR products were run in 1% agarose gel stained with EtBr and visualized under UV light using BioRad ChemiDoc MP Imaging System.

3.2.2.9.Sanger Sequencing of the Cloned CRISPR Plasmids

In order to confirm the sequences of the cloned CRISPR plasmids, isolated plasmid DNAs were sequenced with hU6 forward primer in MEDSANTEK (http://www .medsantek.com.tr/). Analysis of Sanger sequencing was performed with CLC Main Workbench by comparison of sequencing results with hypothetical sequences of the cloned CRISPR plasmids

3.2.2.10. Midiprep Plasmid DNA Isolation for Cloned CRISPR Plasmids

In order to obtain pure and concentrated DNA, midiprep plasmid DNA isolations were performed with PureLink® HiPure Midiprep Plasmid DNA Purification Kit (#K210005) according to the manufacturers' protocol. Concentration and purity of midiprep plasmid DNAs were determined with NanoDrop One^{C} Microvolume UV-Vis Spectrophotometer.

3.2.3. Mammalian Cell Culture

3.2.3.1. U87-MG Cell Line Thawing, Maintenance and Cryopreservation

U87-MG cell line was purchased from ATCC. The first vial was thawed in 10 mL cDMEM. The cells were seeded in a T75 cell culture flask and incubated at 37°C and 5% CO_2. For maintenance of these cells, when the confluency reached to 60-70%, the cells were subcultured at a ratio of 1:3 or 1:5. For subculturing, the medium was aspirated and after washing with 1X DPBS for 2 times, the cells were incubated with Trypsin-EDTA (0.05%) at 37 °C for 5 min and collected in cDMEM. Cells are

centrifuged at 100 g for 10 min. After centrifugation, supernatant was discarded. Cells were resuspended in cDMEM. Cells were subcultured at a ratio of 1:3 or 1:5 to T75 flask.

When the cells needed to be cryopreserved to maintain stocks for further experiments, this protocol was applied. When the cells had a confluency of 60-70% confluency, medium was aspirated. After washing 2 times with 1X DPBS, the cells were incubated with Trypsin-EDTA (0.05%) at 37 °C for 5 min and collected in cDMEM. After centrifugation at 100 g for 10 min, the supernatant was aspirated. The cell pellet was resuspended in freezing medium in cryopreservation tubes and placed in Mr. Frosty Freezing Container at -80 °C. After 24h, the cells were transferred to liquid nitrogen for further storage.

3.2.3.2.Puromycin Concentration Determination

$1x10^5$ U87-MG cells were seeded to each well of 6-well plate. After 24h, the growth medium of the cells was replaced with complete DMEM containing 0.1 µg/mL, 0.25 µg/mL, 0.5 µg/mL, 1 µg/mL, 2 µg/mL, 3 µg/mL, 4 µg/mL and 5 µg/mL puromycin. Every three days, medium of the cells was changed with freshly prepared Puromycin containing medium. 1 weeks later, cells were collected, stained with Trypan Blue and the live cells were counted with hemocytometer. Cell viability was calculated with [Cell viability % = (Live cell number of treated sample/Live cell number of untreated control) x 100] formula.

3.2.4. Small-Scale Transfections

3.2.4.1. Microscopy and Flow Cytometry Analyses of Small-Scale Transfection Optimization

For small-scale transfection optimizations, three different pcDNAGFP: Lipofectamine 3000 ratios (1:1.5,1:3,1:5) were tested. $3x10^5$ cells/well were seeded in a well of 6-well plate. Next day, 2.5 μg pcDNA-GFP plasmid, different amounts of Lipofectamine 3000 (3.75 μL, 7.5 μL and 12.5 μL) and 5uL transfection enhancer were mixed in Opti-MEM. Mixtures were incubated for 20 min at RT. After incubation, mixtures were added onto cells drop by drop. Then, cells were incubated at 37°C and 5% CO_2. 16 h after transfection, the medium of the transfected cells were replaced with fresh cDMEM. 48 h after transfection, GFP positive cells were visualized under FITC channel of ZEISS Axio Vert.A1 inverted fluorescent microscope. For flow cytometry analysis, the following protocol was applied. The medium was aspirated and after washing with 1X DPBS for 2 times, the cells were incubated with Trypsin-EDTA (0.05%) at 37 °C for 5 min and collected in cDMEM. Cells were centrifuged at 100 g for 10 min. After centrifugation, supernatant was discarded. Cell pellets are washed in 500 μL 1X DPBS and centrifuged at 100 g for 10 min. Supernatants were aspirated. The cell pellets were resuspended in 500 μL 1X DPBS and samples were acquired by BD FACSVerse™ to quantify the cell viability with FSC vs SSC dot plots and GFP positive cell percentage with FITC histograms.

3.2.4.2. Small-Scale Transfections of CRISPR Plasmids

After determination of the optimum ratio of DNA:Lipofectamine 3000 for small-scale transfection, U87-MG cells were transfected individually with the cloned

CRISPR plasmids targeting the upstream or downstream regions (CRISPR A, B, C and D) and non-targeting CRISPR plasmids (CRISPR NT-C1 and NT-C2). In these transfections, DNA:Lipofectamine 3000 ratio was used as 1:3. $3x10^5$ cells/well were seeded one day before the experiment. For each CRISPR transfection, 2.5µg DNA, 7.5µL Lipofectamine 3000 and 5µL transfection enhancer were mixed and incubated at RT for 20 min. Then, each mixture was added drop by drop to medium of the seeded cells. 48h after transfection, 0.5 µg/mL Puromycin treatment was started. In every 3-4 days, 0.5 µg/mL Puromycin containing cDMEM was replaced with freshly prepared Puromycin cDMEM. After puromycin enrichment for 1 week, 2.5 $x10^5$ cells were collected for gDNA isolation.

3.2.4.3. Genomic DNA (gDNA) Isolation

After transfection and puromycin enrichment steps that are explained in section 3.2.4, from $2.5x10^5$ cells genomic DNA isolation was performed with Tail Lysis protocol. According to this protocol, lysis buffer was prepared with 10 µL Proteinase K (20 mg/mL) and 500 µL tail lysis buffer (prepared as described in 3.1.3). Cell pellets were resuspended with lysis buffer and incubated at 55°C for 90 min. After incubation, 250 µL 5 M NaCl was added to samples and inverted 20 times. Samples were incubated on ice for 10 min and centrifuged at 3.000 rpm for 60 min at 4 °C. After centrifugation, supernatants were transferred into new tubes. 650 µL isopropanol was added and inverted until it becomes homogenous. Samples were incubated at RT for 15 min and centrifuged at 13.000 rpm for 10 min. Supernatants were discarded. Pellets were washed with 1 mL absolute EtOH and centrifuged at max speed for 10 min. Supernatants were discarded. After discarding the supernatants, pellets were air dried. Then, DNA was dissolved in 200 µL TE with 20 µg/mL RNaseA. DNA samples were stored at 4°C.

3.2.4.4. PCR Amplification of the CRISPR Target Regions

After gDNA isolation, the specific target regions of CRISPR A, B, C and D were PCR amplified with specific primers shown in Table 3.3. PCR components and conditions for amplification of the target regions are shown in Table 3.19 and Table 3.20.

Table 3.19 PCR components for amplification of the target regions

Components	**Amounts**
MyTaq Buffer (5X)	5 µL
Template DNA	1 µL
Forward Primer (5 µM)	1 µL
Reverse Primer (5 µM)	1 µL
MyTaq Polymerase (5U/µL)	0.125 µL
ddH_2O	16.875 µL
Total	25 µL

Table 3.20 PCR conditions for amplification of the target regions

	Temperature	**Time**	
Initial Denaturation	95 °C	3 min	
Denaturation	95 °C	15 s	40X Cycles
Annealing	Variable	15 s	
Extension	72 °C	40 s	
Hold	4 °C	∞	

The annealing temperatures were determined as 60 °C, 52°C and 50°C for amplification of upstream target region A, upstream target region B and downstream target region, respectively. In order to see the specificity of the PCR products, the samples were run in 1% agarose gel stained with EtBr and visualized under UV light using BioRad ChemiDoc MP Imaging System.

3.2.4.5.Restriction Fragment Length Polymorphism (RFLP) Assay

After PCR amplification of the specific target regions, individual editing performances of CRISPR candidates were determined by RFLP assay as described in Table 3.21. RFLP assay conditions were shown in Table 3.22.

As a result of CRISPR A activity, HinfI restriction site was expected to be destroyed in upstream target region A (figure 4.18, left panel). As a result of CRISPR B activity, NciI restriction site was expected to be destroyed in upstream target region B (figure 4.20, left panel). In downstream target region, Aor51HI (AfeI) restriction site was expected to be destroyed upon CRISPR C activity (figure 4.22, left panel). There are two Hinf I restriction sites in the downstream target region and only one of those sites was expected to be destroyed as a result of CRISPR D activity (figure 4.23, left panel). Therefore, in the RFLP assays, the PCR product of upstream target region A was digested with HinfI enzyme to show CRISPR A activity, the PCR product of upstream target region B was digested with NciI enzyme to show CRISPR B activity, the PCR product of downstream target region was digested with Aor51HI (AfeI) enzyme to show CRISPR C activity and the PCR product of downstream target region was digested with HinfI enzyme was used to show CRISPR D activity.

Table 3.21 Digestion components of RFLP assay

Components	Amounts
CutSmart Buffer (10X)	1.5 µL
PCR product	50 ng
Restriction Enzymes	0.5 µL
ddH_2O	up to 15 µL
Total	15 µL

Table 3.22 Digestion conditions of RFLP assay

Temperature	Time
37 °C	2 h
4 °C	∞

The digestion products were run in 2% agarose gel stained with EtBr and visualized under UV light using BioRad ChemiDoc MP Imaging System.

3.2.4.6.T7 Endonuclease I (T7EI) Assay

After the PCR amplification of upstream target region, A, upstream target region B and downstream target region, which was explained in section 3.2.4.4, T7EI assay was performed to analyze induvial editing performances of CRISPR A, B, C and D. T7EI reaction components and conditions are shown in Table 3.23 and Table 3.24, respectively.

Table 3.23 Components and conditions of denaturation and re-annealing steps of T7EI assay

Denaturation and re-annealing components	
Components	**Amounts**
NEB Buffer 2	1 µL
PCR product	50 ng
ddH_2O	up to 9.5 µL
Denaturation and re-annealing conditions	
95 °C	5 min
95- 85 °C	-2 °C/sec
85-25 °C	- 0.1 °C/sec
4°C	∞

Table 3.24 Components and conditions of T7EI digestion

T7EI digestion components	
Components	**Amounts**
Denatured and re-annealed PCR product mix (shown in table 3.23)	9.5 µL
T7 Endonuclease I	0.5 µL
T7EI digestion conditions	
37 °C	15 min
4°C	∞

The products of T7EI assay were run in 2% agarose gel stained with EtBr and visualized under UV light using BioRad ChemiDoc MP Imaging System.

3.2.5. Large- Scale Transfections

3.2.5.1. Microscopy and Flow Cytometry Analyses of Large-Scale Transfection Optimization

For large-scale transfection optimizations, two different pcDNAGFP: Lipofectamine 3000 ratios (1:1.5,1:3) were tested. $3x10^6$ cells/well were seeded in 100-mm cell culture dishes. Next day, 15 μg pcDNA-GFP plasmid, different amounts of Lipofectamine 3000 (22.5 μL, 45 μL) and 30 uL transfection enhancer were mixed in Opti-MEM. Mixtures were incubated for 20 min at RT. After incubation, mixtures were added onto cells drop by drop. Then, cells were incubated at 37°C and 5% CO_2. 16 h later after transfection, the medium of the transfected cells were replaced with fresh cDMEM. 48 h after transfection, GFP positive cells were visualized under FITC channel of ZEISS Axio Vert.A1 inverted fluorescent microscope. For flow cytometry analysis, the following protocol was applied. The medium was aspirated and after washing with 1X DPBS for 2 times, the cells were incubated with Trypsin-EDTA (0.05%) at 37 °C for 5 min and collected in cDMEM. Cells were centrifuged at 100 g for 10 min. After centrifugation, supernatant was discarded. Cell pellets were washed in 500 μL 1X DPBS and centrifuged at 100 g for 10 min. Supernatants were aspirated. The cell pellets were resuspended in 500 μL 1X DPBS and samples were acquired by BD FACSVerse™ to quantify the cell viability with FSC vs SSC dot plots and GFP positive cell percentage with FITC histograms.

3.2.5.2. Large-Scale Transfection of CRISPR Plasmids

After determination of the optimum DNA:Lipofectamine 3000 ratio for large-scale transfection, U87-MG cells were co-transfected with the cloned CRISPR plasmids targeting the upstream or downstream regions (CRISPR A, B, C and D). As, negative controls of the gene editing, non-targeting controls (CRISPR NT-C1 + CRISPR NT-C2) were also co-transfected to U87-MG cells. For the transfections of CRISPR pairs, $3x10^6$ cells/well were seeded to 100-mm cell culture dishes. The next day, 15 µg DNA, 45 µL Lipofectamine 3000 and 30 µL transfection enhancer were mixed in Opti- MEM and incubated at RT for 20 min. After the incubation, the mixture was added to the cells drop by drop. 16 h after the transfections, the medium of the cells were replaced by fresh cDMEM. 48h after the transfections, 0.5 µg/mL puromycin treatment was started. In every 3-4 days, 0.5 µg/mL puromycin containing cDMEM was refreshed. After 1 week of puromycin enrichment, from 2.5 $x10^5$ cells, genomic DNA isolation was performed as explained in section 3.2.4.3 and rest of the cells were cryopreserved for further experiments.

3.2.5.3. Genotyping of U87-MG Cell Pools Co-Transfected with CRISPR Pairs

CRISPR candidates targeting upstream target region (CRISPR A, CRISPR B) and downstream target region (CRISPR C, CRISPR D) were co-transfected. By using the gDNAs that were isolated from CRISPR pair co-transfected cell pools which was explained in section 3.2.4.3, the region between the upstream and downstream target regions were PCR amplified with Upstream_Target_ Region_A_ Fwd and Downstream_Target_Region_Rev primers. The PCR components and conditions are shown in Table 3.25 and Table 3.26, respectively.

Table 3.25 PCR components for genotyping

Components	Amounts
MyTaq Buffer (5X)	5 µL
Template DNA	1 µL
Forward Primer (5 µM)	1 µL
Reverse Primer (5 µM)	1 µL
MyTaq Polymerase (5U/µL)	0.125 µL
ddH_2O	16.875 µL
Total	25 µL

Table 3.26 PCR conditions for genotyping

	Temperature	Time	
Initial Denaturation	95 °C	3 min	
Denaturation	95 °C	15 s	40X Cycles
Annealing	57 °C	15 s	
Extension	72 °C	40 s	
Hold	4 °C	∞	

The PCR products were run in 1% agarose gel stained with EtBr and visualized under UV light using BioRad ChemiDoc MP Imaging System.

3.2.5.4.Single Cell Cloning of CRISPR A + CRISPR C Co-Transfected Cell Pool

Single cell cloning was performed from the CRISPR A + CRISPR C co-transfected cell pool. In 96-well plates, starting with 1000 cell/well concentration, serial dilutions were done until 1 cell/well concentration. The 96-well plates were incubated at 37ºC and 5% CO_2.In every 3-4 days, the growth medium was replaced with fresh cDMEM. Only one colony growing wells were further expanded to 24-well plate, 6-well plate and 100mm cell culture plates. For each single cell clone, gDNA was isolated as explained in section 3.2.4.3 and cryopreserved for further experiments.

3.2.5.5.Genotyping of the Single Cell Colonies Derived from CRISPR A + CRISPR C Co-transfected U87-MG Cell Pool

By using the gDNAs that were isolated from single cell colonies that were derived from CRISPR A + CRISPR C pair co-transfected cell pool, the region between the upstream and downstream target regions were PCR amplified with Upstream_ Target_Region_A_Fwd and Downstream_Target_Region_Rev primers. The PCR components and conditions are shown in Table 3.25 and Table 3.26, respectively. The PCR products were run in 1% agarose gel stained with EtBr and visualized under UV light using BioRad ChemiDoc MP Imaging System.

3.2.6. Sanger Sequencing of the Single Cell Colonies Showing $p53^{-/-}$ Profile

In order to confirm the specific deletion in the *TP53* gene locus, for the single cell clones showing $p53^{-/-}$ profile (colony 2, 16 and 17), the region between the upstream and downstream target regions were PCR amplified with Upstream_ Target_Region_A_Fwd and Downstream_Target_Region_Rev primers. After performing PCR purification with PureLink™ PCR Purification Kit according to manufacturer's protocol, the samples were sequenced by Sanger Sequencing in Medsantek Company. Sequencing results were analyzed by using CLC Main Workbench.

3.2.7. Control of Off-Target Effect in Single Cell Colonies Showing $p53^{-/-}$ Profile

In order to detect if there was an off-target effect due to CRISPR A or CRISPR C in the single cell colonies showing $p53^{-/-}$ profile (colony 2, 16, 17), T7EI assay was performed. For this purpose, by using the gDNAs of single colonies showing $p53^{-/-}$ profile (colony 2, 16, 17), to amplify CRISPR A Off_Target Site (the most possible off-target site for CRISPR A), PCR was carried out with CRISPR_A_Off_Target_fwd and CRISPR_A_Off_Target_rev primers and to amplify CRISPR C Off_Target Site (the most possible off-target site for CRISPR C) PCR was carried out with CRISPR_C_Off_Target_fwd and CRISPR_C_Off_ Target_rev primers. The Off-Target PCR components and conditions are show in Table 3.27 and Table 3.28, respectively.

Table 3.27 Off-target PCR components

Components	Amounts
MyTaq Buffer (5X)	5 µL
Template DNA	1 µL
Forward Primer (5 µM)	1 µL
Reverse Primer (5 µM)	1 µL
MyTaq Polymerase (5U/µL)	0.125 µL
ddH_2O	16.875 µL
Total	25 µL

Table 3.28 Off-target PCR conditions

	Temperature	Time	
Initial Denaturation	95 °C	3 min	
Denaturation	95 °C	15 s	40X Cycles
Annealing	58°C	15 s	
Extension	72 °C	40 s	
Hold	4 °C	∞	

By using PCR products of CRISPR A Off-Target and CRISPR C Off-Target, T7EI assay was carried out as described in section 3.2.4.6. The off-target PCR products were run in 2% agarose gel stained with EtBr and visualized under UV light using BioRad ChemiDoc MP Imaging System.

3.2.8. Western Blot

In order to control p53 protein expression, whole cell proteins were extracted from WT, CRISPR NT-C1+ CRISPR NT-C2 co-transfected cells, CRISPR A + CRISPR C co-transfected cells and single cell colonies showing the $p53^{-/-}$ profile colony 2, colony 16 and colony 17. Cells were collected after trypsinization and centrifuged at 1.000 rpm for 5 min at 4 °C. Supernatants were discarded. Cells were washed with 10 mL ice cold 1X DPBS. Cells were centrifuged at 1.000 rpm for 5 min at 4 °C. Supernatants were discarded. Pellets were resuspended with 1 mL ice cold 1X DPBS. Cells were centrifuged at 1.000 rpm for 5 min at 4 °C. Then, supernatants were discarded. Cells were resuspended with 250 µL cell lysis buffer + protease inhibitor and centrifuged at max speed for 15 min at 4°C. After centrifugation, lysates were collected into new tube and stored at -80 °C. Then, protein concentrations were quantified with Bradford assay (Serva #3922201) according to manufacturer's protocol.

The lysates were incubated in 1X Laemmli Buffer at 95°C for 10 min and then centrifuged at 14.000 rpm for 5 min at 4°C. From the supernatant, 50 µg protein samples were run in SDS gels composed of 4% stacking and 13% separating parts. The compositions of these parts were explained in section 3.1.3. The gels were run in 1X running buffer at 80 V for 2-2.5 h. After running, proteins were transferred to 0.45 µm PVDF membranes in 1X transfer buffer at 250 mA for 120 min at 4°C. Then, the membranes were blocked in 5% non-fat milk in PBS at RT for 1h with continuous shake. After blocking, membranes were washed 3 times with 15 mL PBS-T for 10 min. Primary antibodies (either anti-p53 antibody or anti-β-actin antibody) were diluted with a ratio of 1:1000 in red solution and the membranes were incubated with the primary antibody dilutions at 4°C for 16 h with continuous shake. After primary antibody incubation, membranes were washed 3 times with 15 mL PBS-T for 10 min. Secondary antibodies (either anti-mouse HRP antibody or anti-

rabbit HRP antibody) were diluted with a ratio of 1:10000 in 5% non-fat milk in PBS at RT for 1 h with continuous shake. After secondary antibody incubation, membranes were washed 3 times with 15 mL PBS-T for 10 min. Membranes were then incubated with chemiluminescent substrate at RT for 5 min and then visualized by using BioRad ChemiDoc MP Imaging System.

3.2.9. Trypan Blue Exclusion Assay

In order to assess the proliferation difference of U87-MG cells and U87-MG $p53^{-/-}$ cells, trypan blue exclusion assay was performed. Cells were kept at 37 °C with 5% CO_2. U87-MG cells and U87-MG $p53^{-/-}$ cells were seeded as 2.5 x 10^4 cell/well in 24-well plate and incubated at 37 °C with 5% CO_2. 24h, 48h, 72h, 96h and 120 h after seeding, the cells were trypsinized and collected. The cells were then stained with trypan blue and the live cells were counted. This experiment was performed with three replicates and repeated three times. The statistical analysis of the results was done with two-way ANOVA in GraphPad Prism.

3.2.10. Wound Healing Assay (Scratch Assay)

In order to compare the migration abilities of U87-MG cells and U87-MG $p53^{-/-}$ cells, wound healing assay was performed. U87-MG cells and U87-MG $p53^{-/-}$ cells were seeded as 8.5 x 10^4 cells/well in 24-well plates in cDMEM with 10%FBS. Cells were incubated at 37 °C with 5% CO_2. 24h after the seeding, for each well the wound area was created by scratching the middle of the wells with 200 μL tip. After the scratch, the medium was replaced with cDMEM containing 1%FBS. For the control groups, the medium was replaced with 10%FBS. In order to track the wound

closure, images of the wound area were taken with ZEISS Axio Vert.A1 inverted microscope at 0, 24, 48 and 72 h time points This experiment was performed with three replicates and repeated three times. The wound areas were quantified with MRI Wound Healing Tool- Image J macros. The percentage of the wound closure was calculated by this formula: Wound Closure % = $(1-(WA_t / WA_0)) X 100$. The statistical analysis of the results was performed with two-way ANOVA in GraphPad Prism.

3.2.11. Colony Formation Assay

In order to compare the colony formation abilities of U87-MG cells and U87-MG $p53^{-/-}$ cells, colony formation assay was performed. U87-MG cells and U87-MG $p53^{-/-}$ cells were seeded as 2 x 10^3 cells/well in 6-well plates in cDMEM. The cells were incubated at 37 °C with 5% CO_2 and every 3-4 days the growth medium was replaced with fresh cDMEM. After 20 days of incubation, the cells were washed 2 times with 1X DPBS and fixed with methanol for 20 min. After fixation, cells were washed 2 times with 1X DPBS and stained with 0.5% crystal violet solution at RT for 10 min. After the staining, the excess dye was removed and the wells were washed two times with dH_2O. Then, the plates were air-dried for 30 min. After taking the images of the well-plates, crystal violet was solubilized with 10 % acetic acid and the absorbance was measured at 590 nm by Thermo VarioSkan. This experiment was performed with three replicates and repeated three times. The statistical analysis of the results was performed with two sample student t-test in GraphPad Prism.

4. RESULTS

4.1. Cloning gRNA Candidates into pSp-Cas9(BB)-2A-Puro (PX459) V2.0 Plasmid

4.1.1. Diagnostic Digestion of the pSp-Cas9(BB)-2A-Puro (PX459) V2.0 Plasmid

For gRNA cloning, pSp-Cas9(BB)-2A-Puro (PX459) V2.0 plasmid (Addgene plasmid # 62988) was planned to use. Before cloning experiments, diagnostic digestions of the plasmid with different restrictions enzymes were performed. According to the plasmid map that is shown in Figure 4.1A. PstI, EcoRI, EcoRV, NotI, BglI, and SacI restriction sites were selected for further digestion reactions. The expected bands as the results of PstI, EcoRI, EcoRV, NotI, BglI, SacI single digestions and EcoRV+NotI double digestion were shown in Figure 4.1B and the results of these restriction digestion reactions were shown in Figure 4.1C. As it can be observed from Figure 4.1C, all the band sizes of the restriction enzyme digestion products were correct and matching with the expected band sizes.

A.

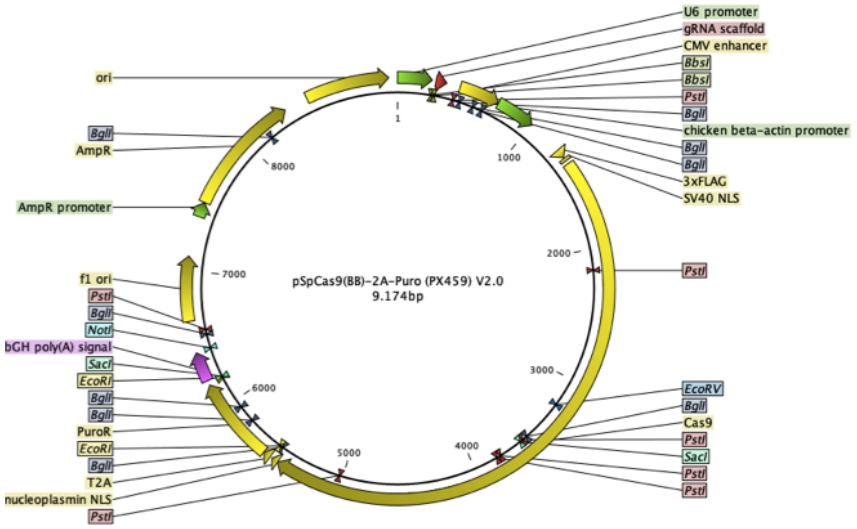

B.

Restriction Enzyme	Expected Bands
PstI	3016bp, 1743bp, 1547bp, 1422bp, 1212bp, 204bp, 30bp
EcoRI	8505bp, 669bp
EcoRV	9174bp (Linearization of the Plasmid)
NotI	9174bp (Linearization of the Plasmid)
EcoRV+NotI double digestion	5964bp, 3210bp
BglI	2901bp, 1956bp, 1625bp, 1480bp, 603bp, 303bp, 131bp, 104bp, 71bp
SacI	6576bp, 2598bp

C.

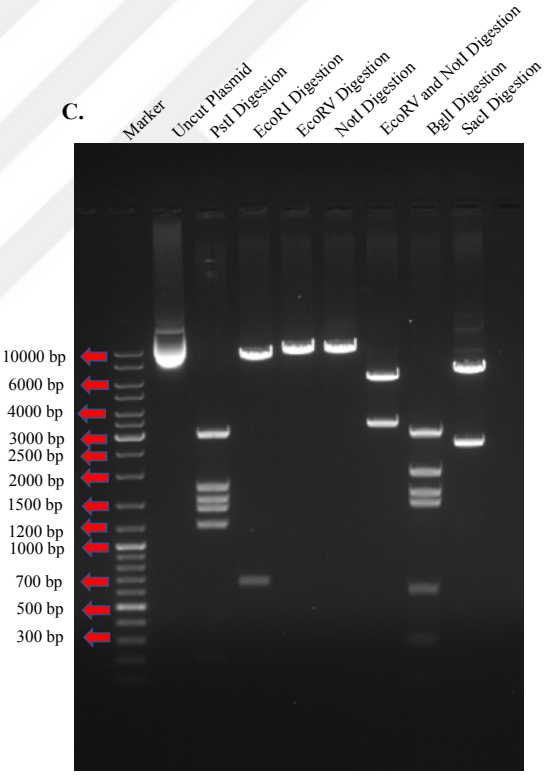

Figure 4.1 Diagnostic digestion of pSp-Cas9(BB)-2A-Puro (PX459) V2.0 plasmid with different restriction enzymes. **(A)** The map of pSp-Cas9(BB)-2A-Puro (PX459) V2.0 plasmid. **(B)** Expected band sizes after indicated restriction enzyme digestions. **(C)** The results of the restriction enzyme digestions. The restriction enzyme digestion products were loaded to 1% agarose gel and run at 120 V for 2 h. Sizes of some marker bands are indicated with arrows. Uncut plasmid lane shows the undigested pSp-Cas9(BB)-2A-Puro (PX459) V2 plasmid.

4.1.2. Oligonucleotide Annealing and Cloning into pSp-Cas9(BB)-2A-Puro (PX459) V2.0 Plasmid

In order to create U87-MG $p53^{-/-}$ cell line, two target regions were determined as upstream and downstream target regions in the *TP53* gene locus as shown in Figure 3.1. Considering these target regions, four gRNA candidates (gRNA A, B, C and D) were designed. gRNA A and B were designed to target the upstream target region whereas gRNA C and D were designed to target the downstream target region as shown in Figure 3.1. In addition, two non-targeting gRNAs (gRNA NT-C1 and NT-C2), which do not target anywhere in the genome, were planned to use as negative controls.

For each gRNA (A, B, C, D, NT-C1 and NT-C2), the top strand oligonucleotide (gRNA target sequence) and the bottom strand oligonucleotide (reverse complement of gRNA target sequence) were annealed individually. As shown in Figure 4.2, compared to individual top and bottom oligonucleotide lanes, in annealed oligo lanes, there are bright bands which indicate the successful annealing process.

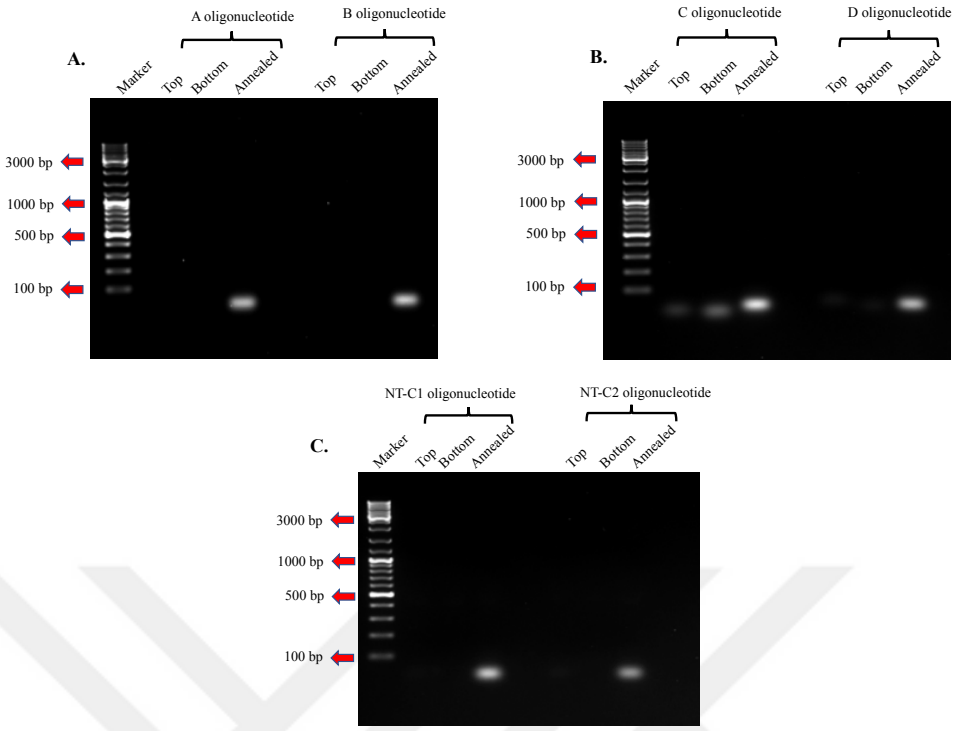

Figure 4.2 The results of top and bottom oligonucleotide annealing of each gRNA candidates and non-targeting gRNAs. Oligonucleotide annealing results for **(A)** gRNA A and B **(B)** gRNA C and D **(C)** gRNA NT-C1 and NT-C2. The products of each annealing reaction were loaded into 2% agarose gel and run at 90 V for 30 min. For each annealing reaction, top and bottom single stranded oligonucleotides were also loaded as controls of the reactions. Sizes of some marker bands are indicated with red arrows.

The annealed oligonucleotides of each gRNA candidate and each non-targeting control were cloned into pSp-Cas9(BB)-2A-Puro (PX459) V2.0 plasmid by using BbsI restriction enzyme and T4 DNA ligase. After ligation reactions, the cloned plasmids were transformed into chemically competent *E.coli* DH5α strain and spread on LB agar medium containing Ampicillin for positive selection. After growth for 16 h at 37°C, the bacterial colonies were observed. For each CRISPR cloning, 10 colonies were selected for further growth in LB containing Ampicillin for plasmid DNA isolation. After 16 h of growth in LB containing Ampicillin, the miniprep plasmid DNAs were isolated. In order to screen the cloned plasmids, PCR reactions were carried out. In these PCR reactions, hU6fwd primer was used as

forward primer, and as reverse primer, bottom oligonucleotides specific to each different gRNA candidate and non-targeting control gRNAs were used. For each PCR reaction, there was also the PCR negative control in which there was no template DNA. In Figure 4.3, the PCR products of CRISPR A cloning, in Figure 4.4, the PCR products of CRISPR B cloning, in figure 4.5, the PCR products of CRISPR C cloning, in Figure 4.6, the PCR products of CRISPR D cloning, in Figure 4.7, the PCR products of CRISPR NT-C1 cloning, and in Figure 4.8, the PCR products of CRISPR NT-C2 cloning are shown. The expected PCR product size for the correctly cloned CRISPR plasmids is 274 bp and as seen from the Figures from 4.3 to 4.8 for A, C, D, NT-C1 and NT-C2 10 out of 10 bacterial clones and for B 9 out of 10 bacterial clones had successfully cloned plasmids.CRISPR A cloning, CRISPR B cloning, CRISPR C cloning, CRISPR D cloning, CRISPR NT-C1 cloning and CRISPR NT-C2 cloning are shown in Figure 4.3, Figure 4.4, Figure 4.5, Figure 4.6, Figure 4.7 and Figure 4.8 respectively.

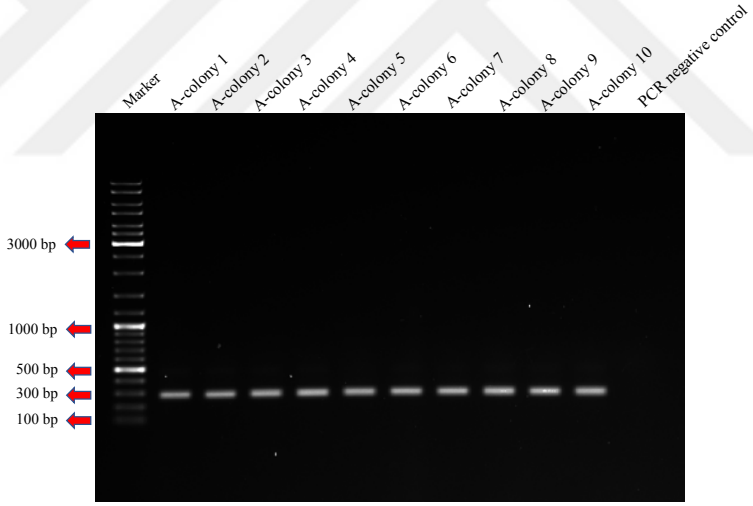

Figure 4.3 PCR screening of CRISPR cloning for candidate A. The cloned plasmids that were isolated from 10 different bacterial colonies were PCR amplified with hU6 fwd as forward primer and bottom oligonucleotide for gRNA A as reverse primer. The products of each PCR reaction were loaded into 1% agarose gel and run at 100 V for 60 min. The expected size of the PCR product is 274 bp. The negative control of the PCR reaction does not include template DNA. Sizes of some marker bands are indicated with red arrows.

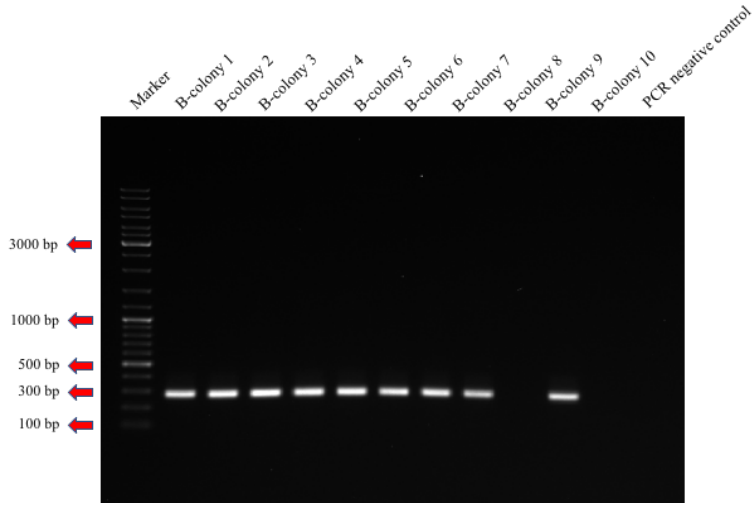

Figure 4.4 PCR screening of CRISPR cloning for candidate B. The cloned plasmids that were isolated from 10 different bacterial colonies were PCR amplified with hU6 fwd as forward primer and bottom oligonucleotide for gRNA B as reverse primer. The products of each PCR reaction were loaded into 1% agarose gel and run at 100 V for 60 min. The expected size of the PCR product is 274 bp. The negative control of the PCR reaction does not include template DNA. Sizes of some marker bands are indicated with red arrows.

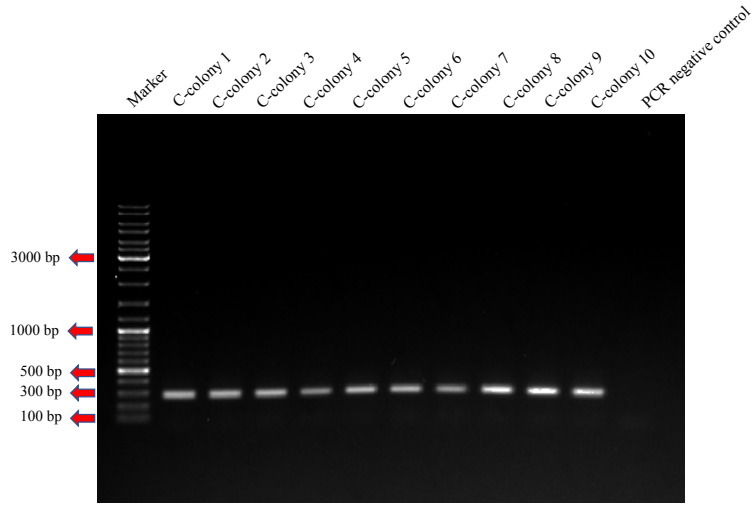

Figure 4.5 PCR screening of CRISPR cloning for candidate C. The cloned plasmids that were isolated from 10 different bacterial colonies were PCR amplified with hU6 fwd as forward primer and bottom oligonucleotide for gRNA C as reverse primer. The products of each PCR reaction were loaded into 1% agarose gel and run at 100 V for 60 min. The expected size of the PCR product is 274 bp. The negative control of the PCR reaction does not include template DNA. Sizes of some marker bands are indicated with red arrows.

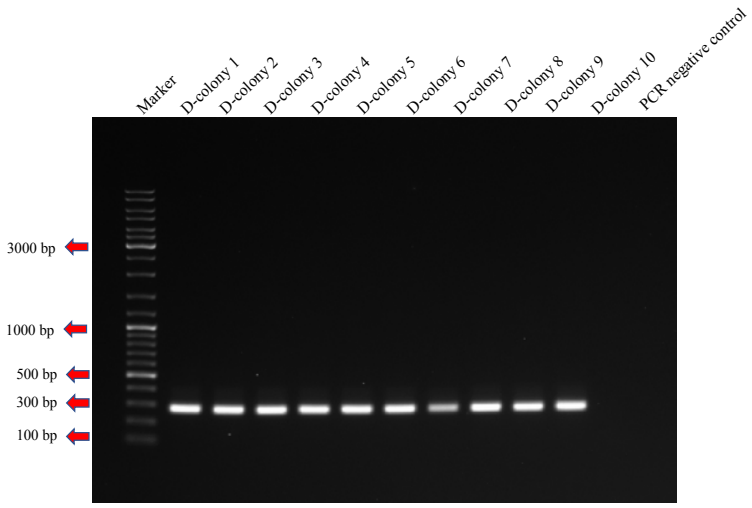

Figure 4.6 PCR screening of CRISPR cloning for candidate D. The cloned plasmids that were isolated from 10 different bacterial colonies were PCR amplified with hU6 fwd as forward primer and bottom oligonucleotide for gRNA D as reverse primer. The products of each PCR reaction were loaded into 1% agarose gel and run at 100 V for 60 min. The expected size of the PCR product is 274 bp. The negative control of the PCR reaction does not include template DNA. Sizes of some marker bands are indicated with red arrows.

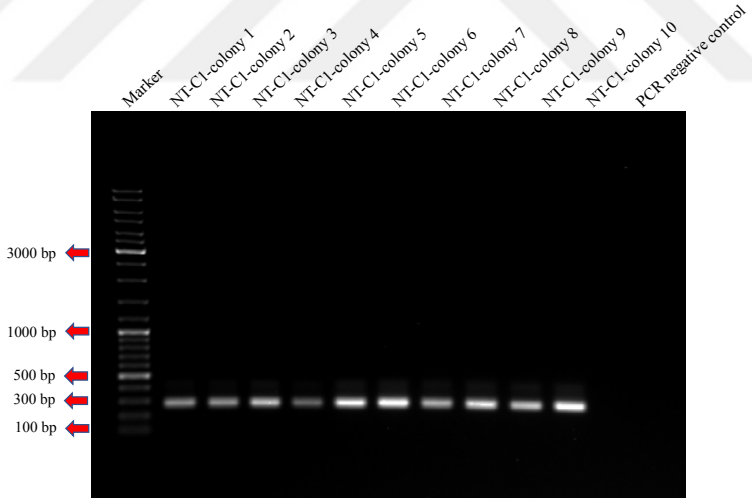

Figure 4.7 PCR screening of CRISPR cloning for NT-C1. The cloned plasmids that were isolated from 10 different bacterial colonies were PCR amplified with hU6 fwd as forward primer and bottom oligonucleotide for gRNA NT-C1 as reverse primer. The products of each PCR reaction were loaded into 1% agarose gel and run at 100 V for 60 min. The expected size of the PCR product is 274 bp. The negative control of the PCR reaction does not include template DNA. Sizes of some marker bands are indicated with red arrows.

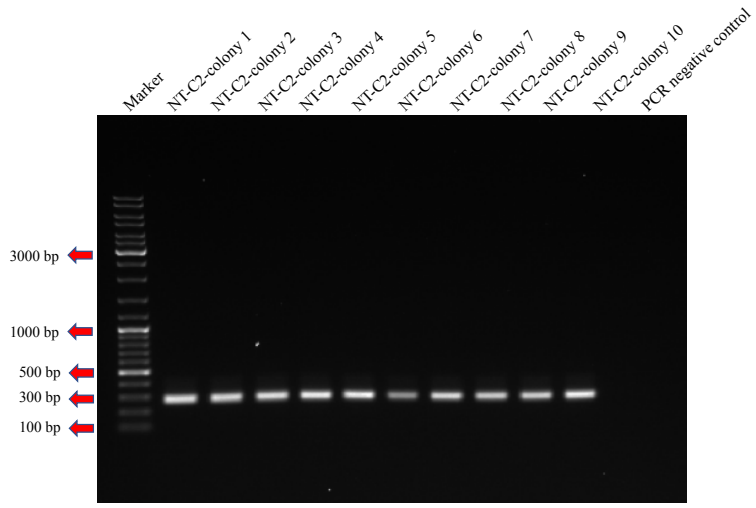

Figure 4.8 PCR screening of CRISPR cloning for NT-C2. The cloned plasmids that were isolated from 10 different bacterial colonies were PCR amplified with hU6 fwd as forward primer and bottom oligonucleotide for gRNA NT-C2 as reverse primer. The products of each PCR reaction were loaded into 1% agarose gel and run at 100 V for 60 min. The expected size of the PCR product is 274 bp. The negative control of the PCR reaction does not include template DNA. Sizes of some marker bands are indicated with red arrows.

4.1.3. Confirmation of the Cloned CRISPR Plasmids with Sanger Sequencing

The plasmid DNAs that were isolated from three different bacterial colonies were sequenced for further confirmation. For each cloning, out of three clones, at least one clone has 100% correct DNA sequence. The comparison of the expected sequence after cloning and the 100% matching sequencing results are shown in Figure 4.9 for candidate A, in Figure 4.10 for candidate B, in Figure 4.11 for candidate C, in Figure 4.12 for candidate D, in Figure 4.13 for non-targeting control NT-C1, and in Figure 4.14 for non-targeting control NT-C2.

From now on, candidate A colony 3 is denoted as **CRISPR A,** candidate B colony 5 is denoted as **CRISPR B,** candidate C colony 9 is denoted as **CRISPR C,** candidate D colony 4 is denoted as **CRISPR D,** non-targeting control NT-C1 colony 8 is denoted as **CRISPR NT-C1,** and non-targeting control NT-C2 colony 8 is denoted as **CRISPR NT-C2.**

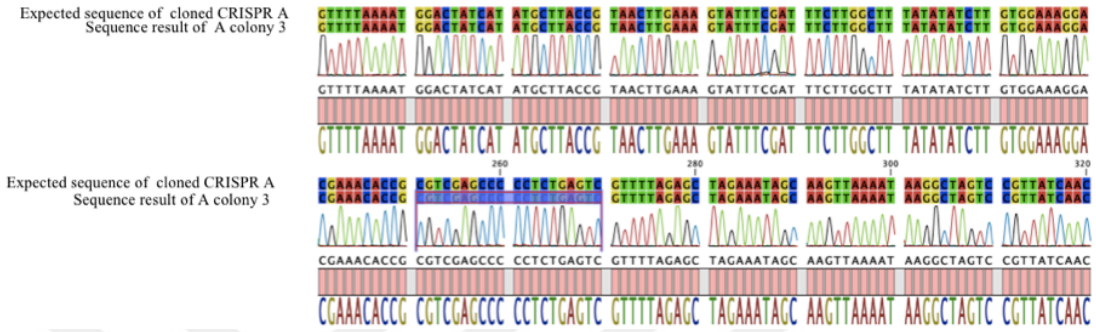

Figure 4.9 Sanger sequencing result of candidate A colony 3. The expected sequence after CRISPR cloning and sequencing result of candidate A colony 3 were compared by using CLC Main Workbench Software. The sequence of gRNA A is highlighted as blue. CRISPR candidate A colony 3, has 100% match with the theoretical expected sequence.

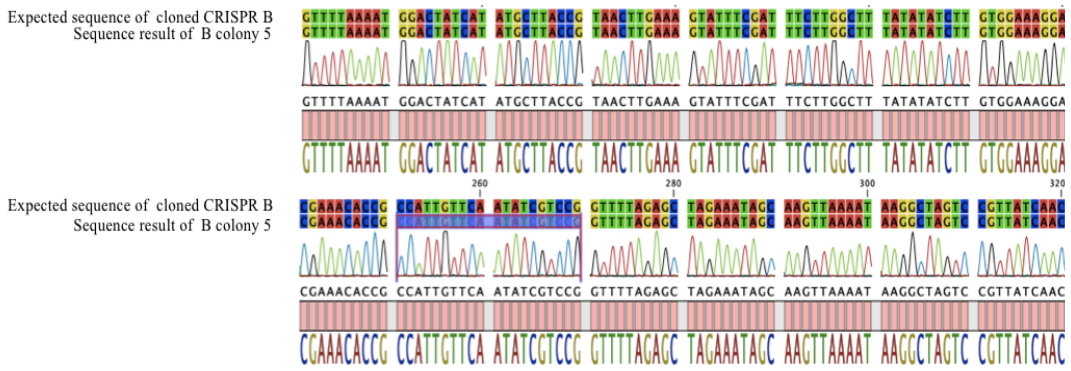

Figure 4.10 Sanger sequencing result of candidate B colony 5. The expected sequence after CRISPR cloning and sequencing result of candidate B colony 5 were compared by using CLC Main Workbench Software. The sequence of gRNA B is highlighted as blue. CRISPR candidate B colony 5, has 100% match with the theoretical expected sequence.

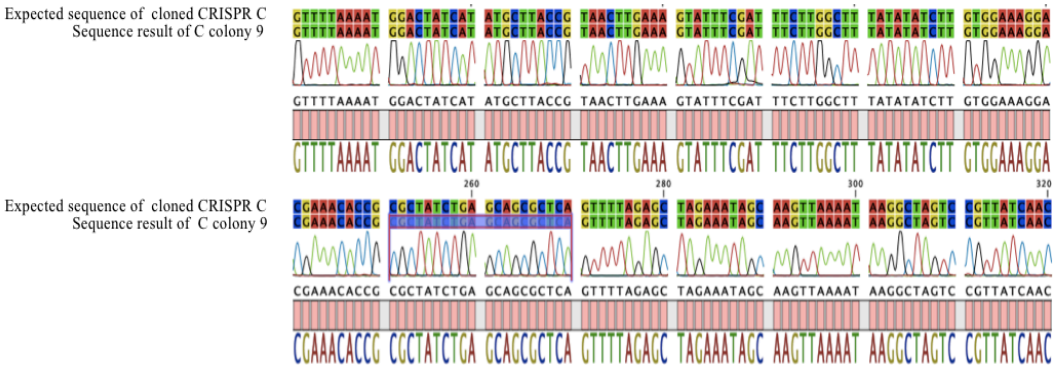

Figure 4.11 Sanger sequencing result of candidate C colony 9. The expected sequence after CRISPR cloning and sequencing result of candidate C colony 9 were compared by using CLC Main Workbench Software. The sequence of gRNA C is highlighted as blue. CRISPR candidate C colony 9, has 100% match with the theoretical expected sequence.

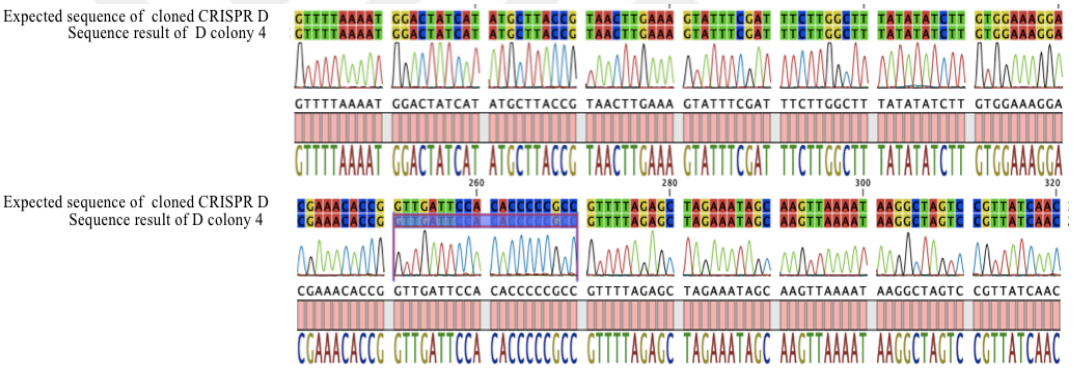

Figure 4.12 Sanger sequencing result of candidate D colony 4. The expected sequence after CRISPR cloning and sequencing result of candidate D colony 4 were compared by using CLC Main Workbench Software. The sequence of gRNA D is highlighted as blue. CRISPR candidate D colony 4, has 100% match with the theoretical expected sequence.

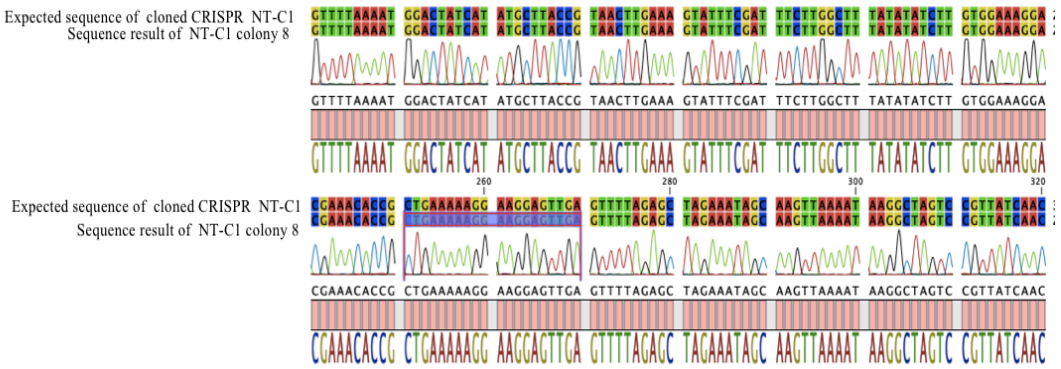

Figure 4.13 Sanger sequencing result of NT-C1 colony 8. The expected sequence after CRISPR cloning and sequencing result of NT-C1 colony 8 were compared by using CLC Main Workbench Software. The sequence of gRNA NT-C1 is highlighted as blue. CRISPR NT-C1 colony 8, has 100% match with the theoretical expected sequence.

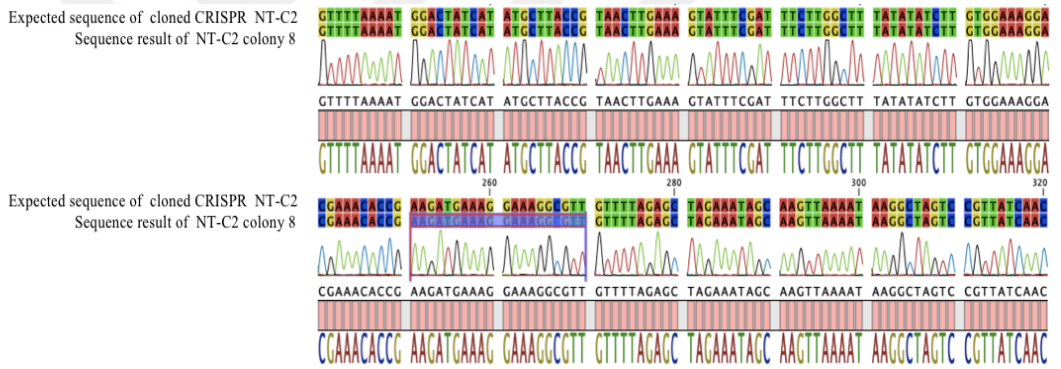

Figure 4.14 Sanger sequencing result of NT-C2 colony 8. The expected sequence after CRISPR cloning and sequencing result of NT-C2 colony 8 were compared by using CLC Main Workbench Software. The sequence of gRNA NT-C2 is highlighted as blue. CRISPR NT-C2 colony 8, has 100% match with the theoretical expected sequence.

4.2. Determination of Puromycin Concentration for Enrichment of the Transfected Population

After the delivery of the cloned CRISPR plasmids, in order to enrich the transfected cells in the total cell population, the transfected cells were planned to treat with Puromycin for a limited time period. Therefore, in order to determine the optimum concentration for this enrichment, U87-MG cells were treated with different concentrations of Puromycin (0.1 μg/mL, 0.25 μg/mL, 0.5 μg/mL, 1 μg/mL, 2 μg/mL, 3 μg/mL, 4 μg/mL and 5 μg/mL) for one week. After one-week treatment, the cell viability % was determined by trypan blue exclusion assay. As seen from Figure 4.15, the cell viability was decreased to 55.50% for 0.1 μg/mL concentration, 4.06% for 0.25 μg/mL concentration and 0.18% for 0.5 μg/mL concentration. For 1 μg/mL concentration and all the above concentrations, the cell viability % was 0. In this study, the aim was not the stable selection of the transfected cells. On the other hand, the aim was only the enrichment of the transfected cells. Therefore, for the enrichment of the transfected cells in the cell population, the optimum concentration of Puromycin was determined as 0.5 μg/mL.

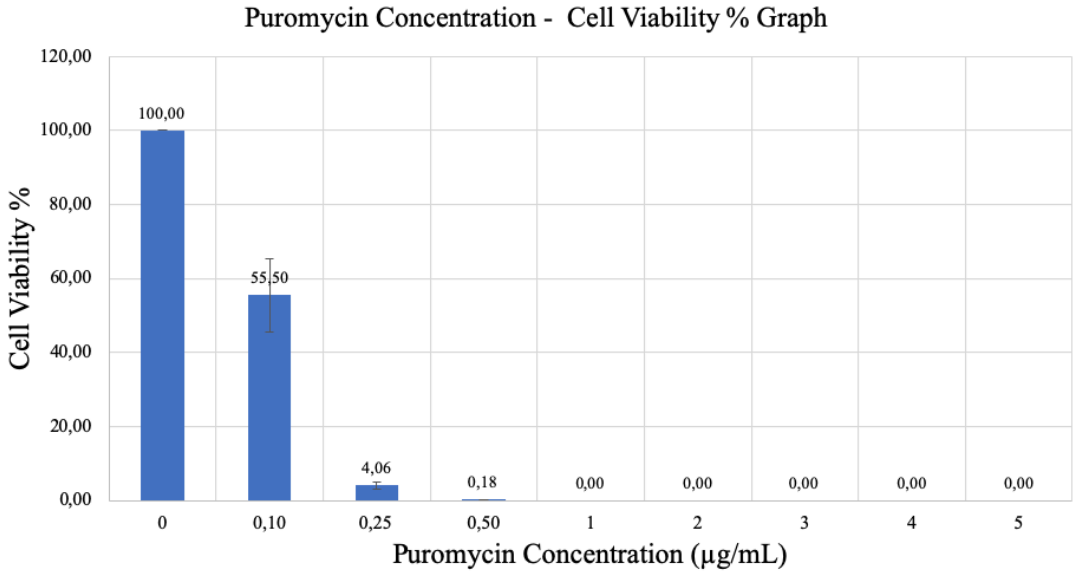

Figure 4.15 Cell Viability % vs Puromycin concentration graph. U87-MG cells were treated with 0.1 µg/mL, 0.25 µg/mL, 0.5 µg/mL, 1 µg/mL, 2 µg/mL, 3 µg/mL, 4 µg/mL and 5 µg/mL Puromycin for one week. After one week, for each concentration, cell viability % was determined by trypan blue exclusion assay.

4.3.Small-Scale Transfection Optimization

In order to visualize the individual editing performances, the individual CRISPR candidates were transfected into $3x10^5$ cells in 6-wells. In this thesis, this scale of transfection is named as small-scale transfections. Prior to the CRISPR candidate transfections, to find the optimum conditions for small-scale transfections, different DNA: Lipofectamine 3000 ratios were tried and the results of these optimization experiments are explained in section 4.3.1 and 4.3.2.

4.3.1. Microscopy Results of Small-Scale Transfection Optimization

The CRISPR plasmids of the candidates and the non-targeting CRISPR plasmids were planned to be transiently transfected to U87-MG cells with Lipofectamine 3000 in 6-well plates. In order to, find the optimum transfection conditions for small-scale transfections, different DNA:Lipofectamine 3000 ratios were tested. For small scale transfections (2.5 µg DNA into $3x10^5$ cells/well in 6-well plates), three different pcDNAGFP:Lipofectamine 3000 ratios (1:1.5,1:3,1:5) were used. 48 h after transfection, the GFP expressing cells were visualized in FITC channel of ZEISS Axio Vert.A1 inverted microscope with 10X magnification. As seen in Figure 4.16, as the pcDNAGFP:Lipofectamine 3000 increased, the number of GFP expressing cells also increased. However, their morphologies were also changing. Especially, in 1:5 ratio, the morphology was resembling apoptotic cell morphology. By considering not only GFP positive cell percentage, but also the cellular health, among the three different conditions, 1:3 was determined as the optimum pcDNAGFP:Lipofectamine 3000 ratio.

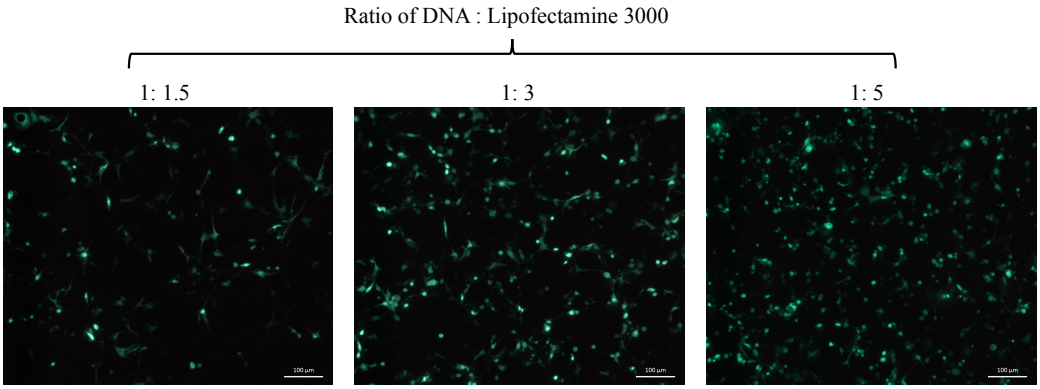

Figure 4.16 Microscopy images of GFP expressing cells that are transfected with different pcDNAGFP:Lipofectamine 3000 ratios for small-scale transfection experiments. U87-MG cells were transfected with 1:1.5, 1:3 and 1:5 ratios of pcDNAGFP:Lipofectamine 3000 to optimize small-scale transfections (2.5 µg DNA into $3x10^5$ cells/well in 6-well plates). After 48 h, the transfected cells were visualized in FITC channel of ZEISS Axio Vert.A1 inverted microscope with 10X magnification. The green cells are the GFP expressing cells. The 100 µm scale bars are shown at the right end corners of each image.

4.3.2. Flow Cytometry Results of Small- Scale Transfection Optimization

The transfected cells that were visualized under fluorescent microscope (explained in section 4.3.1) were also further analyzed with flow cytometer to quantify the transfection efficiency. In Figure 4.17, left panels show the Forward Scatter (FSC) vs Side Scatter (SSC) dot plots of the cell populations. FCS indicates the size of the cells whereas SSC indicates the granularity of the cells. After gating to the live cell population (P1 gate), FITC histograms of live cell populations were plotted. On the right panel of Figure 4.17, FITC histograms of the live cell populations are shown. The FITC positive cell gate (P2) which is determined according to untransfected (GFP negative) cells, indicates the GFP positive cell percent in the live cell population. As seen in Figure 4.17, when pcDNAGFP:Lipofectamine 3000 ratio was 1:1.5, the transfection efficiency was 22.39%, when pcDNAGFP:Lipofectamine 3000 ratio was 1:3, the transfection efficiency was 60.37%, when pcDNAGFP:Lipofectamine 3000 ratio was 1:5, the transfection efficiency was 72.84%. Although, the efficiency of transfection was increasing with the increasing ratio of pcDNAGFP:Lipofectamine 3000, the live cell population in P1 gate was resembling apoptotic cell morphology. Therefore, in consistent with microscopy results, flow cytometry results also indicated that 1:3 ratio was determined as the optimum ratio if both transfection efficiency and cell viability were together considered.

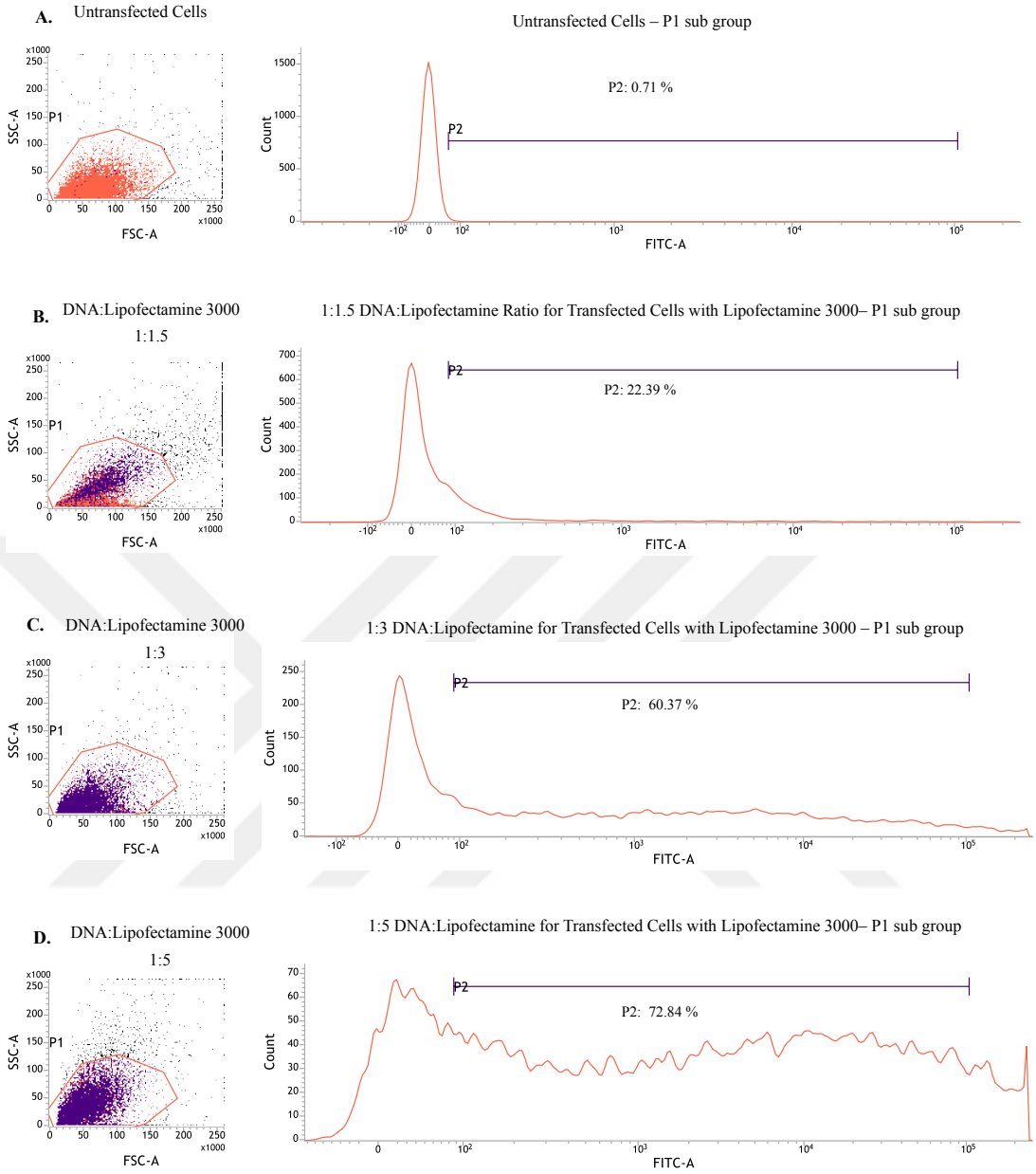

Figure 4.17 Flow cytometry results of cells that are transfected with different pcDNAGFP:Lipofectamine 3000 ratios for small - scale transfection experiments. U87-MG cells were transfected with 1:1.5, 1:3 and 1:5 ratios of pcDNAGFP :Lipofectamine 3000 to optimize small-scale transfections (2.5 µg DNA into $3x10^5$ cells/well in 6-well plates). After 48 h, **(A)** untransfected cells **(B)** transfected cells with 1:1.5 ratio of pcDNAGFP:Lipofectamine 3000 **(C)** transfected cells with 1:3 ratio of pcDNAGFP:Lipofectamine 3000 **(D)** transfected cells with 1:5 ratio of pcDNAGFP:Lipofectamine 3000, were analyzed with flow cytometry. FSC vs SSC dot plots are on the left panel and FITC histograms are on the right panel. FSC represents cell size and SSC represents cell granularity. P1 gate in FSC vs SSC dot plots indicate live cell population. P2 gate in FITC histograms indicate GFP positive cell population. Untransfected cell population was the negative control for the GFP expression.

4.4.Comparison of Individual Gene Editing Performances of CRISPR Candidates by RFLP and T7EI Assays

In order to see the individual gene editing performances of CRISPR candidates, the cloned and confirmed CRISPR candidate plasmids (A, B, C and D) and non-targeting CRISPR control plasmids (NT-C1 and NT-C2) were individually transfected to U87-MG cells with the optimized DNA: Lipofectamine 3000 ratio (1:3). After 48 h, the cell population was treated with 0.5 µg/mL Puromycin for one week to enrich the transfected cell population. Following this enrichment, gDNA was isolated. After PCR amplification of the specific target regions, Restriction Fragment Length Polymorphism (RFLP) and T7 Endonuclase I (T7EI) assays were performed in order to observe individual gene editing performances.

As the upstream target region is a long region, this region as upstream target region A and upstream target region B were PCR amplified in order to perform RFLP analysis of CRISPR A and B, respectively. To assess the gene editing performance of CRISPR A, the upstream target region A was amplified by performing PCR with Upstream_Target_Region_A_Fwd and Upstream_Target_ Region_A_Rev primers. PCR amplification of upstream target region A is expected to give a PCR product of 666 bp. As seen in Figure 4.18 left panel, the HinfI restriction site in this region, is expected to be destroyed as the result of CRISPR A activity. In the presence of HinfI restriction enzyme, PCR product (666 bp) of the wild type (WT, untransfected cells) and non-targeting controls (NT-C1 and NT-C2) populations, were expected to be cleaved into two bands as a band of 381 bp and a band of 285 bp. However, in the cell population that were transfected with CRISPR A, in addition to these bands, undigested band of 666 bp was seen as a result of HinfI restriction site destruction due to IN-DELs caused by CRISPR A activity. As seen from Figure 4.18 right panel, there is an intensity increase in the undigested PCR

product band in the presence of HinfI restriction enzyme, compared to WT and other non-targeting controls (NT-C1 and NT-C2).

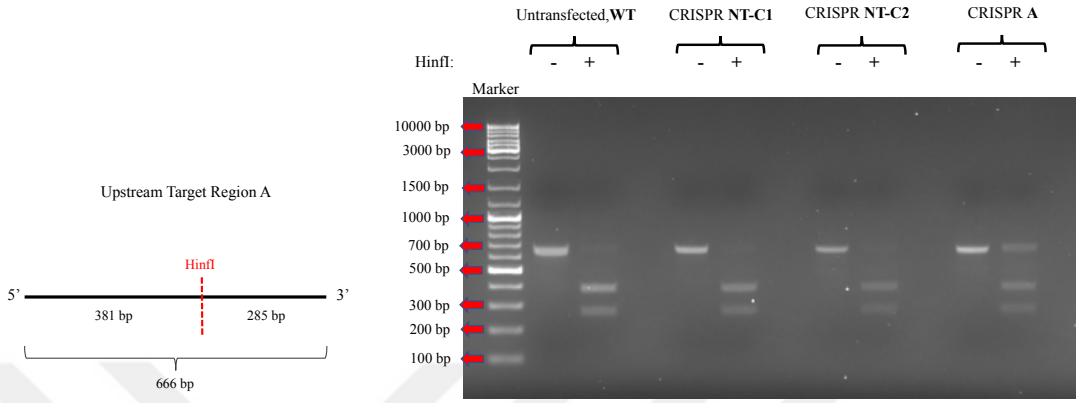

Figure 4.18 RFLP assay results of CRISPR A. For RFLP analysis, upstream target region A of untransfected (WT) cells, non-targeting control CRISPR NT-C1 transfected, non-targeting control CRISPR NT-C2 transfected and CRISPR A transfected cells, were PCR amplified with Upstream_Target_Region_A_Fwd and Upstream_ Target_ Region_ A_Rev primers. Schematic representation of upstream target region A is shown on the left panel. In the upstream target region A, the HinfI restriction site that is expected to be destroyed as the result of CRISPR A activity is shown with red dashed line. The expected band sizes are indicated on the schematic representation. The PCR products were digested with HinfI restriction enzyme and the digestion products were loaded into 2% agarose and run at 100 V for 60 min. The gel image is shown on the right panel. Sizes of some marker bands are indicated with red arrows. (-) indicates the absence of HinfI restriction enzyme, (+) indicates the presence of HinfI restriction enzyme.

T7 endonuclease I (T7EI) mismatch detection assays are used to identify gene editing performance of CRISPR candidates at their specific target site. In T7EI assay, the target region of CRISPR candidate was PCR amplified. After denaturation and re-annealing of the PCR product, unmatched DNA sequences are formed due to IN-DELs created as a result of CRISPR/Cas9 activity. T7EI is capable of recognizing and cleaving these unmatched DNA sequences. Upstream target region CRISPR A was amplified by PCR with Upstream_Target_Region_A_Fwd and Upstream_Targe t_Region_ A_Rev primers. After PCR amplification of the target region, the PCR products were subjected to T7EI assay protocol and the band patterns in the absence

and presence of T7EI were analyzed. As it can be seen from Figure 4.19, the PCR product of CRISPR A transfected cells were digested efficiently with T7EI, indicating the activity of CRISPR A in the upstream target region. In untransfected cells (WT), non-targeting control CRISPR transfected cells (NT-C1 and NT-C2), T7EI digestion resulted in intact uncut bands due to lack of CRISPR A activity. However, in CRISPR A transfected cells, in the presence of T7EI, a portion of the denatured and re-annealed PCR product was digested which indicates the activity of CRISPR A. As the sample was derived from a heterogenous cell pool, a portion of the denatured and re-annealed PCR product was undigested.

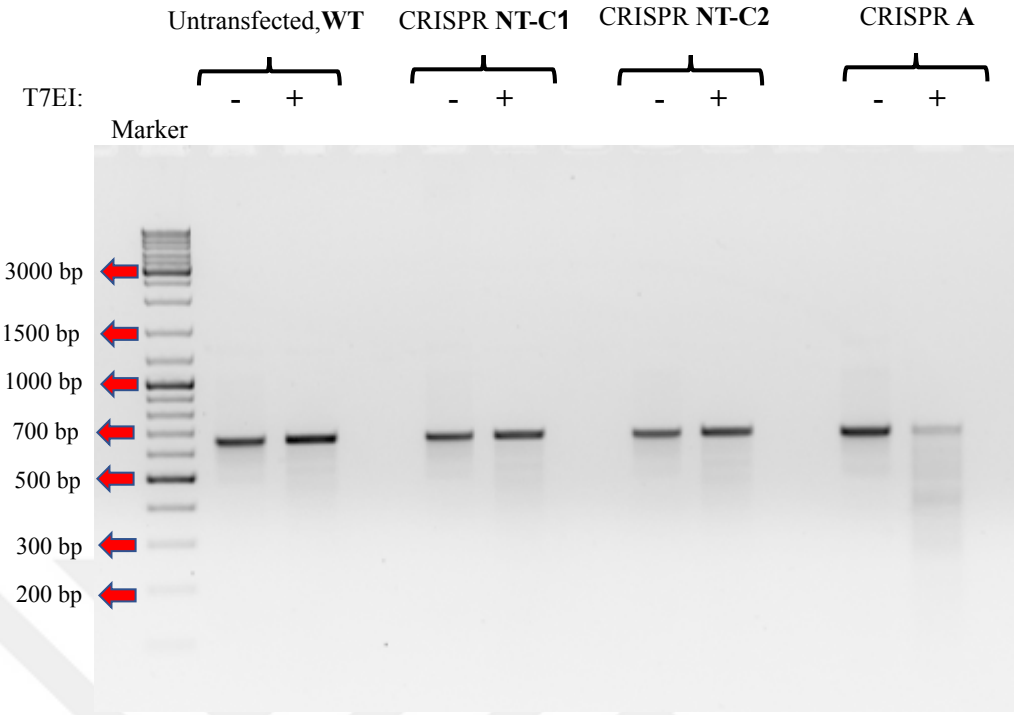

Figure 4.19 T7EI assay results of CRISPR A. For T7EI analysis, upstream target region A of untransfected (WT) cells, non-targeting control CRISPR NT-C1 transfected cells, non-targeting control CRISPR NT-C2 transfected cells and CRISPR A transfected cells were PCR amplified with Upstream_Target_Region _A_Fwd and Upstream_ Target_ Region_ A_Rev primers. The PCR products were subjected to T7EI assay protocol and products were loaded into 2% agarose and run at 100 V for 60 min. Sizes of some marker bands are indicated with red arrows. (-) indicates the absence of T7EI endonuclease enzyme, (+) indicates the presence of T7EI endonuclease enzyme.

In order to assess the gene editing performance of CRISPR B, the upstream target region B was amplified by performing PCR with Upstream_Target _Region_B_Fwd and Upstream_Target_Region_B_Rev primers. PCR amplification of upstream target region B is expected to give a PCR product of 648 bp. As seen in Figure 4.20 left panel, the NciI restriction site in this region, is expected to be destroyed as the result of CRISPR B activity. In the presence of NciI restriction enzyme, PCR product (648 bp) of the wild type (WT, untransfected cells) and non-targeting controls (NT-C1 and NT-C2) populations, were expected to be cleaved into two bands as a band of 452 bp and a band of 196 bp. However, in the cell population

that were transfected with CRISPR B, in addition to these bands, undigested band of 648 bp was seen as a result of NciI restriction site destruction due to IN-DELs caused by CRISPR B activity. As seen from Figure 4.20 right panel, there is an intensity increase in the undigested PCR product band in the presence of NciI restriction enzyme, compared to WT and other non-targeting controls (NT-C1 and NT-C2).

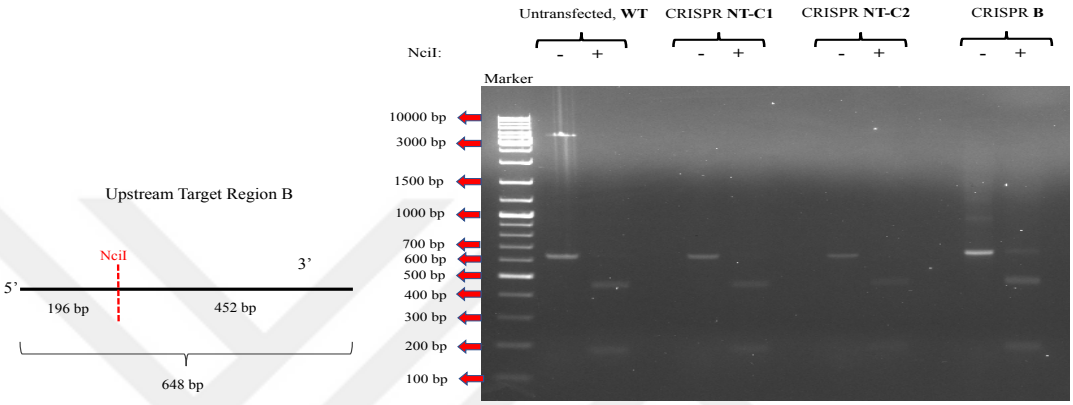

Figure 4.20 RFLP assay results of CRISPR B. For RFLP analysis, upstream target region B of untransfected (WT) cells, non-targeting control CRISPR NT-C1 transfected, non-targeting control CRISPR NT-C2 transfected and CRISPR B transfected cells, were PCR amplified with Upstream_Target_Region_B_Fwd and Upstream_Target_Region_B_Rev primers. Schematic representation of upstream target region B is shown on the left panel. In the upstream target region B, the NciI restriction site that is expected to be destroyed as the result of CRISPR B activity is shown with red dashed line. The expected band sizes are indicated on the schematic representation. The PCR products were digested with NciI restriction enzyme and the digestion products were loaded into 2% agarose and run at 100 V for 60 min. The gel image is shown on the right panel. Sizes of some marker bands are indicated with red arrows. (-) indicates the absence of NciI restriction enzyme, (+) indicates the presence of NciI restriction enzyme.

Upstream target region CRISPR B was amplified by performing PCR with Upstream_Target_Region_B_Fwd and Upstream_Target_Region_B_Rev primers. After PCR amplification of the target region, the PCR products were subjected to T7EI assay protocol and the band patterns in the absence and presence of T7EI were analyzed. As it can be seen from Figure 4.21, PCR product of CRISPR B transfected cells were digested efficiently with T7EI, indicating the activity of CRISPR B in the

upstream target region. In untransfected cells (WT), non-targeting control CRISPR transfected cells (NT-C1 and NT-C2), T7EI digestion resulted in intact uncut bands due to lack of CRISPR B activity. However, in CRISPR B transfected cells, in the presence of T7EI, denatured and re-annealed PCR product was digested completely.

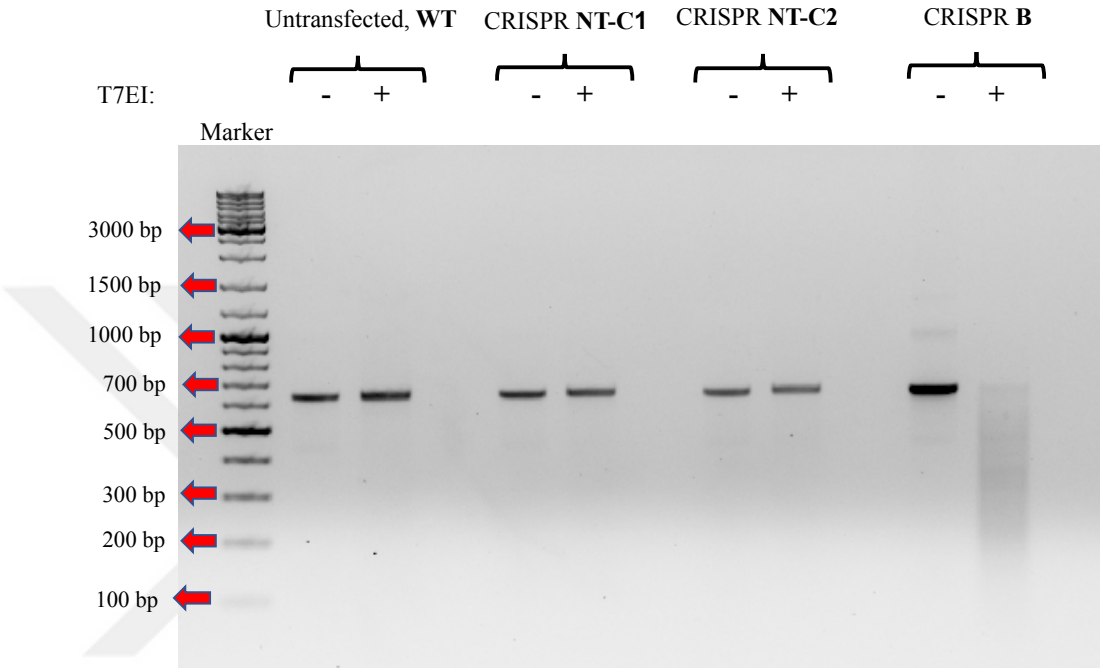

Figure 4.21 T7EI assay results of CRISPR B. For T7EI analysis, upstream target region B of untransfected (WT) cells, non-targeting control CRISPR NT-C1 transfected cells, non-targeting control CRISPR NT-C2 transfected cells and CRISPR B transfected cells were PCR amplified with Upstream_ Target_Region _B_Fwd and Upstream_Target_Region_B_Rev primers. The PCR products were subjected to T7EI assay protocol and products were loaded into 2% agarose and run at 100 V for 60 min. Sizes of some marker bands are indicated with red arrows. (-) indicates the absence of T7EI endonuclease enzyme, (+) indicates the presence of T7EI endonuclease enzyme.

In order to confirm the gene editing performance of CRISPR C, the downstream target region was amplified by performing PCR with Downstream_ Target_Region_Fwd and Downstream_Target_Region_Rev primers. PCR amplification of downstream target region is expected to give a PCR product of 884 bp. As seen in Figure 4.22 left panel, the Aor51HI restriction site in this region, is

expected to be destroyed as the result of CRISPR C activity. In the presence of Aor51HI restriction enzyme, PCR product (884 bp) of the wild type (WT, untransfected cells) and non-targeting controls (NT-C1 and NT-C2) populations, were expected to be cleaved into two bands as a band of 725 bp and a band of 159 bp. As seen from Figure 4.22 right panel, the band patterns of digestion products and the intensities of the undigested PCR product in the presence of Aor51HI were similar in the WT, non-targeting controls (NT-C1 and NT-C2) and CRISPR C transfected samples.

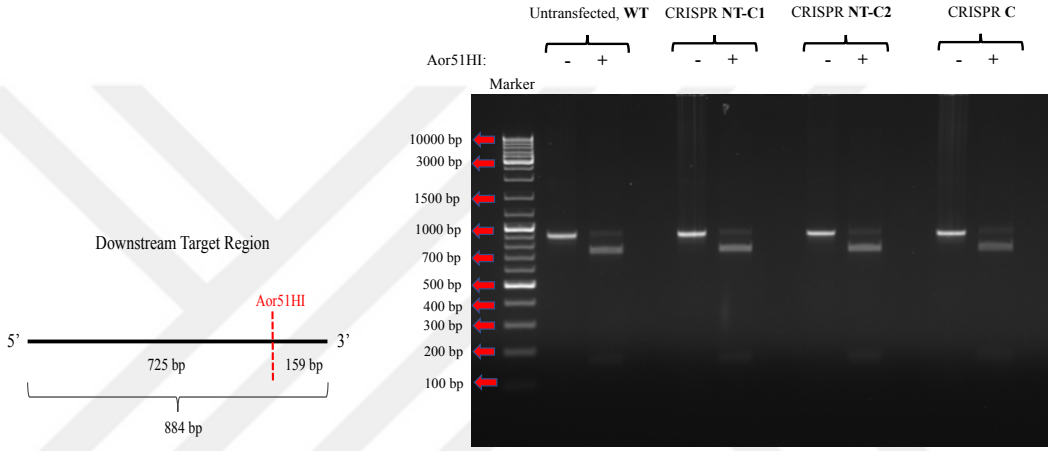

Figure 4.22 RFLP assay results of CRISPR C. For RFLP analysis, downstream target region of untransfected (WT) cells, non-targeting control CRISPR NT-C1 transfected, non-targeting control CRISPR NT-C2 transfected and CRISPR C transfected cells, were PCR amplified with Downstream_Target_Region_Fwd and Downstream_Target_Region_Rev primers. Schematic representation of downstream target region is shown on the left panel. In the downstream target region, the Aor51HI restriction site that is expected to be destroyed as the result of CRISPR C activity is shown with red dashed line. The expected band sizes are indicated on the schematic representation. The PCR products were digested with Aor51HI restriction enzyme and the digestion products were loaded into 2% agarose and run at 100 V for 60 min. The gel image is shown on the right panel. Sizes of some marker bands are indicated with red arrows. (-) indicates the absence of Aor51HI restriction enzyme, (+) indicates the presence of Aor51HI restriction enzyme.

Downstream target region was amplified by performing PCR with Downstream_Target_Region_Fwd and Downstream_Target_Region_Rev primers. After PCR amplification of the target region, the PCR products were subjected to

T7EI assay protocol and the band patterns in the absence and presence of T7EI were analyzed. As it can be seen from Figure 4.23, PCR product of CRISPR C transfected cells were digested with T7EI, indicating the activity of CRISPR C in the downstream target region. In untransfected cells (WT), non-targeting control CRISPR transfected cells (NT-C1 and NT-C2), T7EI digestion resulted in intact uncut bands due to lack of CRISPR C activity. In CRISPR C transfected cells, in the presence of T7EI, most of the denatured and re-annealed PCR product was digested. As the sample was derived from a heterogenous cell pool, a portion of the denatured and re-annealed PCR product was undigested.

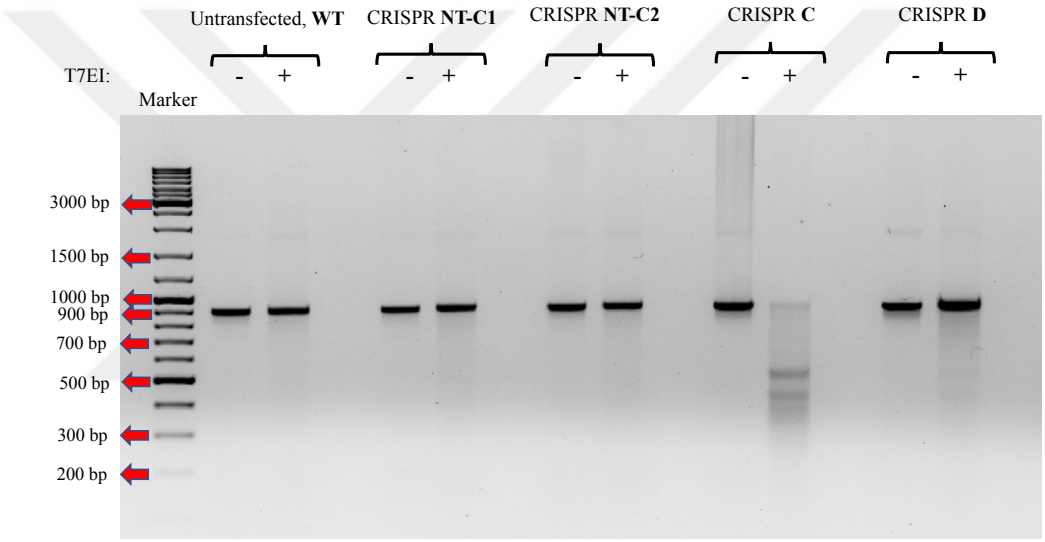

Figure 4.23 T7EI assay results of CRISPR C and CRISPR D. For T7EI analysis, downstream target region of untransfected (WT) cells, non-targeting control CRISPR NT-C1 transfected cells, non-targeting control CRISPR NT-C2 transfected cells, CRISPR C and CRISPR D transfected cells were PCR amplified with Downstream _Target_Region_Fwd and Downstream_Target_Region_Rev primers. The PCR products were subjected to T7EI assay protocol and products were loaded into 2% agarose and run at 100 V for 60 min. Sizes of some marker bands are indicated with red arrows. (-) indicates the absence of T7EI endonuclease enzyme, (+) indicates the presence of T7EI endonuclease enzyme.

In order to confirm the gene editing performance of CRISPR D, the downstream target region was amplified by performing PCR with Downstream_Target_Region_Fwd and Downstream_Target_Region_Rev primers.

PCR amplification of downstream target region is expected to give a PCR product of 884 bp. There are two HinfI resctriction sites in this region. The HinfI restriction site indicated with "*" in Figure 4.24 left panel is expected to be destroyed as the result of CRISPR D activity. In the presence of HinfI restriction enzyme, PCR product (884 bp) of the wild type (WT, untransfected cells) and non-targeting controls (NT-C1 and NT-C2) populations, were expected to be cleaved into three bands as a band of 626 bp, a band of 176 bp and a band of 82 bp. The band patterns of digestion products and the intensities of the undigested PCR product in the presence of HinfI were similar in the WT, non-targeting controls (NT-C1 and NT-C2) and CRISPR D transfected samples.

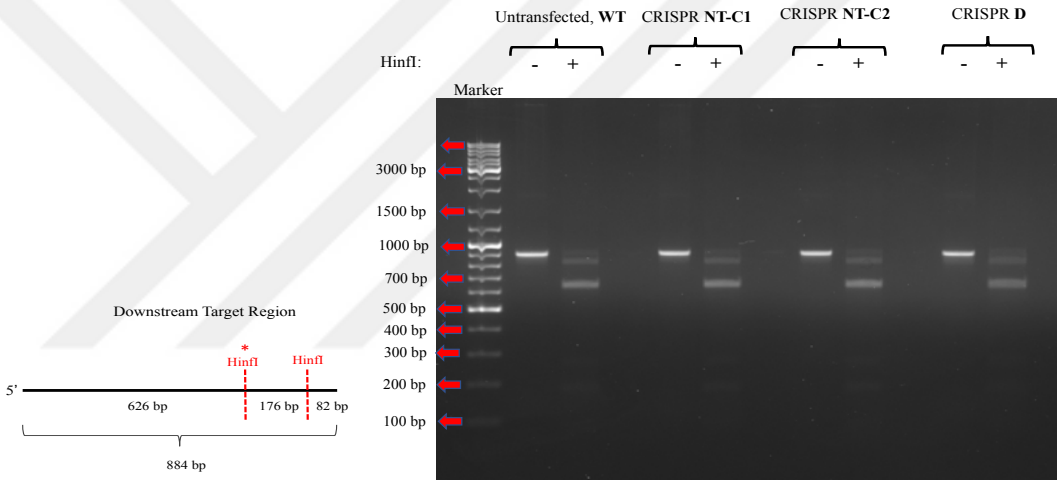

Figure 4.24 RFLP assay results of CRISPR D. For RFLP analysis, downstream target region of untransfected (WT) cells, non-targeting control CRISPR NT-C1 transfected, non-targeting control CRISPR NT-C2 transfected and CRISPR D transfected cells, were PCR amplified with Downstream_Target_Region_Fwd and Downstream_Target_Region_Rev primers. Schematic representation of downstream target region is shown on the left panel. The two HinfI restriction sites are shown with red dashed lines. The HinfI restriction site that is expected to be destroyed by CRISPR D activity is indicated with "*". The expected band sizes are indicated on the schematic representation. The PCR products were digested with HinfI restriction enzyme and the digestion products were loaded into 2% agarose and run at 100 V for 60 min. The gel image is shown on the right panel. Sizes of some marker bands are indicated with red arrows. (-) indicates the absence of HinfI restriction enzyme, (+) indicates the presence of HinfI restriction enzyme.

Downstream target region was amplified by performing PCR with Downstream_Target_Region_Fwd and Downstream_Target_Region_Rev primers.

After PCR amplification of the target region, the PCR products were subjected to T7EI assay protocol and the band patterns in the absence and presence of T7EI were analyzed. As it can be seen from Figure 4.23, PCR product of CRISPR D transfected cells were digested with T7EI, indicating the activity of CRISPR D in the downstream target region. In untransfected cells (WT), non-targeting control CRISPR transfected cells (NT-C1 and NT-C2), T7EI digestion resulted in intact uncut bands due to lack of CRISPR D activity. As it can be seen from Figure 4.23, in CRISPR D transfected cells, there was only a faint smear in the presence of T7EI and most of the denatured and re-annealed PCR product was intact.

4.5. Large-Scale Transfection Optimization

For further CRISPR pair co-transfection experiments, the transfected cells were going to be subjected to not only gDNA isolation and single cell cloning but also protein isolation for western blot experiments, expansion for further characterization experiments and cryopreservation. Therefore, the scale-up of the transfection experiments was needed. For the large-scale transfections, $3x10^6$ cells were transfected in 100-mm cell culture dishes. In the following sections 4.5.1 and 4.5.2, transfection optimization results of large-scale transfections were explained.

4.5.1. Microscopy Results of Large-Scale Transfection Optimization

In order to, find the optimum transfection conditions for large-scale transfections, different DNA:Lipofectamine 3000 ratios were tested. For large-scale transfections (15 µg DNA into $3x10^6$ cells in 100-mm cell culture dishes), three different pcDNAGFP:Lipofectamine 3000 ratios (1:1.5,1:3) were used. 48 h after transfection, the GFP expressing cells were visualized in FITC channel of ZEISS Axio Vert.A1 inverted microscope with 10X magnification. As seen in Figure 4.25, as the pcDNAGFP:Lipofectamine 3000 increased, the number of GFP expressing cells also increased. By considering GFP positive cell percentage, 1:3 was determined as the optimum pcDNAGFP:Lipofectamine 3000.

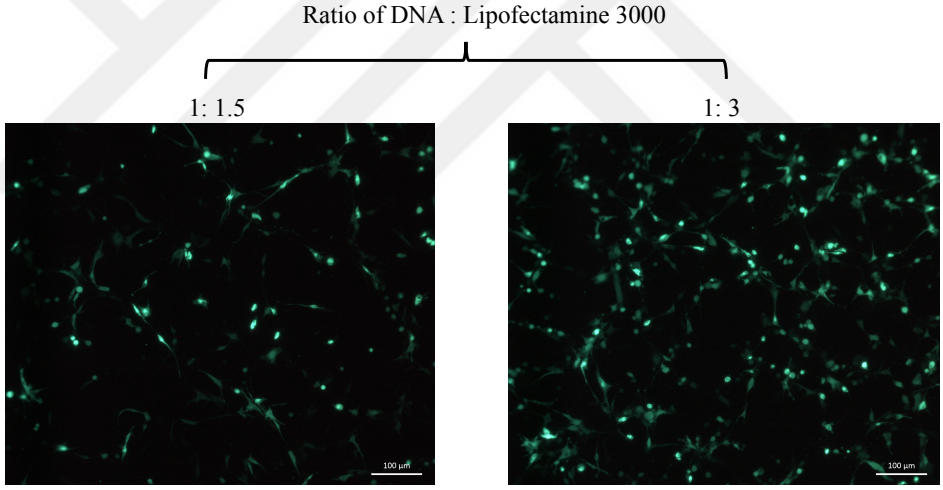

Figure 4.25 Microscopy images of GFP expressing cells that are transfected with different pcDNAGFP:Lipofectamine 3000 ratios for large-scale transfection experiments. U87-MG cells were transfected with 1:1.5 and 1:3 ratios of pcDNAGFP:Lipofectamine 3000 to optimize large-scale transfections (15 µg DNA into $3x10^6$ cells in 100-mm cell culture dishes). After 48 h, the transfected cells were visualized in FITC channel of ZEISS Axio Vert.A1 inverted microscope with 10X magnification. The green cells are the GFP expressing cells. The 100 µm scale bars are shown at the right end corners of each image.

4.5.2. Flow Cytometry Results of Large-Scale Transfection Optimization

The transfected cells that were visualized under fluorescent microscope (explained in section 4.5.1) were also further analyzed with flow cytometer to quantify the transfection efficiency. In Figure 4.26, left panels show the Forward Scatter (FSC) vs Side Scatter (SSC) dot plots of the cell populations. FCS indicates the size of the cells whereas SSC indicates the granularity of the cells. After gating to the live cell population (P1 gate), FITC histograms of live cell populations were plotted. On the right panel of Figure 4.26, FITC histograms of the live cell populations are shown. The FITC positive cell gate (P2) which is determined according to untransfected cells (GFP negative cells), indicates the GFP positive cell percent in the live cell population. As seen in Figure 4.26, when pcDNAGFP:Lipofectamine 3000 ratio was 1:1.5, the transfection efficiency was 23.08%, when pcDNAGFP:Lipofectamine 3000 ratio was 1:3, the transfection efficiency was 47.46%.Therefore, in consistent with microscopy results, flow cytometry results also indicated that 1:3 ratio was the optimum ratio for considering the transfection efficiencies.

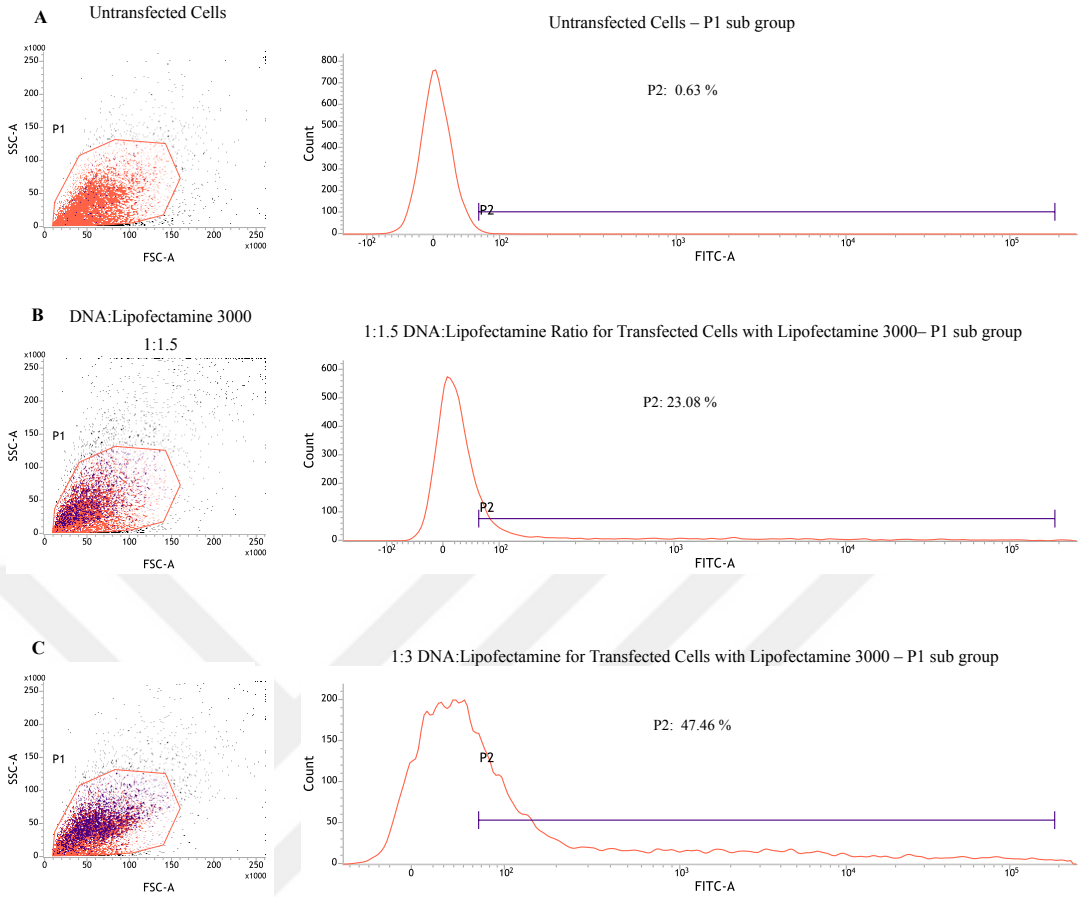

Figure 4.26 Flow cytometry results of cells that are transfected with different pcDNAGFP:Lipofectamine 3000 ratios for large-scale transfection experiments. U87-MG cells were transfected with 1:1.5 and 1:3 ratios of pcDNAGFP: Lipofectamine 3000 to optimize large-scale transfections (15 µg DNA into $3x10^6$ cells/well in 100 mm cell culture). After 48 h, **(A)** untransfected cells **(B)** transfected cells with 1:1.5 ratio of pcDNAGFP:Lipofectamine 3000 **(C)** transfected cells with 1:3 ratio of pcDNAGFP:Lipofectamine 3000 were analyzed with flow cytometry. FSC vs SSC graphs are on the left panel and FITC histograms are on the right panel. FSC represents cells size and SSC represents cell granularity. P1 gate in FSC vs SSC dot plots indicate live cell population. P2 gate in FITC histograms indicate GFP positive cell population. Untransfected cell population was the negative control for the GFP expression.

4.6.Gene Editing Results of Co-transfected CRISPR Pairs

To target the upstream and downstream target regions in the *TP53* gene locus simultaneously and delete the region in between, CRISPR A or B and CRISPR C or D were co-transfected as pairs to U87-MG cells. As negative control, non-targeting CRISPRs (NT-C1, NT-C2) were also co-transfected as pairs. As mentioned before, CRISPR A and B were designed for upstream target region whereas CRISPR C and D were designed for downstream target region. Therefore, for the desired deletion in the genome, CRISPR A+ CRISPR C, CRISPR A+ CRISPR D, CRISPR B+ CRISPR C and CRISPR B+ CRISPR D for non-targeting controls CRISPR NT-C1+ CRISPR NT-C2 co-transfections were performed with the optimized DNA: Lipofectamine 3000 ratio (1:3). As controls of the experiment, single transfections of each CRISPR pair were also performed. 48h after transfection, 0.5 µg/mL Puromycin treatment was started. For enrichment of the transfected cell population, 0.5 µg/mL Puromycin treatment continued for one week. After genomic DNA isolation, the region starting with upstream target region and ending with downstream target region was PCR amplified with Upstream_Target_Region_A_Fwd and Downstream_Target _Region _Rev primers. For untransfected (WT) cells and CRISPR NT-C1+ CRISPR NT-C2 co-transfected cells, the expected PCR product size was 2022 bp and as seen in Figure 4.27, their PCR product size were correct. However, for each co-transfected CRISPR pairs, in addition to WT PCR product, there was a new and shorter PCR product (indicated with blue arrows in Figure 4.27) due to CRISPR pair activity.

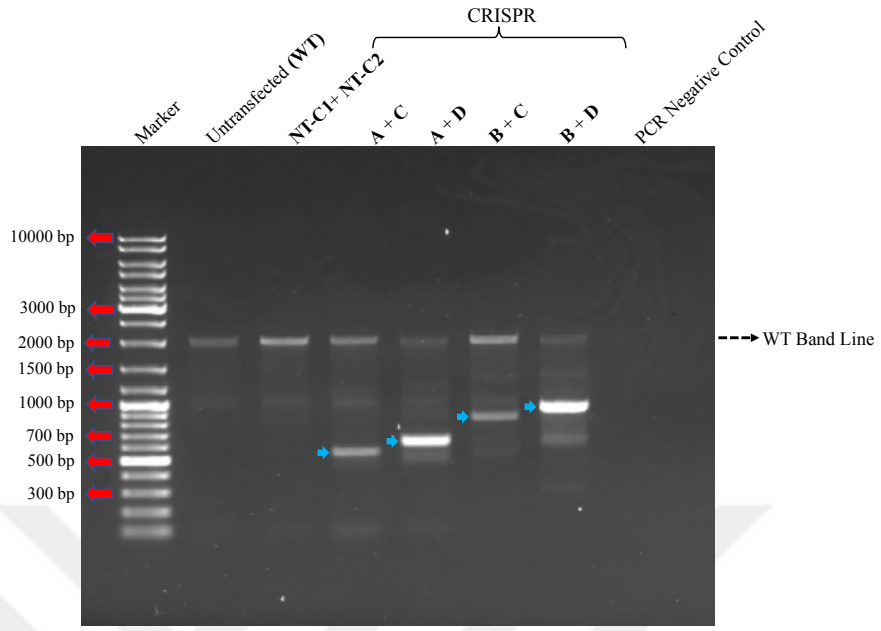

Figure 4.27 Result of CRISPR activities of co-transfected CRISPR candidates. After transfection of CRISPR candidates that target upstream target region and downstream target region, regions in between two target sites were amplified with Upstream_Target_Region_A_Fwd and Downstream_Target_Region_Rev primers. Blue arrows illustrate size of PCR products after CRISPR activities. The PCR products were loaded into 1% agarose and run at 100 V for 60 min. Sizes of some marker bands are indicated with red arrows. The negative control of the PCR reaction does not include template DNA.

To confirm the results of gene editing in CRISPR pair co-transfected cells, the PCR reactions with Upstream_Target_Region_A_Fwd and Downstream_Target _Region_Rev primers were repeated. This time for each CRISPR pair, in addition to CRISPR pair co-transfected sample, PCR amplification was also performed for the single CRISPR transfection controls in order to show the specificity of the newly formed PCR products due to CRISPR pair activities.

The results of gene editing due to CRISPR A+ CRISPR C pair activity are shown in Figure 4.28. As a result of PCR amplification, in untransfected cells (WT), CRISPR NT-C1 transfected cells, CRISPR NT-C2 transfected cells, CRISPR NT-C1+ CRISPR NT-C2, CRISPR A transfected cells and CRISPR C transfected cells, 2022 bp WT band was observed. In CRISPR A + CRISPR C co-transfected cells, in addition to 2022 bp WT band, the shorter PCR product as a result of the deletion in the *TP53* gene locus performed by the CRISPR pair was observed again which is consistent with the results shown in Figure 4.28.

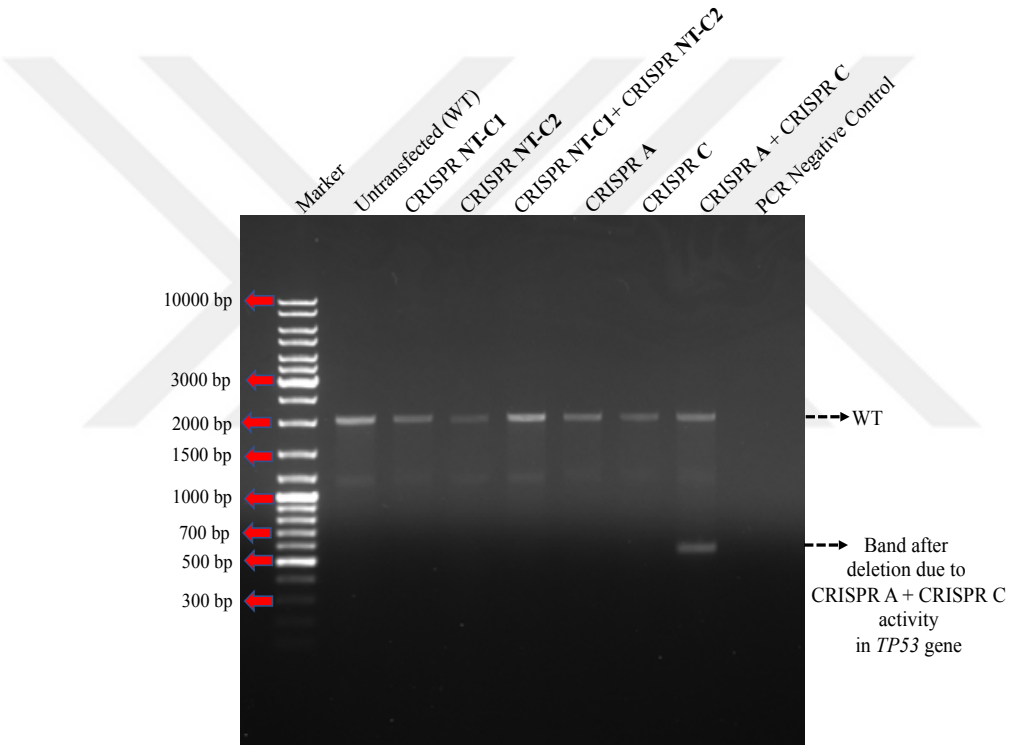

Figure 4.28 Results of gene editing due to CRISPR A+ CRISPR C pair activity in U87-MG cells. After co-transfection of CRISPR A + CRISPR C, region in between two target sites was amplified by performing PCR with Upstream_Target_Region _A_Fwd and Downstream_Target_Region_Rev primers. PCR products were loaded into 1% agarose and run at 100 V for 60 min. Sizes of some marker bands are indicated with red arrows. The negative control of the PCR reaction does not include template DNA.

The results of gene editing due to CRISPR A+ CRISPR D pair activity are shown in Figure 4.29. As a result of PCR amplification, in untransfected cells (WT), CRISPR NT-C1 transfected cells, CRISPR NT-C2 transfected cells, CRISPR NT-C1+ CRISPR NT-C2, CRISPR A transfected cells and CRISPR D transfected cells, 2022 bp WT band was observed. In CRISPR A + CRISPR D co-transfected cells, in addition to 2022 bp WT band, the shorter PCR product as a result of the deletion in the *TP53* gene locus performed by the CRISPR pair was observed again which is consistent with the results shown in Figure 4.29.

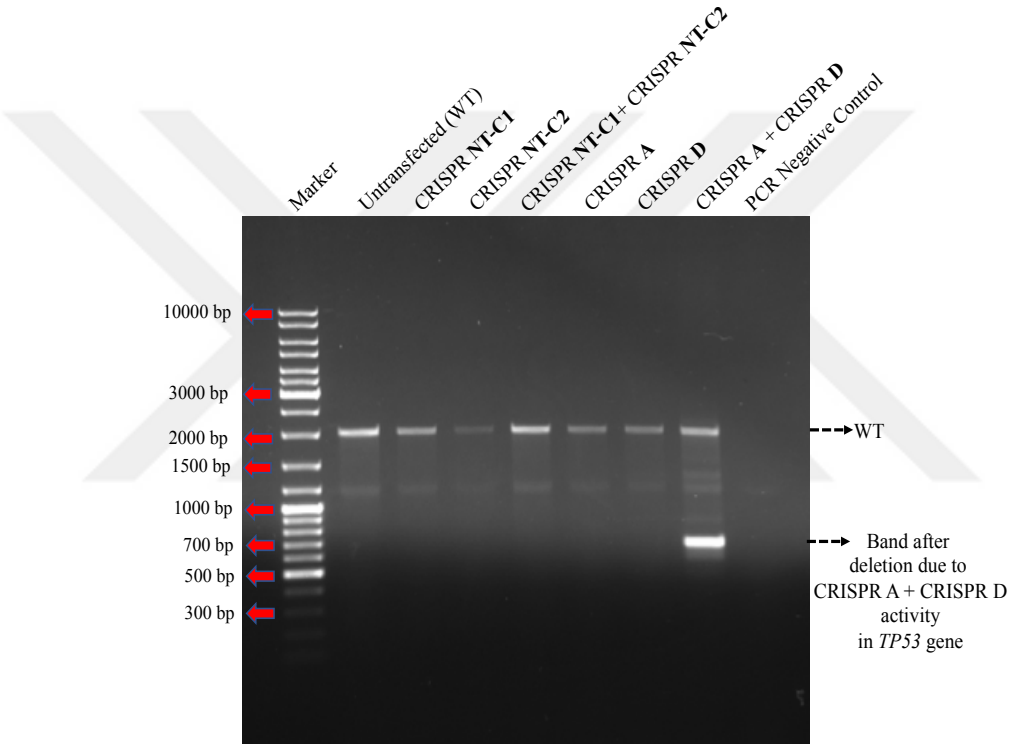

Figure 4.29 Results of gene editing due to CRISPR A+ CRISPR D pair activity in U87-MG cells. After co-transfection of CRISPR A + CRISPR D, region in between two target sites was amplified by performing PCR with Upstream_Target_Region _A_Fwd and Downstream_Target_Region_Rev primers. PCR products were loaded into 1% agarose and run at 100 V for 60 min. Sizes of some marker bands are indicated with red arrows. The negative control of the PCR reaction does not include template DNA.

The results of gene editing due to CRISPR B+ CRISPR C pair activity are shown in Figure 4.30. As a result of PCR amplification, in untransfected cells (WT), CRISPR NT-C1 transfected cells, CRISPR NT-C2 transfected cells, CRISPR NT-C1+ CRISPR NT-C2, CRISPR A transfected cells and CRISPR D transfected cells, 2022 bp WT band was observed .In CRISPR B + CRISPR C co-transfected cells, in addition to 2022 bp WT band, the shorter PCR product as a result of the deletion in the *TP53* gene locus performed by the CRISPR pair was observed again which is consistent with the results shown in Figure 4.30.

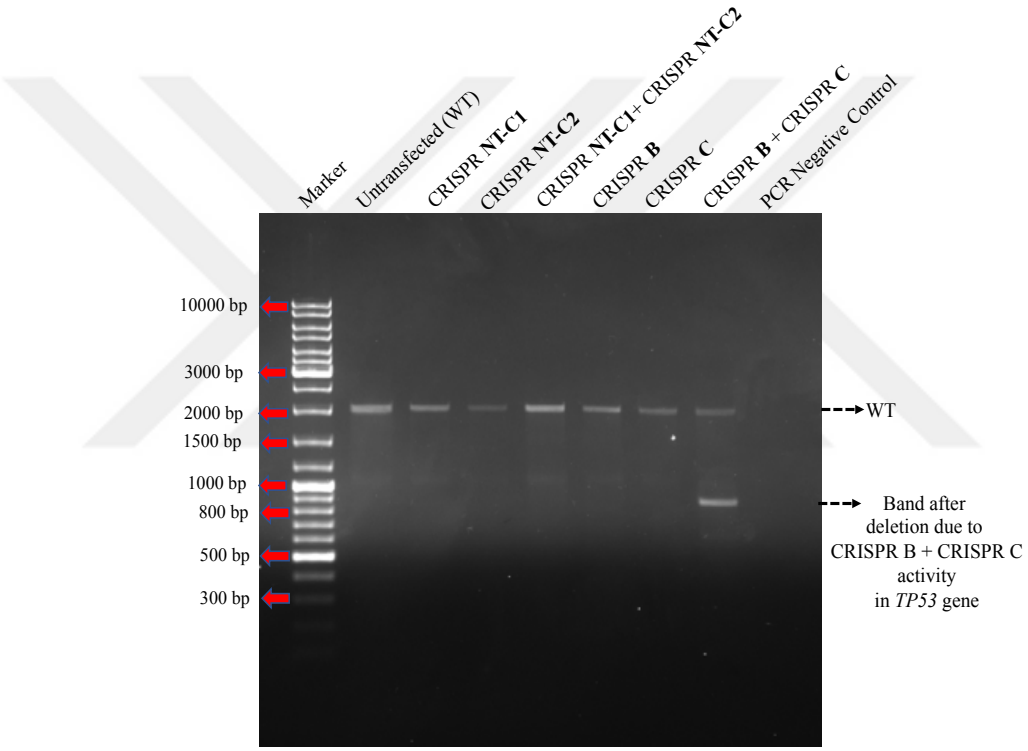

Figure 4.30 Results of gene editing due to CRISPR B+ CRISPR C pair activity in U87-MG cells. After co-transfection of CRISPR B + CRISPR C, region in between two target sites was amplified by performing PCR with Upstream_Target_Region _A_Fwd and Downstream_Target_Region_Rev primers. PCR products were loaded into 1% agarose and run at 100 V for 60 min. Sizes of some marker bands are indicated with red arrows. The negative control of the PCR reaction does not include template DNA.

The results of gene editing due to CRISPR B+ CRISPR D pair activity are shown in Figure 4.31. As a result of PCR amplification, in untransfected cells (WT), CRISPR NT-C1 transfected cells, CRISPR NT-C2 transfected cells, CRISPR NT-C1+ CRISPR NT-C2, CRISPR B transfected cells and CRISPR D transfected cells, 2022 bp WT band was observed. In CRISPR B + CRISPR D co-transfected cells, in addition to 2022 bp WT band, the shorter PCR product as a result of the deletion in the *TP53* gene locus performed by the CRISPR pair was observed again which is consistent with the results shown in Figure 4.31.

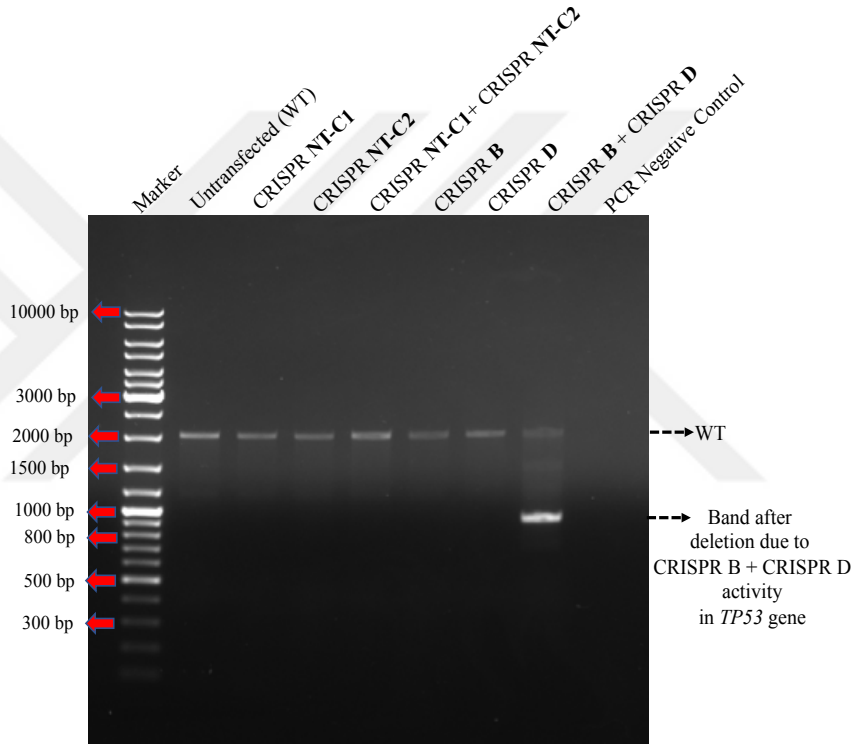

Figure 4.31 Results of gene editing due to CRISPR B+ CRISPR D pair activity in U87-MG cells. After co-transfection of CRISPR B + CRISPR D, region in between two target sites was amplified by performing PCR with Upstream_Target_Region _A_Fwd and Downstream_Target_Region_Rev primers. PCR products were loaded into 1% agarose and run at 100 V for 60 min. Sizes of some marker bands are indicated with red arrows. The negative control of the PCR reaction does not include template DNA.

4.7. Genotyping of The Single Cell Colonies Derived from CRISPR A and CRISPR C Co-transfected Cells

CRISPR candidates were co-transfected as pairs and each pair successfully deleted the desired region as shown in Figures 4.27, 4.28, 4.29, 4.30 and 4.31. Although all of the CRISPR candidate pairs worked successfully, CRISPR A + CRISPR C pair co-transfected cell pool was selected for single cell cloning and further experiments due to the reason that this CRISPR pair is the pair that deletes the longest region in the *TP53* gene locus.

After the expansion of these single cell clones, gDNA isolation was performed. In order to screen these colonies, PCR reactions were carried out to amplify the region in between upstream target region and downstream target region by performing PCR. In these PCR reactions, Upstream_Target_Region_A_Fwd primer was used as forward primer and Downstream_Target_Region_Rev primer was used as reverse primer. For each PCR reaction, untransfected (WT) cells, CRISPR NT-C1 + CRISPR NT-C2 and CRISPR A+ CRISPR C co-transfected cell pool were used as control.

PCR products of untransfected (WT) cells, CRISPR NT-C1+ CRISPR NT-C2 co-transfected cell pool, CRISPR A + CRISPR C co-transfected cell pool and single cell colonies derived from CRISPR A + CRISPR C co-transfected cell pool are shown in Figure 4.32. For each PCR reaction, there was also the PCR negative control in which there was no template. In untransfected (WT) and CRISPR NT-C1+ CRISPR NT-C2 transfected cells, the length of the PCR product is 2022 bp due to lack of CRISPR activity. In CRISPR A + CRISPR C co-transfected cell pool in addition to 2022 bp WT band, there was the newly formed PCR product as a result of specific CRISPR A + CRISPR C pair activity. Among the 40 single cell colonies,

one colony (colony 3) showed $p53^{+/-}$ profile by ending up with both a WT PCR product and a PCR product indicating the desired deletion in the *TP53* gene locus. In addition, there were three colonies (colony 2, colony 16 and colony 17) showing $p53^{-/-}$ profile by ending up with a single PCR product as a result of the desired deletion in the *TP53* gene locus and no WT PCR product.

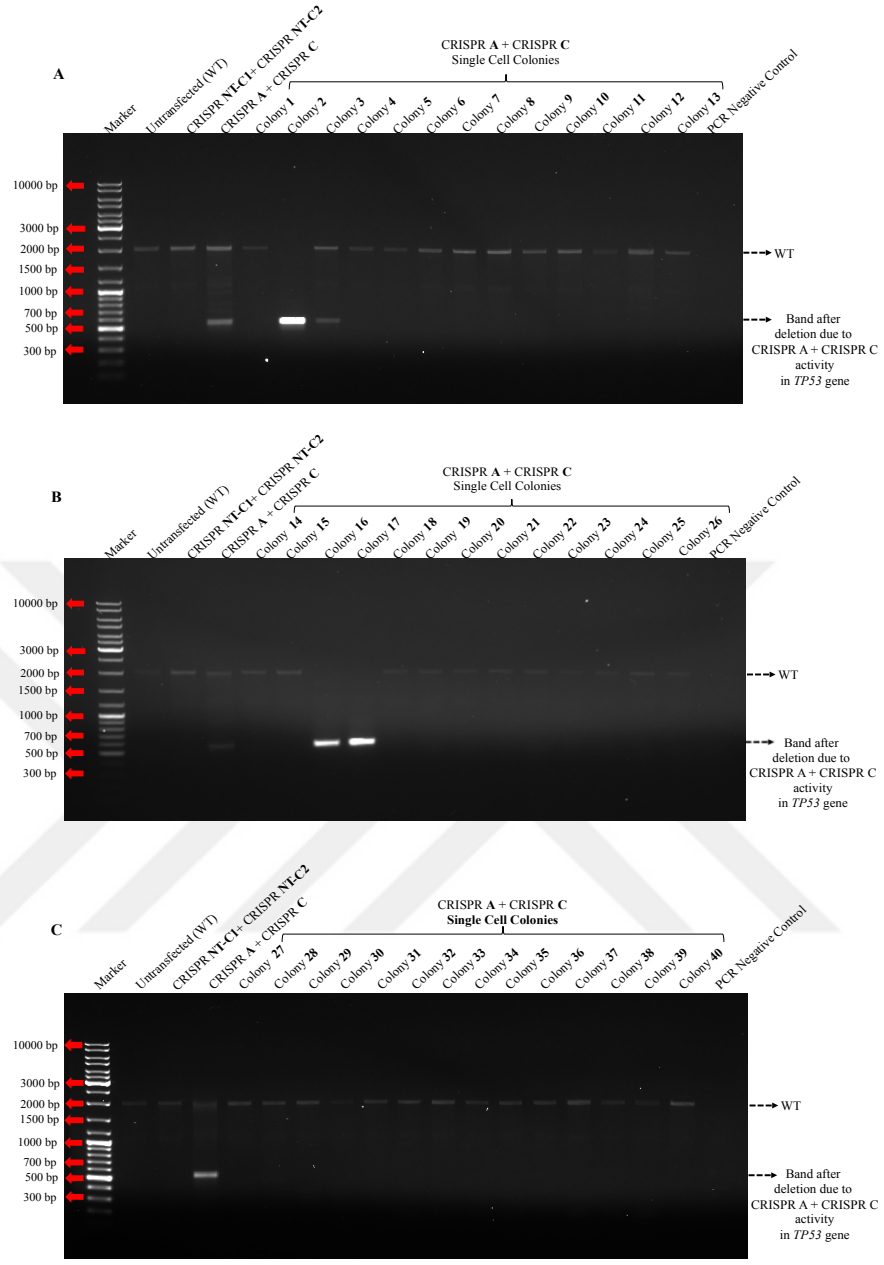

Figure 4.32 Genotyping of single-cell colonies derived from CRISPR A + CRISPR C co-transfected cell pool. After isolating gDNAs from the untransfected cells U87-MG cells (WT), CRISPR NT-C1+ CRISPR NT-C2 co-transfected cell pool, CRISPR A + CRISPR C co-transfected cell pool and single cell clones derived from CRISPR A + CRISPR C transfected cell pool, by using Upstream_Target_Region_A_Fwd primer and Downstream_Target_Region_Rev primer, PCR amplification was performed. The PCR products of single cell clones 1-12 **(A)**, 13-26 **(B)** and 27-40 **(C)** are run in 1% agarose gel at 100V for 60 min. The negative control of the PCR reaction does not include template DNA. Sizes of some marker bands are indicated with red arrows.

4.8. Confirmation of the Single-Cell Colonies Showing $p53^{-/-}$ Profile with Sanger Sequencing

In order to confirm the deletion in between upstream and downstream target regions in the *TP53* gene locus, PCR products of the single cell clones, which showed $p53^{-/-}$ profile (colony 2, colony 16 and colony 17) in genotyping experiments, were sequenced. The sequencing results for colony 2, colony 16 and colony 17 are shown in Figures 4.33, 4.34 and 4.35, respectively. When the sequencing results were compared with WT *TP53* gene sequence, it was clearly seen that the desired regions were deleted in the *TP53* gene locus of these three colonies.

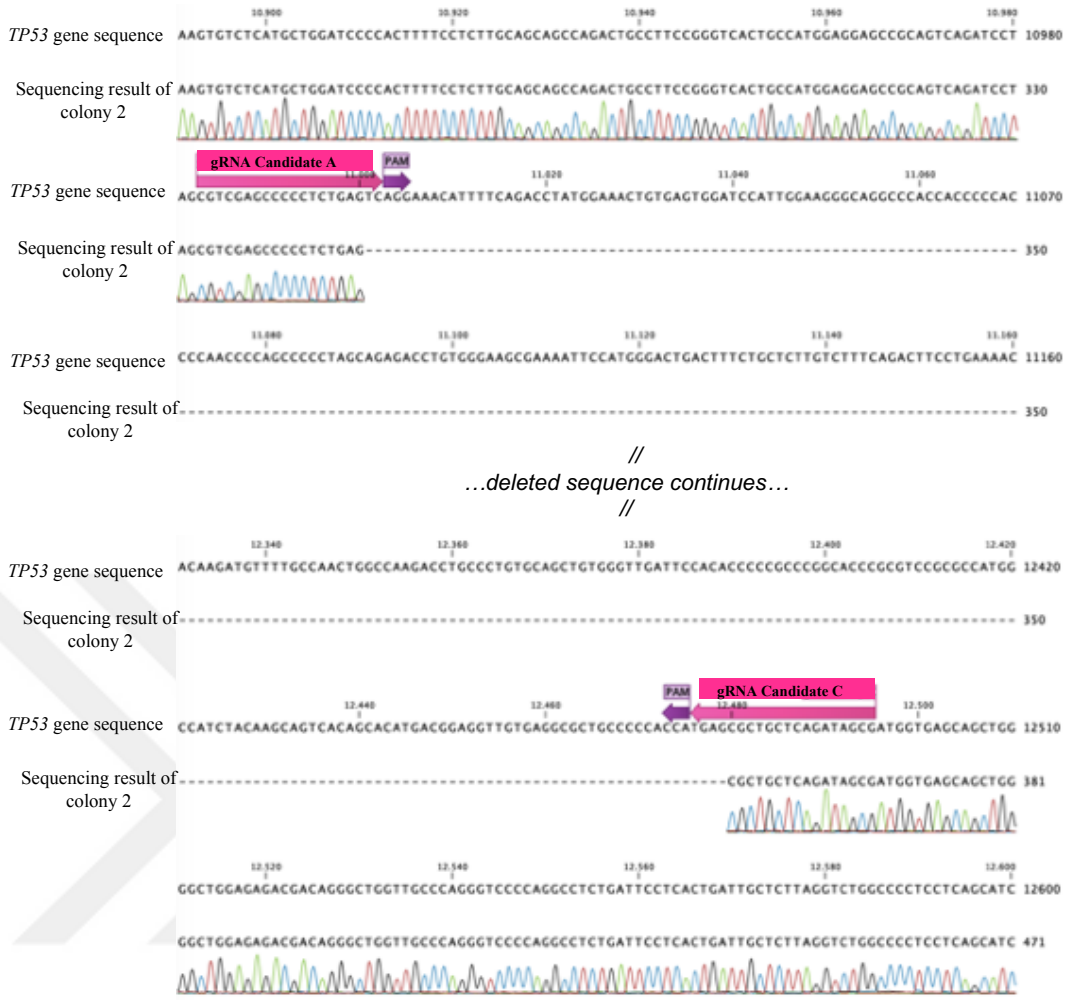

Figure 4.33 Sanger sequencing result of single cell colony 2. Sequence in between upstream target region and downstream target region of colony 2 was compared with WT *TP53* sequence using CLC Main Workbench Software. The sequences of gRNA A and gRNA C are indicated with pink arrows, and their PAM sequences are indicated with purple arrows in the reference *TP53* gene sequence.

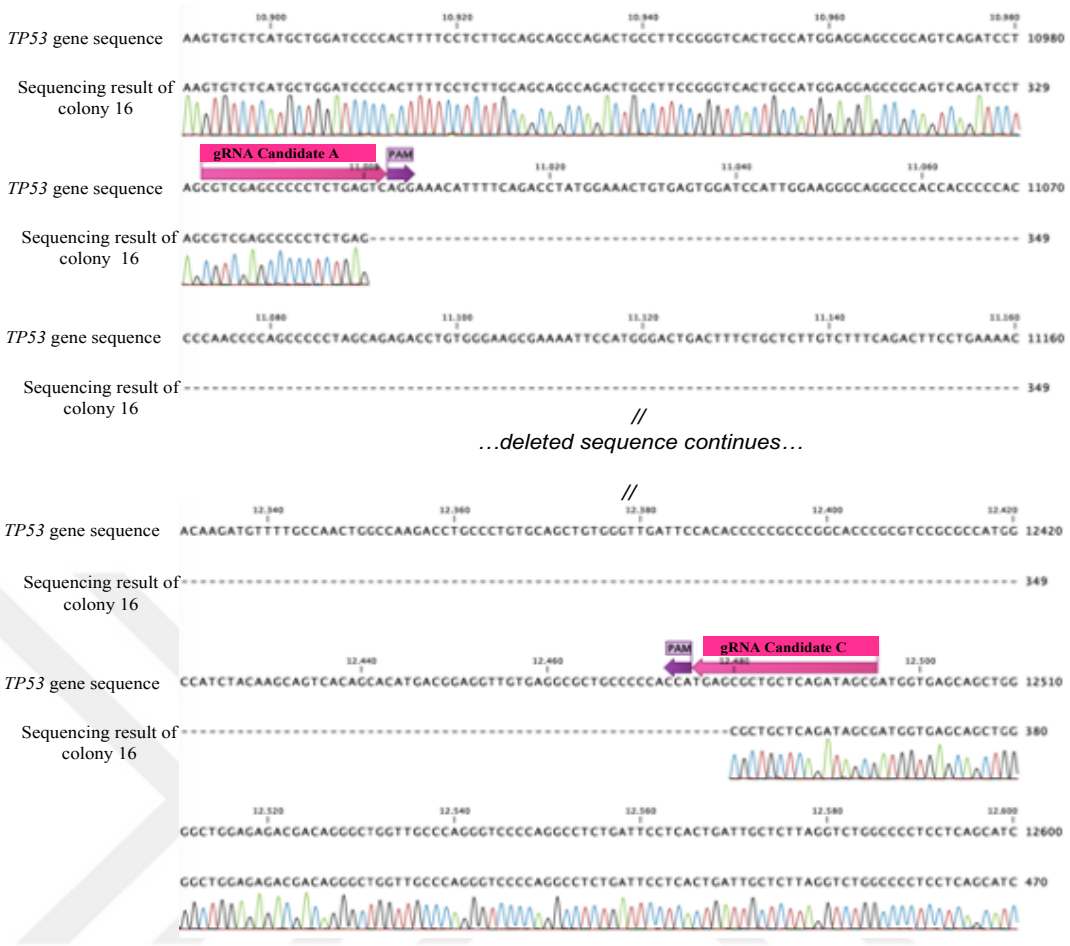

Figure 4.34 Sanger sequencing result of single cell colony 16. Sequence in between upstream target region and downstream target region of colony 16 was compared with WT *TP53* sequence using CLC Main Workbench Software. The sequences of gRNA A and gRNA C are indicated with pink arrows, and their PAM sequences are indicated with purple arrows in the reference *TP53* gene sequence.

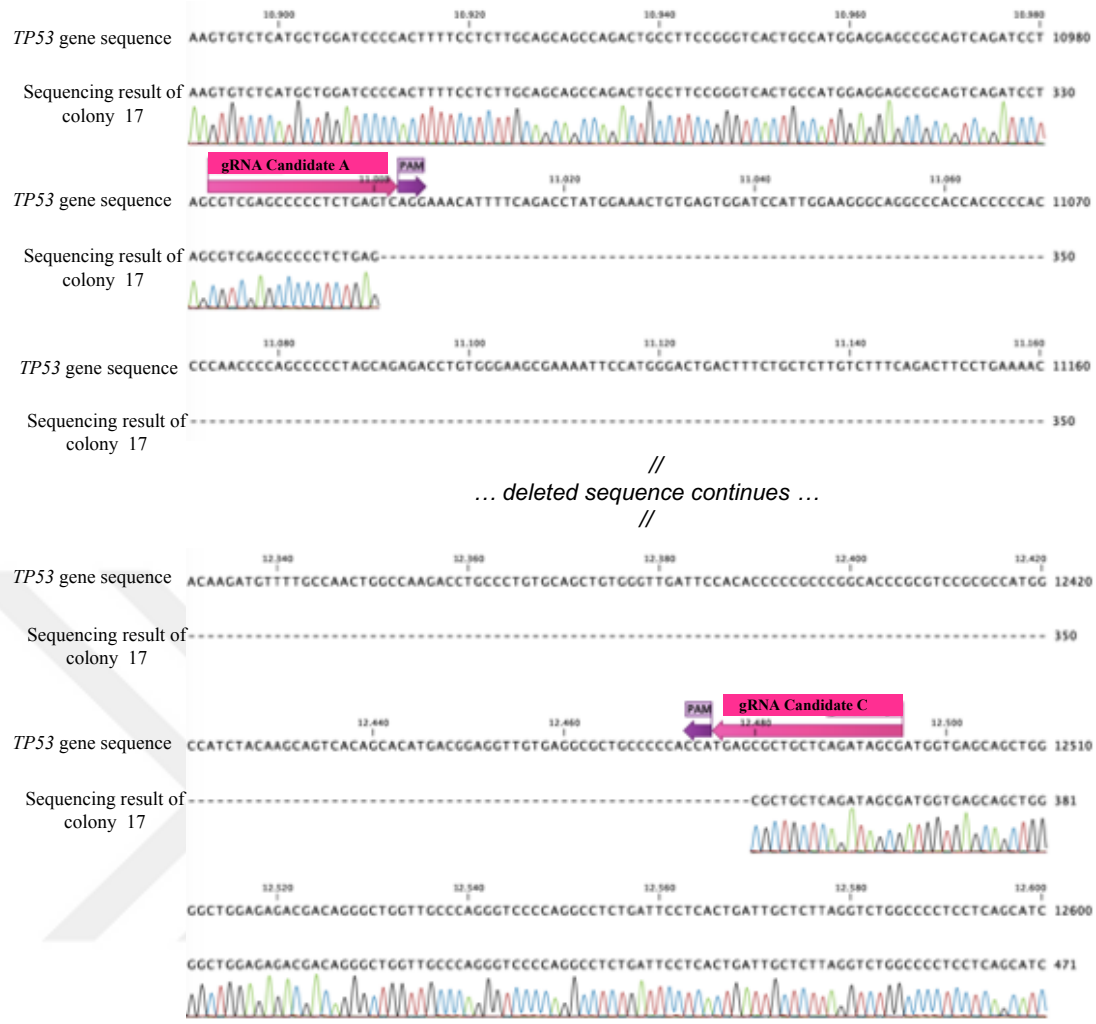

Figure 4.35 Sanger sequencing result of single cell colony 17. Sequence in between upstream target region and downstream target region of colony 17 was compared with WT *TP53* sequence using CLC Main Workbench Software. The sequences of gRNA A and gRNA C are indicated with pink arrows, and their PAM sequences are indicated with purple arrows in the reference *TP53* gene sequence.

4.9.Off-Target Analysis of the Single-Cell Colonies Showing $p53^{-/-}$ Profile

In order to check if there is any off-target effect of the CRISPR A + CRISPR C pair in these single cell colonies, the most probable off-target sites for both gRNA A and gRNA C were analyzed with T7EI assay.

CRISPR A Off-Target region of untransfected (WT) cells, CRISPR NT-C1 + CRISPR NT-C2 co-transfected cells and single cell colonies showing $p53^{-/-}$ profile (colony 2, colony 16 and colony 17) were PCR amplified by using CRISPR_A_Off_ Target_fwd and CRISPR_A_Off_Target_rev primers. These the PCR products were subjected to T7EI assay. As seen from Figure 4.36, in the presence of T7EI the PCR products of single cell clones showing $p53^{-/-}$ profile, were still intact and not digested similar to untransfected (WT) cells and non-targeting control (CRISPR NT-C1 + CRISPR NT-C2) co-transfected cells. This result indicates that there was no off-target effect of CRISPR A.

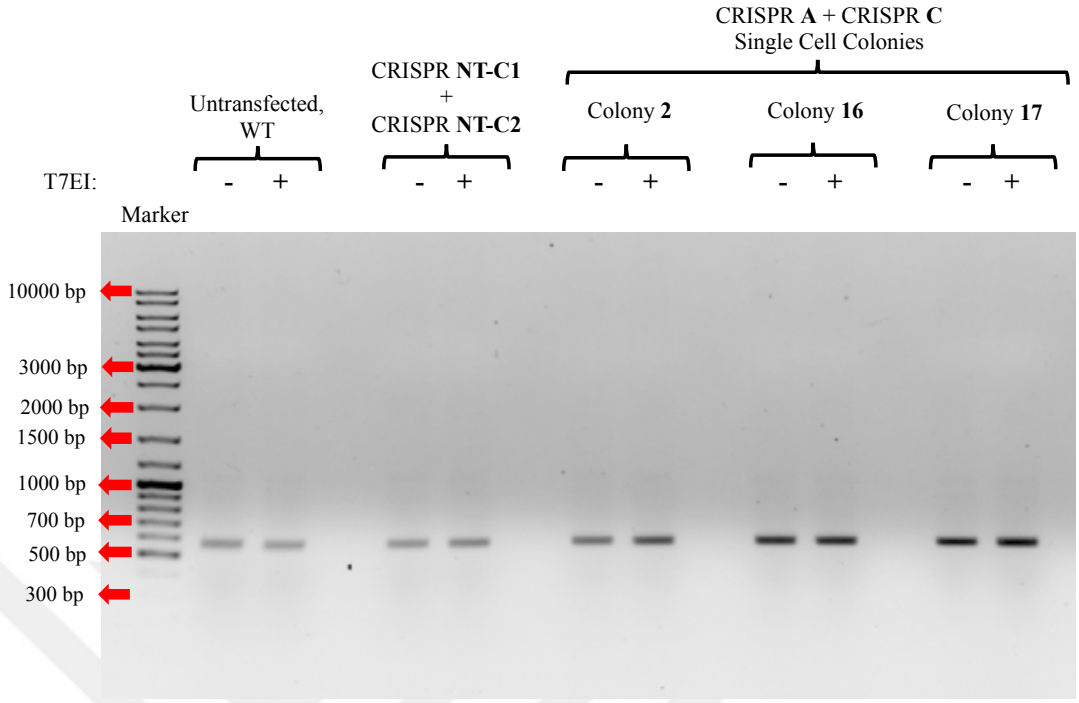

Figure 4.36 Off-target analysis of CRISPR A. CRISPR A off-target region of untransfected (WT) cells, NT-C1+NT-C2 co-transfected cells, single cell colonies showing $p53^{-/-}$ profile were PCR amplified by using CRISPR_A_Off_Target_fwd and CRISPR_ A_Off_Target_rev primers. The PCR product size is 567 bp and with these PCR products, T7EI assay was performed. The products were loaded into 2% agarose gel and run at 100 V for 60 min. Sizes of some marker bands are indicated with red arrows. (-) shows the absence of T7EI and (+) shows the presence of T7EI.

CRISPR C Off-Target region of untransfected (WT) cells, CRISPR NT-C1 + CRISPR NT- C2 co-transfected cells and single cell colonies showing $p53^{-/-}$ profile (colony 2, colony 16 and colony 17) were PCR amplified by using CRISPR_C_Off_ Target_fwd and CRISPR_C_Off_Target_rev primers. These the PCR products were subjected to T7EI assay. As seen from Figure 4.37, in the presence of T7EI the PCR products of single cell clones showing $p53^{-/-}$ profile, were still intact and not digested similar to untransfected (WT) cells and non-targeting control (CRISPR NT-C1 + CRISPR NT-C2) co-transfected cells. This result indicates that there was no off-target effect of CRISPR C.

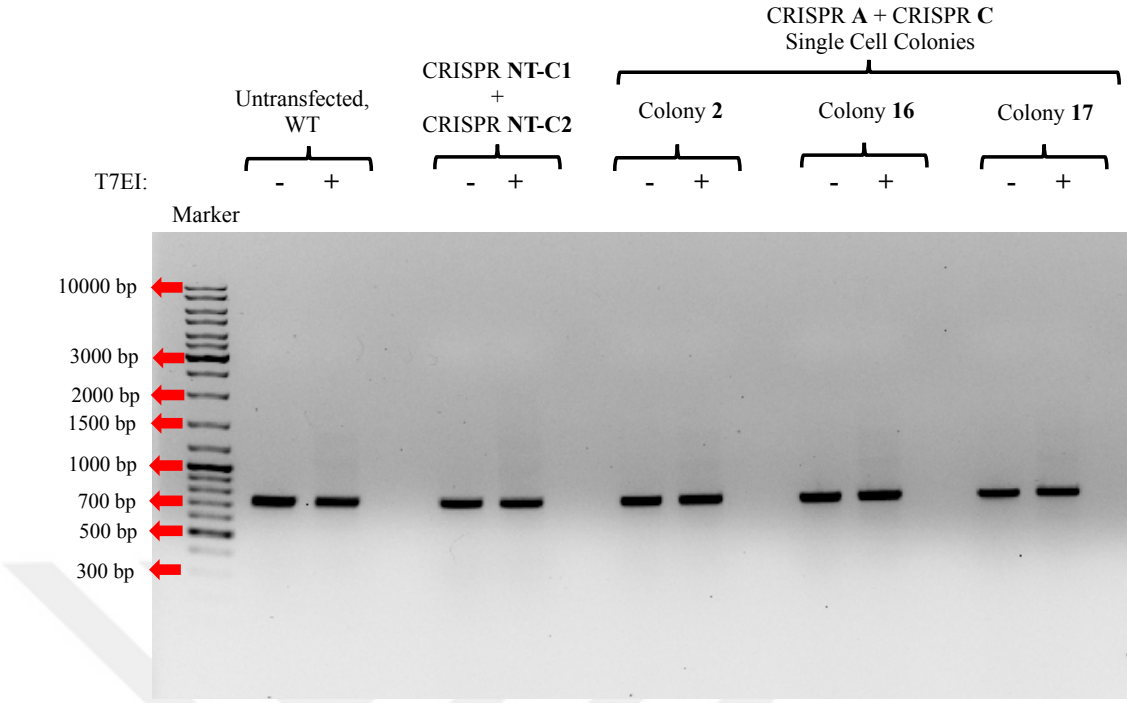

Figure 4.37 Off-target analysis of CRISPR C. CRISPR C off-target region of untransfected (WT) cells, NT- C1+NT- C2 co-transfected cells, single cell colonies showing $p53^{-/-}$ profile were PCR amplified by using CRISPR_C_Off_Target_fwd and CRISPR_ C_Off_Target_rev primers. The PCR product size is 747 bp and with these PCR products, T7EI assay was performed. The products were loaded into 2% agarose gel and run at 100 V for 60 min. Sizes of some marker bands are indicated with red arrows. (-) shows the absence of T7EI and (+) shows the presence of T7EI.

4.10. Western Blot Results of Single Cell Colonies Showing $p53^{-/-}$ Profile

p53 protein levels of untransfected cells (WT), non-targeting control (CRISPR NT-C1+ CRISPR NT-C2) co-transfected cell pool, CRISPR A + CRISPR C co-transfected cell pool and single cell colonies showing $p53^{-/-}$ profile (colony 2, colony 16 and colony 17) were assessed by western blot. As seen from Figure 4.38, the p53 protein was expressed in untransfected cells (WT), non-targeting control (CRISPR NT-C1+ CRISPR NT-C2) co-transfected cell pool, CRISPR A + CRISPR C co-transfected cell pool. On the other hand, the p53 protein expression was not

detected in the single cell colonies (colony 2, colony 16 and colony 17) which were derived from CRISPR A + CRISPR C cell pool. β-actin was used as loading control and as it can be seen, the protein levels of β-actin were similar in all samples.

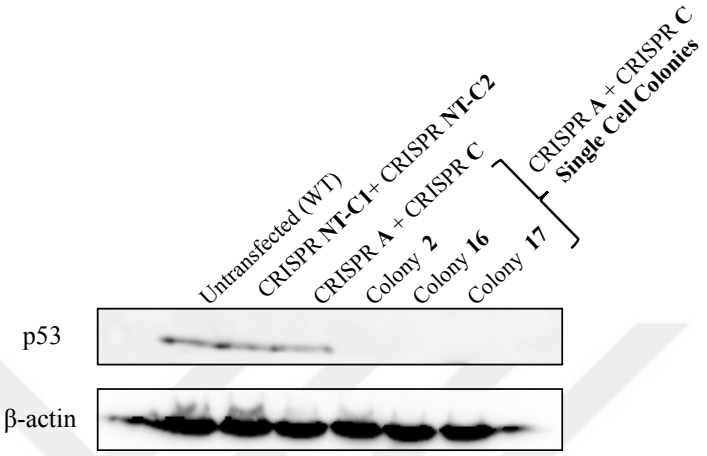

Figure 4.38 Confirmation of p53 expression loss in single cell colonies 2, 16 and 17. Western blotting was performed by using the whole cell lysates that were extracted from untransfected (WT) cells, non-targeting control co-transfected cell pool (CRISPR NT-C1+ CRISPR NT-C2), CRISPR A + CRISPR C co-transfected cell pool and single cell colonies 2, 16 and 17. The western blot result showing p53 expression, is shown in the upper panel. In the lower panel, the western blot result of β-actin, as house-keeping control, is shown. The membranes were visualized by using BioRad ChemiDoc MP Imaging System.

4.11. Characterization of U87-MG $p53^{-/-}$ Cell Line

Among the three single cells colonies of which $p53^{-/-}$ profile were confirmed at both gene and protein levels with no off-target effect, single cell colony 2 was continued with for further characterization experiments. In the following sections, single cell colony 2 is named as U87-MG $p53^{-/-}$ cell line.

4.11.1. Characterization of U87-MG p53$^{-/-}$ Cells: Cell Proliferation

As it is known that p53 controls cell proliferation, the first characterization aspect for the newly generated U87-MG p53$^{-/-}$ cells was cell proliferation difference compared to U87-MG cells. The proliferation of U87-MG (WT) cells and U87-MG p53$^{-/-}$ cells were determined by trypan blue exclusion assay in a time-dependent manner. The live cell number was determined 24h, 48h, 72h, 96h and 120h after seeding. This experiment was repeated three different times with three replicates. As seen in Figure 4.39, U87-MG p53$^{-/-}$ cells proliferated significantly faster than U87-MG (WT) cells.

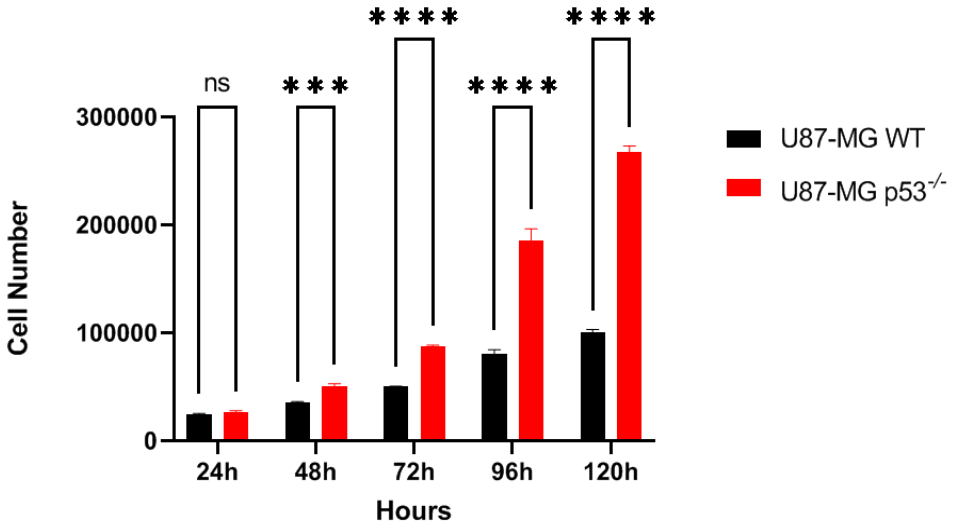

Figure 4.39 The results of trypan blue exclusion assay. 24h, 48h, 72h, 96h and 120h after cell seed, the viable U87-MG (WT) and U87-MG p53$^{-/-}$ cells were determined by trypan blue exclusion assay. The black bars indicate the number of viable U87-MG (WT) cells and the red bars indicate the number of viable U87-MG p53$^{-/-}$ cells at the indicated time points. The results of three independent experiments each of which had three technical replicates were analyzed by two-way ANOVA statistical test. p values less than 0.0001 ($p < 0.0001$) are shown with four asterisks. p values less than 0.001 ($p < 0.001$) are shown with three asterisks. “ns” is indicating “not significant”.

4.11.2. Characterization of U87-MG $p53^{-/-}$ Cells: Migration

In order to characterize the newly generated $p53^{-/-}$ cell line further, migration abilities of U87-MG (WT) cells and U87-MG $p53^{-/-}$ cells were also compared by wound healing assay. 24h, 48h and 72 h after formation of the wound area, the closure of the wound was traced. For each time point, the wound closure percentage was calculated by considering the initial wound area (WA_0). In this experimental set up, there were two growth medium conditions: 1%FBS and 10%FBS. 1%FBS condition was used for testing the migration abilities of the cells and 10% FBS condition was the control of the experiment. In Figure 4.40, the representative images of the results of three different experiments each of which had three replicates, are shown. As seen in Figures 4.40 and 4.41, in 10%FBS condition, 24h and 48h after the wound formation, the wound closure percentages of U87-MG $p53^{-/-}$ cells were significantly higher than that of U87-MG WT cells. 72h after the wound formation, there was not a significant change in the wound closure percentages of U87-MG WT and U87-MG $p53^{-/-}$ cells. In 1%FBS conditions, the wound closure percentages of U87-MG WT and U87-MG $p53^{-/-}$ cells were not significantly different in any time points. These results indicate that there was not a significant difference in the migration abilities of U87-MG WT and U87-MG $p53^{-/-}$ cells in 1% FBS conditions.

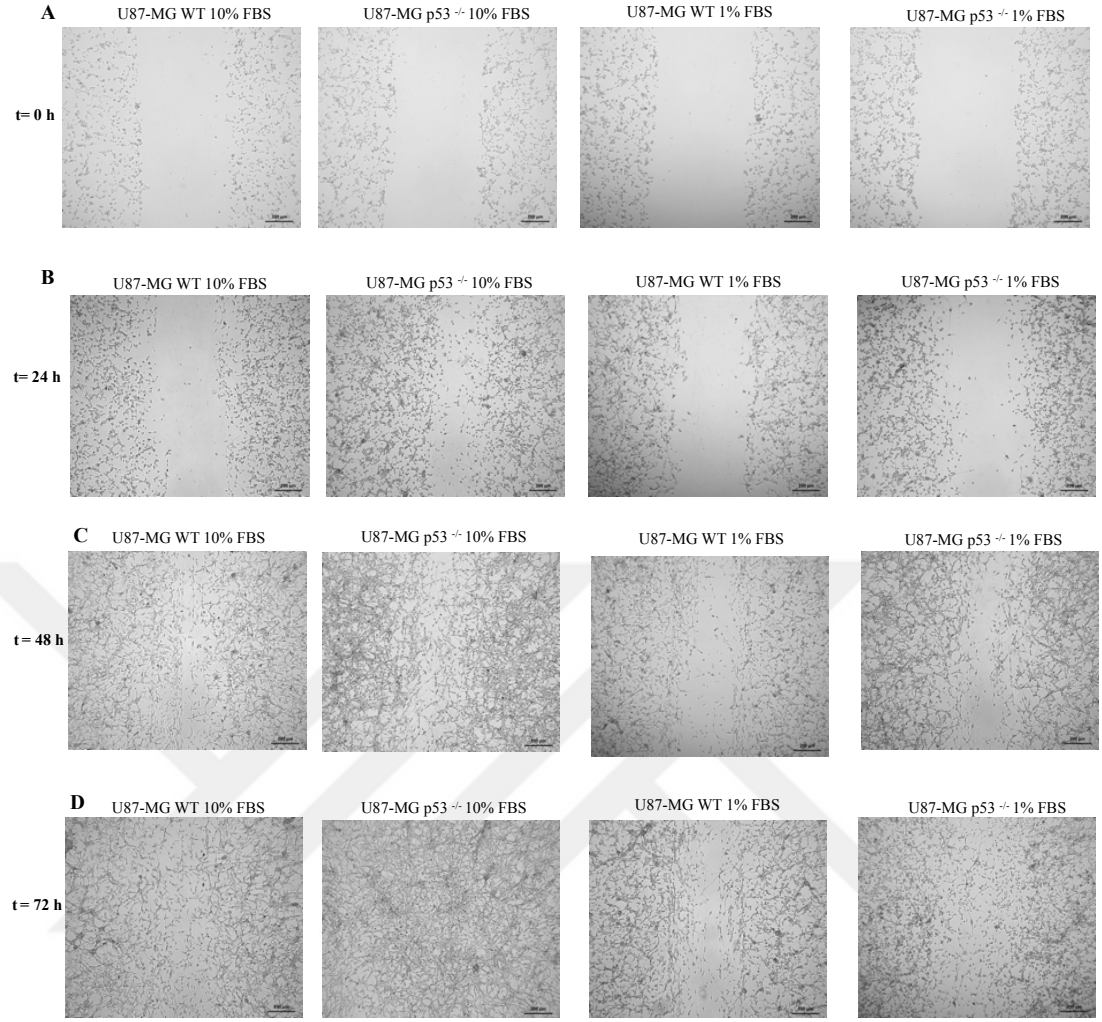

Figure 4.40 Microscopy images of the wound healing assay. 24h after cell seed, the cell-free wound area was created (t = 0) and this area was visualized at 0h, 24h, 48h and 72h after its formation by using ZEISS Axio Vert.A1 inverted microscope in bright field channel. This experiment was repeated three times and each of the experiments had three replicates. Representative microscopy images for each sample show the wound area at (A) t = 0h (B) t = 24h (C) t = 48h and (D) t = 72h time points.

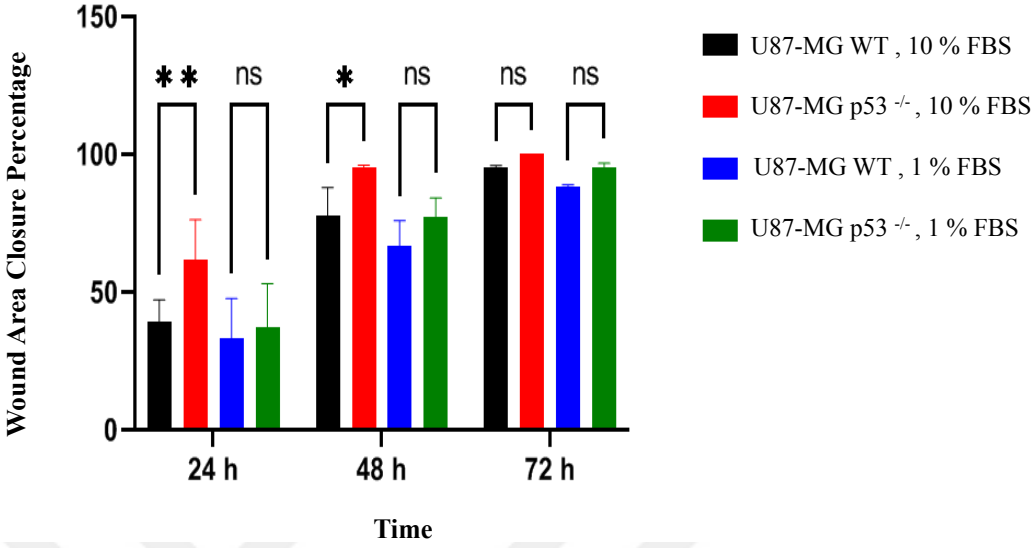

Figure 4.41 Results of the wound healing assay. 24h after cell seed, the cell-free wound area was created (t = 0) and 0h, 24h, 48h and 72h after its formation, this area was visualized by using ZEISS Axio Vert.A1 inverted microscope in bright field channel. This experiment was repeated three times and each of the experiments had three replicates. (Representative images are shown in Figure 4.40) The wound areas at the indicated time points were quantified by using MRI Wound Healing Tool Image J macros and wound closure percentage was calculated as explained in section 3.2.10. The results were analyzed by two-way ANOVA statistical test. p values less than 0.05 ($p < 0.05$) are shown with one asterisk and p values less than 0.01 ($p < 0.01$) are shown with two asterisks. "ns" is indicating "not significant". The color codes of the samples are shown on the right panel.

4.11.3. Characterization of U87-MG $p53^{-/-}$ Cells: Colony Formation

For further characterization of newly generated $p53^{-/-}$ cell line, the colony formation abilities U87-MG (WT) cells and U87-MG $p53^{-/-}$ cells were compared by colony formation assay. In this assay, 2000 cells/well were seeded in 6-well plates and after 20 days, the cells were stained with crystal violet to visualize the forming colonies. The representative images of the colonies formed by U87-MG (WT) cells

and U87-MG $p53^{-/-}$ cells are shown in Figure 4.42A. In addition, in order to quantify the visible results, after solubilization of the crystal violet that stained the cells in each well, the absorbance was measured at 590 nm. In Figure 4.43B, the results of three different experiments each of which had three replicates, are shown. Considering the results shown in Figure 4.43, the colony formation ability of U87-MG $p53^{-/-}$ cells are significantly higher than U87-MG (WT) cells.

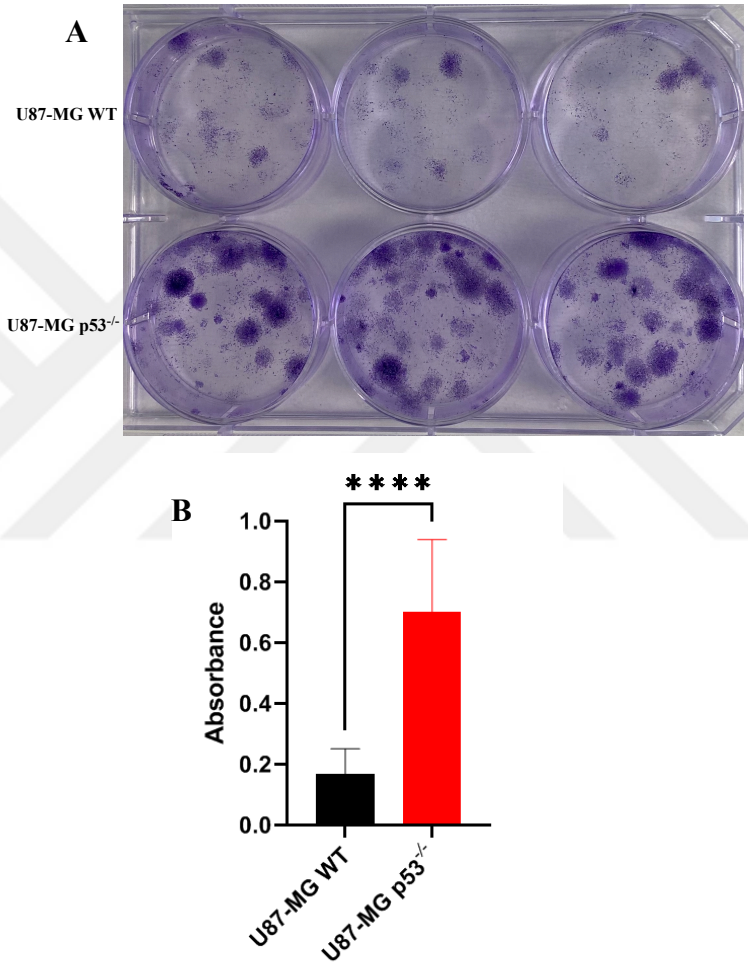

Figure 4.42 Results of the colony formation assay. 2000 cells/well were seeded in 6-well plates and after 20 days, the cells were stained with crystal violet to visualize the forming colonies. This experiment was repeated three times with three replicates. **(A)** Representative images of colonies formed by U87-MG cells and U87-MG $p53^{-/-}$ cells **(B)** Quantification of the crystal violet dye that stained the cells. The black bars indicate U87-MG (WT) cells and the red bars indicate the U87-MG $p53^{-/-}$ cells. The results were analyzed by using student two sample t-test. p values less than 0.0001 ($p < 0.0001$) are shown with four asterisks.

5. DISCUSSION AND COCLUSION

p53 is a tumor suppressor protein that has crucial roles in cell cycle, senescence, apoptosis, autophagy, cell metabolism and DNA repair (146). The p53 protein is found to be mutant in 50% of cancers (1). In 85% of glioblastoma tumors, p53 and the p53 signaling pathway are deregulated (147). In order to study mutant p53 protein in glioblastoma cell line model which lacks p53 expression, is needed. Therefore, the aim of this thesis aim was to create a p53 knockout glioblastoma cell line via targeting the *TP53* gene locus by CRISPR/ Cas9 system.

Before constructing the CRISPR plasmids, the pSp-Cas9(BB)-2A-Puro (PX459) V2.0 plasmid was digested with different restriction enzymes to confirm the plasmid prior to all experiments. Seven diagnostic digestions, which were theoretically ending up with a unique band patterns, were performed. The sizes of the digestion products were consistent with the expected sizes based on the plasmid map. Therefore, the plasmid was considered to be correct and used for further cloning experiments.

As can be seen in Figure 3.1, the *TP53* gene has three different promoters that are used to express the full-length p53 protein and its isoforms. Therefore, in order to guarantee the inhibition of the expression of all p53 isoforms, two target regions (upstream target region and downstream target region) were determined in the *TP53* gene locus to target with CRISPR/Cas9 system. For each target region, two guide RNAs were designed: gRNA A, gRNA B, gRNA C and gRNA D. The sequences of two non-targeting gRNAs (gRNA NT-C1 and gRNA NT-C2) were obtained from (148). A crucial step before starting CRISPR/Cas9 genome editing system was the design of gRNA candidates. lt is known that one of the limitations of CRISPR is off-

target effects. In order to avoid off-target effects and to achieve the highest editing efficiency of the gRNA at the target site, gRNAs should be designed with a length of 17-24 base pairs. Shorter gRNA sequences would be expected to minimize off-target effects. The GC content of the gRNA was another important consideration in gRNA design. The range of GC content should be 40-80 % in total. lf the GC content is high, lt is known that RNA-DNA duplex is stabilized and off-target effect is prevented due to destabilizing off-target hybridization (145,149,150,151,152,153). gRNA A, B, C and D were designed by considering the predicted efficiency, IN-DEL, out-of-frame and off-target scores.

Four gRNA candidates (gRNA A, gRNA B, gRNA C and gRNA D) and two non-targeting gRNA controls (NT-C1 and NT-C2) were annealed and phosphorylated for ligation step. The annealing reaction products were run in agarose gel which was stained with EtBr. EtBr is an intercalating agent and it is known to stain dsDNA more effectively than ssDNA (154,155,156). Therefore, the annealed oligonucleotide lanes were brighter than the top and bottom oligonucleotide lanes for each gRNA. The faint bands that were seen in some top and/or bottom oligonucleotide lanes although they were single stranded DNA, might be due to self-annealing of the individual oligonucleotides. Self-annealing is most commonly seen in repeat sequences or in oligonucleotides that are high in GC content (157). Single stranded product has open conformation, resulting in a higher stokes radius, more drag and run faster (158).

Annealed oligonucleotides for each gRNA candidates were ligated to pSp-Cas9(BB)-2A-Puro (PX459) V2.0 plasmid by using Golden Gate assembly. Type IIS restriction enzymes such as BbsI and BsmBI are used for Golden Gate assembly. The BbsI restriction enzyme recognizes its restriction site and digests the pSp-Cas9(BB)-2A-Puro (PX459) V2.0 plasmid from outsite of recognition sequence to form sticky

ends. Annealed oligonucleotides with their phosphorylated ends were ligated to the digested pSp-Cas9(BB)-2A-Puro (PX459) V2.0 plasmid. As negative control of the ligation reactions, there were also ligation reactions without insert (annealed oligonucleotides) in order to see the efficiency of cloning. Because if there were empty undigested plasmids and/or self-ligated empty plasmids, they would also cause colony growth.

After ligation, the ligation products were treated with Exonuclease V enzyme, which degrades single-stranded DNA but does not harm the circular DNA. After treatment; cloned plasmids were transformed into chemically competent *E. coli* (DH5α). In the samples without insert (annealed oligos), there were no colonies. However, for each CRISPR cloning reaction, there were at least 300-350 colonies on LB Agar plates with Ampicillin. This amplification in colony number, was an indicator of successful cloning of annealed oligos into pSp-Cas9(BB)-2A-Puro (PX459) V2.0 plasmid.

For each cloning, 10 colonies were selected after transformation. In order to find the correctly cloned CRISPR plasmids, the plasmid DNAs were isolated from bacterial colonies and screened by performing PCR. In all PCR reactions, there was PCR negative control that did not contain template in the reaction. As there were not any PCR products in the PCR negative control samples, the PCR products observed in template containing samples were concluded to be specific. Size of the PCR products was matching with the expected band size considering the theoretical sequence after cloning. As it can be seen from the Figures 4.3.- 4.8, the presence of the insert was confirmed in the plasmid DNAs of 10 out of 10 bacterial colonies for CRISPR A, C and D cloning and 9 out of 10 bacterial colonies for CRISPR B cloning. These results indicated that the efficiency of the CRISPR plasmid construction was high. For each cloning, cloned plasmids from three different

bacterial colonies were sequenced for further confirmation. As shown in Figures 4.9 - 4.14, for each cloning out of three clones, at least one clone has 100 % correct DNA sequence when compared with the hypothetical plasmid sequence after cloning.

Prior to enrichment steps after transfections, puromycin concentration was determined. In the literature, the concentrations of puromycin used for selection of U87-MG cells are variable (from 0.8 μg/mL to 5 μg/mL) (159,160). In order to determine concentration for this enrichment, U87-MG cells were treated with different concentrations of Puromycin (0.1 μg/mL, 0.25 μg/mL, 0.5 μg/mL, 1 μg/mL, 2 μg/mL, 3 μg/mL, 4 μg/mL and 5 μg/mL) for one week. Cell viability percent was quantified by performing trypan blue exclusion assay. Trypan blue dye stains dead cells. Live cells are seen as unstained or colorless. For 1 μg/mL concentration and all the above concentrations of Puromycin, there were no viable cells. For 0.5 μg/mL concentration of Puromycin, cell viability was 0.18 %. In order to avoid CRISPR/Cas9 stable expression due to integration into the genome and to achieve enrichment rather than selection, 0.5 μg/mL was determined as the optimum Puromycin concentration for U87-MG cells.

U87-MG cells are considered as hard to transfect cells (161). Lipofectamine 3000, which is the transfection reagent, is the most commonly used reagent for the transfection of U87-MG cells (162,163,164,165,166). Most of the transfection reagents are toxic for the cells (167,168). Therefore, for highest cell viability and transfection efficiency, the DNA:transfection reagent ratio should be optimized. In this study, transfection experiments were performed in two different scales: small-scale and large-scale transfections. Small-scale transfections were performed in 6-well plates with $3x10^5$ cells/well whereas large-scale transfections were performed in 100-mm cell culture petri dishes with $3x10^6$ cells/dish. For small-scale transfection optimizations, three different DNA:Lipofectamine 3000 ratios were tested: ratios of

1:1.5, 1:3 and 1:5. 48 h after transfection, the GFP expressing cells were visualized in the FITC channel of fluorescent microscope.

As shown in Figure 4.16, as the pcDNAGFP:Lipofectamine 3000 ratio increased, the number of GFP expressing cells also increased. After fluorescent microscopy analysis, for quantification of the GFP positive cell percent in the cell population, flow cytometry analysis was performed. Flow cytometry is a method for analysis of single cell or multiple cells in suspended salt-based buffer solution. There are two types of scatter for the visible light: Forward Scatter (FSC) and Side Scatter (SSC). X-axis (FSC) represents cell size. Y-axis (SSC) represents granularity of the cell (169,170,171,172). By considering FSC vs SSC dot plots, the gate for the live cell population was determined as P1 gate. For the live cell population gate (P1), FITC histograms were plotted to observe the GFP positive cells. By using the untransfected cells (GFP negative cells), the threshold for GFP expression and the gate for GFP expressing cells (P2) were determined. By considering the GFP positive cell percent, the transfection efficiency was evaluated for each sample. As it can be seen from Figure 4.17, for small-scale transfections, the highest transfection efficiency was 72.84% when the DNA:Lipofectamine 3000 ratio was 1:5. However, cells were resembling apoptotic cell morphology. When cells undergo apoptosis, cells swell and increase in their granularity. In late apoptosis, cells burst and shrink (173,174). By considering not only GFP expression level but also their healthy morphology, among the three different conditions, 1:3 ratio was determined as the optimum DNA:Lipofectamine 3000 ratio. For large-scale transfection optimizations, two different DNA:Lipofectamine 3000 ratios were tested: ratios of 1:1.5 and 1:3. As shown in Figures 4.25 and 4.26, as the DNA:Lipofectamine 3000 increased, the number of GFP expressing cells also increased. By considering both microscopy and flow cytometry results, 1:3 was determined as the optimum DNA:Lipofectamine 3000 ratio. The percentage of GFP positive cells in the 1:3 ratio pcDNAGFP:Lipofectamine 3000 for small-scale and large-scale transections was 60.37 % and 47.46 %, respectively. It can be clearly seen that although the optimum

DNA:Lipofectamine 3000 ratio was same for both small-scale and large-scale transfections, the transfection efficiencies were not the same. As the scale of the transfection experiment increases, in other words as there were more cells, more DNA and larger area for growth, the transfection was more difficult.

DSBs are generated by CRISPR-Cas9 to activate DNA repair mechanisms for genome editing. Small insertions or deletions (IN-DELs) and other complex by-products, including large deletions, result from the repair of DSBs. RFLP and T7EI assays are most commonly used assays to analyze the gene editing performance. To assess the gene editing performance of CRISPR candidates with RFLP, the upstream and downstream target regions were amplified by performing PCR with region specific primers. The recognition sites of the restriction enzymes were expected to be destroyed as a result of CRISPR activity so that the restriction enzymes could no longer recognize and cleave the restriction site. Therefore, in the RFLP assays, the PCR product of the upstream target region A was digested with HinfI enzyme to show CRISPR A activity, the PCR product of the upstream target region B was digested with NciI enzyme to show CRISPR B activity, the PCR product of the downstream target region was digested with Aor51HI (AfeI) enzyme to show CRISPR C activity and the PCR product of the downstream target region was digested with HinfI enzyme was used to show CRISPR D activity. In the presence of restriction enzymes, PCR product of the wild type (WT, untransfected cells) and non-targeting controls (NT-C1 and NT-C2) populations, were cleaved into two digestion products. For the cell populations that were transfected with either CRISPR A or CRISPR B, in addition to the cleaved PCR products, there were also undigested PCR products indicating the destruction of the restriction sites due to IN-DELs caused by CRISPR activity. However, the uncut band intensity was similar to the control groups for CRISPR C and CRISPR D in the presence of restriction enzymes as shown in Figures 4.18, 4.20, 4.22 and 4.24.

T7 endonuclease I (T7EI) assays are also performed to determine the gene editing performance of CRISPR candidates at their specific target site. In the T7EI assay, target regions were PCR amplified with site specific primers. Heteroduplexes were formed after denaturation and re-annealing of the PCR product due to IN-DELs. T7EI is capable of recognizing and cleaving these unmatched DNA sequences. After PCR amplification of the target regions, the PCR products were subjected to T7EI protocol and the band patterns in the absence and presence of T7EI were analyzed. In the presence of T7EI, the denatured and re-annealed PCR products of the wild type (WT, untransfected cells) and non-targeting control transfected cells (NT-C1 and NT-C2) were intact due to lack of CRISPR activity. The denatured and re-annealed PCR products of the cells that were transfected with CRISPR candidates were efficiently digested in the presence of T7EI, indicating the activity of CRISPR A, B and C in their target region. However, in CRISPR D transfected cells, in the presence of T7EI, only a minute portion of the denatured and re-annealed PCR product was digested.

The sensitivity of RFLP assay and the T7EI assay are different from each other. Although the activity of CRISPR C was not clearly evident from the results of the RFLP assay, the results of the T7EI assay indicated that CRISPR C was also able to edit its target site efficiently. The RFLP assay detects only IN-DELs that are generated in the restriction site in the target region. However, in T7EI assay, IN-DELs in the entire target region can be detected. Therefore, the difference between the results of two assays may be due to the IN-DELs not being located at the restriction site but at another site in the target region. Although CRISPR A, B and C were efficient in editing their specific target regions, CRISPR D was not as successful as the other CRISPR candidates in editing its specific target by considering its RFLP and T7EI assay results.

As mentioned before, CRISPR A and B were designed for upstream target region whereas CRISPR C and D were designed for downstream target region. Therefore, for the desired deletion in the genome, CRISPR A + CRISPR C, CRISPR A + CRISPR D, CRISPR B + CRISPR C and CRISPR B + CRISPR D were co-transfected to U87-MG cells. As the negative control of the gene editing, CRISPR NT-C1 + CRISPR NT-C2 were co-transfected to U87-MG cells. After genomic DNA isolation from these cells, the region starting with upstream target region and ending with downstream target region was PCR amplified.

For untransfected (WT) cells and the cells co-transfected with CRISPR NT-C1 + NT-C2, the size of the amplified PCR product was 2022 bp. However, for each CRISPR pair co-transfected sample, in addition to WT PCR product, there was a new and shorter PCR product (indicated with blue arrows in Figure 4.27) due to CRISPR pair activity. As shown in Figure 4.27, for U87-MG cells that were co-transfected with CRISPR pairs, in addition to the expected PCR products there were also other new PCR products of different lengths which may be due to IN-DELs and/or deletions in the target region. As the CRISPR pair co-transfected cells were cell pools, it is possible to have multiple versions of mutations in the cell pool due to CRISPR activity. The PCR amplifications were repeated including the CRISPR single-transfected samples to show the specificity of the new PCR products generated only by the activity of the CRISPR pairs. The CRISPR candidates were unable to delete the desired regions when they were transfected individually as shown in Figures 4.28, 4.29, 4.30 and 4.31. In other words, the desired deletions in between the upstream and downstream target regions were observed only in the presence of CRISPRs as pairs. This indicates the specificity of the PCR products that were produced as a result of CRISPR pair activity. Interestingly, the gene editing efficiencies of these CRISPR candidates were much higher when they were co-transfected as pairs.

By considering the genotyping PCR results of CRISPR pair co-transfected cell pools, all CRISPR pairs (CRISPR A + CRISPR C, CRISPR A + CRISPR D, CRISPR B + CRISPR C and CRISPR B + CRISPR D), managed to delete the sequences in between their target sites. In the beginning, the aim was to find the CRISPR pair that would efficiently delete the desired region between the target sites in the *TP53* gene locus. However, all CRISPR pairs worked efficiently and therefore the strategy for the selection of the CRISPR pairs for further studies has been changed. As CRISPR A + CRISPR C pairs delete the longest region in the *TP53* gene locus, CRISPR A + CRISPR C co-transfected cells were selected in order to find the single cell clone bearing biallelic deletion in the *TP53* gene locus.

CRISPR A + CRISPR C co-transfected cells were actually a cell pool that was composed of cells with different genotypes. Because after the delivery of the plasmids of the CRISPR pair, there were different possibilities. For example, the uptake of neither CRISPR A or CRISPR C by some cells, the uptake of only CRISPR A or CRISPR C by some cells or although the uptake of CRISPR pairs, monoallelic deletion by some cells or the uptake of CRISPR pairs and biallelic deletion by some cells. Therefore, single cell cloning was performed to find the cell clone that had the homozygous deletion in the TP53 gene locus. In order to screen single cell colonies, PCR reactions were carried out to amplify the region in between the upstream target region and the downstream target region by performing PCR. Among the 40 single cell colonies, one colony (colony 3) showed $p53^{+/-}$ profile by ending up with both a WT PCR product and a PCR product indicating the desired deletion in the *TP53* gene locus. In addition, there were three colonies (colony 2, colony 16 and colony 17) showing $p53^{-/-}$ profile by ending up with a single PCR product as a result of the desired deletion in the *TP53* gene locus. The remaining colonies showed the WT profile. According to the single cell cloning, the number of $p53^{-/-}$ colonies was higher than that $p53^{+/-}$ cells. Seeding the cell at low density is the stressful process for the cells. Therefore, $p53^{-/-}$ cells cope with stress by preventing cell cycle arrest and inhibiting apoptosis compared to $p53^{+/-}$ cells (175). Proliferation

rate of the $p53^{-/-}$ cells is faster than that of $p53^{+/-}$ cells (176). Therefore, $p53^{-/-}$ cells have selective advantage as a result of their genotype.

In order to confirm the deletion in between the upstream and downstream target regions of the *TP53* gene locus, the PCR products from the single cell colonies, that showed $p53^{-/-}$ profile (colony 2, colony 16 and colony 17), were sequenced. As clearly seen from Figures 4.33, 4.34 and 4.35, the desired regions were deleted in the TP53 gene locus of these three colonies.

One of the limitations of the CRISPR/Cas9 system is the off-target effect. Off-target effect is non-specific and/or undesired genomic modification in the genome. Designed gRNA targets different regions of the genome with low affinity and gRNA can tolerate one/or more mismatches. The designed gRNA recognizes genomic loci with sequences that are similar to the target, and then Cas9 acts on non-targeted sites in the genome to generate cleavages. In off target effect, mismatches that are close to the 5' region of the target site are better tolerated by gRNA but, mismatches that close to the 3' region of the target site are not better tolerated by gRNA due to the PAM recognition sequence. In order to reduce the off-target effect, gRNAs are designed with the lowest off-target score. Lowest off-target score means highest score to guide detection (116,177). In order to check if there is any off-target effect of the CRISPR A + CRISPR C pair in these single cell colonies, the most probable off-target sites for both gRNA A and gRNA C were analyzed by performing T7EI assay. CRISPR A and C off-target regions of untransfected (WT) cells, CRISPR NT-C1 + NT-C2 co-transfected cells and colonies showing $p53^{-/-}$ profile (colony 2, colony 16 and colony 17) were PCR amplified. As seen in Figures 4.36 and 4.37, the denatured and re-annealed PCR products of the single colonies having $p53^{-/-}$ profile were intact in the presence of T7EI similar to all negative controls. These results indicate that there were no off-target effects.

Although the biallelic deletion in the TP53 gene locus was confirmed in colony 2, 16 and 17, the lack of p53 protein expression had to be also confirmed as the aim was the inhibition of p53 protein expression in the newly generated cell line. Therefore, p53 protein levels of untransfected cells (WT), non-targeting control (CRISPR NT-C1+ NT-C2) co-transfected cell pool, CRISPR A + CRISPR C co-transfected cell pool and colonies showing $p53^{-/-}$ profile (colony 2, colony 16 and colony 17) were determined by performing Western Blot. The expression of the endogenous p53 protein was detected in untransfected (WT), non-targeting control (NT-C1 + NT-C2) co-transfected cells and CRISPR A+ CRISPR C co-transfected cells whereas in the colonies showing the $p53^{-/-}$ profile (colony 2, colony 16 and colony 17) p53 protein expression was not detected.CRISPR A+ CRISPR C co-transfected cells was a cell pool so in addition to gene edited cells, there were also WT cells in which there were no CRISPR activity therefore there was p53 protein expression. As β-actin is a housekeeping protein, it was used as a loading control in the western blot experiment. In normal conditions, the endogenous p53 protein expression is low (64). In order to detect the expression of the p53 protein in the western blot experiment, a high amount of the total protein extract (50 μg) was loaded to each well of the SDS gel. Therefore, even at low exposure, the band intensities of housekeeping β-actin protein were saturated. By considering the western blot results, it is concluded that the biallelic deletion in TP53 gene locus in U87-MG cells resulted in lack of p53 expression in single cell colonies 2, 16 and 17.

After the confirmation of being $p53^{-/-}$ at both gene and protein levels, U87-MG $p53^{-/-}$ cells (colony 2) were further characterized by assessing their cell proliferation, cell migration and colony formation abilities.Since the p53 protein regulates the cell cycle, the first characterization aspect for the newly generated U87-MG $p53^{-/-}$ cell line was the difference in cell proliferation compared to U87-MG cells. The proliferation of U87-MG (WT) cells and U87-MG $p53^{-/-}$ cells were determined by performing trypan blue exclusion assay in a time-dependent manner. The live cell population was determined at 24 h, 48 h, 72 h, 96 h and 120 h after the

seeding. As seen in Figure 4.39, U87-MG $p53^{-/-}$ cells proliferated significantly faster than U87-MG (WT) cells. p53 tumor suppressor protein plays role in cell cycle arrest. p53 indirectly down-regulates the expression of genes that are crucial for progression through the cell division cycle (178). Therefore, p53-deficient cells exhibit accelerated proliferation. This is consistent with the literature (179,180,181,182).

In order to analyze also the long-term cell proliferation, colony formation ability of U87-MG $p53^{-/-}$ cells were compared with U87-MG (WT) cells. The stress factor for the cells in this experiment is cell seeding at low density. Cells will enter the lag phase of growth if they are seeded at too low a density. In the lag phase, cells grow slowly or die out (183). The transcription of p21 is activated after stress condition (184). Cyclin-dependent kinase inhibitor p21 blocks CDK-1/Cyclin B and CDK-2/Cyclin E to cause cell cycle arrest at G1 and S phase, allowing p53 to prevent cells from growing and dividing. Cells undergo senescence and apoptosis (185,186). When p53 is absence, cells continue to proliferate by losing the ability to regulate the cell cycle, which is not affected even by stress (187). As seen in Figure 4.42, although U87-MG cells were having difficulties in proliferation and colony formation, U87-MG $p53^{-/-}$ cells were still proliferating and forming colonies despite the low cell seed density stress factor. This is consistent with the literature (188,189,190).

Wound healing assay was performed to compare the migration abilities of U87-MG cells and U87-MG $p53^{-/-}$ cells. Wound closure was tracked after 24, 48 and 72 hours of wound formation. For each time point, the wound closure percentage was calculated by considering the initial wound area (WA_0). In this experimental set up, 1%FBS and 10%FBS were two growth medium conditions. 1%FBS condition was used for testing the migration abilities of the cells and 10% FBS condition was the control of the experiment. As seen in Figures 4.40 and 4.41, in 10% FBS condition,

24h and 48h after the wound formation, the wound closure percentages of U87-MG $p53^{-/-}$ cells were significantly higher than that of U87-MG WT cells. However, in 10% FBS condition the cells were both proliferating and migrating. Since it was also observed that U87-MG $p53^{-/-}$ cells were proliferating significantly faster than U87-MG cells in trypan blue exclusion and colony formation assays, the significant difference of U87-MG $p53^{-/-}$ cells in wound closure was mainly due to higher cell proliferation rate. Therefore, the wound closure only in 1%FBS conditions were considered as the condition to test the migration abilities. In 1%FBS conditions, the wound closure percentages of U87-MG WT and U87-MG $p53^{-/-}$ cells were not significantly different in any time point. In other words, the migration abilities of U87-MG cells and U87-MG $p53^{-/-}$ cells were not significantly different from each other. In the literature, the p53 null tumors are commonly known to have benign phenotype (191,192,193,194,195,196,197). In benign tumors, there is only tumor formation due to cell proliferation, but there is no migration and invasion as there is in malignant tumors (198).

In conclusion, in this study U87-MG $p53^{-/-}$ cell line was aimed to be created via targeting two different regions in the *TP53* gene locus by CRISPR/Cas9 system. In order to target the *TP53* gene, four gRNAs (A, B, C and D) were designed and successfully cloned into pSp-Cas9(BB)-2A-Puro (PX459) V2.0 plasmid. Gene editing performances of the cloned CRISPR plasmids were analyzed both individually and as pairs. U87-MG $p53^{-/-}$ cell line was generated as a result of biallelic deletion in the *TP53* gene locus. This newly generated cell line is characterized from the perspectives of cell proliferation, migration and colony formation abilities. In conclusion, this created U87-MG $p53^{-/-}$ cell line model can be used for further p53 mutant studies in glioblastoma.

6. REFERENCES

1. Marei HE, Althani A, Afifi N, et al. p53 signaling in cancer progression and therapy. Cancer Cell Int. 2021 ;21 (1):703.

2. Gualberto A, Aldape K, Kozakiewicz K, Tlsty TD. An oncogenic form of p53 confers a dominant, gain-of-function phenotype that disrupts spindle checkpoint control. Proc Natl Acad Sci U S A. 1998;95(9):5166-5171.

3. Gencel-Augusto J, Lozano G. p53 tetramerization: at the center of the dominant-negative effect of mutant p53. Genes Dev. 2020;34(17-18):1128-1146.

4. Bock C, Datlinger P, Chardon F, et al. High-content CRISPR screening. Nat Rev Methods Primers. 2022;2(1):9.

5. Tandon N, Thakkar K, LaGory E, Liu Y, Giaccia A. Generation of Stable Expression Mammalian Cell Lines Using Lentivirus. Bio-Protocol. 2018;8(21).

6. Dropulić B. Lentiviral vectors: their molecular design, safety, and use in laboratory and preclinical research. Hum Gene Ther. 2011;22(6):649-657.

7. Nagai H, Kim YH. Cancer prevention from the perspective of global cancer burden patterns. J Thorac Dis. 2017;9(3):448-451.

8. Stass SA, Mixson J. Oncogenes and tumor suppressor genes: therapeutic implications. Clin Cancer Res. 1997;3(12 Pt 2):2687-2695.

9. Ferguson LR, Chen H, Collins AR, Connell M, Damia G, Dasgupta S, et al. Genomic instability in human cancer: Molecular insights and opportunities for therapeutic attack and prevention through diet and nutrition. Seminars in Cancer Biology. 2015 Dec;35: S5–24.

10. Hanahan D, Weinberg RA. Hallmarks of Cancer: The Next Generation. Cell. 2011 Mar ; 144 (5) :646–74.

11. Vogelstein B, Papadopoulos N, Velculescu VE, Zhou S, Diaz LA, Kinzler KW. Cancer Genome Landscapes. Science. 2013 Mar 29;339(6127):1546–58.

12. Lee EY, Muller WJ. Oncogenes and Tumor Suppressor Genes. Cold Spring Harbor Perspectives in Biology. 2010 Oct 1;2(10): a003236–a003236.

13. Sherr CJ. Principles of Tumor Suppression. Cell. 2004 Jan;116(2):235–46.

14. Osborne C, Wilson P, Tripathy D. Oncogenes and Tumor Suppressor Genes in Breast Cancer: Potential Diagnostic and Therapeutic Applications. The Oncologist. 2004 Jul 1;9(4):361–77.

15. Robert Allan Weinberg. The Biology of Cancer. Second Edition. Garland Science. 2014.

16. Alberts Bruce, Johnson Alexander, Lewis Julian, Morgan David, Raff Martin, Roberts Keith, Walter Peter. Molecular Biology of the Cell. Sixth Edition. Garland Science. 2008.

17. Simanshu DK, Nissley DV, McCormick F. RAS Proteins and Their Regulators in Human Disease. Cell. 2017 Jun;170(1):17–33.

18. Desilets A, Ho AL. Targeting HRAS in Head and Neck Cancer: Lessons From the Past and Future Promise. Cancer J. 2022;28(5):363-368.

19. Bannoura SF, Uddin MH, Nagasaka M, et al. Targeting KRAS in pancreatic cancer: new drugs on the horizon. Cancer Metastasis Rev. 2021;40(3):819-835.

20. Muñoz-Couselo E, Adelantado EZ, Ortiz C, García JS, Perez-Garcia J. NRAS-mutant melanoma: current challenges and future prospect. Onco Targets Ther. 2017;10:3941-3947.

21. Miller MS, Miller LD. RAS Mutations and Oncogenesis: Not all RAS Mutations are Created Equally. Front Genet. 2012;2:100.

22. Eilers M, Eisenman RN. Myc's broad reach. Genes Dev. 2008 Oct 15;22(20):2755–66.

23. Xu-Monette ZY, Deng Q, Manyam GC, et al. Clinical and Biologic Significance of MYC Genetic Mutations in De Novo Diffuse Large B-cell Lymphoma. Clin Cancer Res. 2016;22(14):3593-3605.

24. Zhu HQ, Gao FH. Regulatory Molecules and Corresponding Processes of BCR-ABL Protein Degradation. J Cancer. 2019;10(11):2488-2500.

25. Ross TS, Mgbemena VE. Re-evaluating the role of BCR/ABL in chronic myelogenous leukemia. Mol Cell Oncol. 2014;1(3):e963450.

26. Kelly WJ, Shah NJ, Subramaniam DS. Management of Brain Metastases in Epidermal Growth Factor Receptor Mutant Non-Small-Cell Lung Cancer. Front Oncol. 2018;8:208.

27. Zeng F, Harris RC. Epidermal growth factor, from gene organization to bedside. Seminars in Cell & Developmental Biology. 2014 Apr; 28:2–11.

28. Sigismund S, Avanzato D, Lanzetti L. Emerging functions of the EGFR in cancer. Mol Oncol. 2018;12(1):3-20.

29. Weinberg RA. The retinoblastoma protein and cell cycle control. Cell. 1995 May;81(3):323–30.

30. Ballatori SE, Hinds PW. Osteosarcoma: prognosis plateau warrants retinoblastoma pathway targeted therapy. Signal Transduct Target Ther. 2016;1:16001.

31. Mandigo AC, Tomlins SA, Kelly WK, Knudsen KE. Relevance of pRB Loss in Human Malignancies. Clin Cancer Res. 2022;28(2):255-264.

32. Lin K, Baritaki S, Vivarelli S, Falzone L, Scalisi A, Libra M, et al. The Breast Cancer Protooncogenes HER2, BRCA1 and BRCA2 and Their Regulation by the iNOS/NOS2 Axis. Antioxidants. 2022 Jun 17;11(6):1195.

33. Karami F, Mehdipour P. A comprehensive focus on global spectrum of BRCA1 and BRCA2 mutations in breast cancer. Biomed Res Int. 2013;2013:928562.

34. Lakhani SR, Manek S, Penault-Llorca F, et al. Pathology of ovarian cancers in BRCA1 and BRCA2 carriers. Clin Cancer Res. 2004;10(7):2473-2481.

35. Ostrom QT, Bauchet L, Davis FG, Deltour I, Fisher JL, Langer CE, et al. The epidemiology of glioma in adults: a "state of the science" review. Neuro-Oncology. 2014 Jul 1;16(7):896–913.

36. Oronsky B, Reid TR, Oronsky A, Sandhu N, Knox SJ. A Review of Newly Diagnosed Glioblastoma. Front Oncol. 2021 Feb 5; 10:574012.

37. Hanif F, Muzaffar K, Perveen K, Malhi S, Simjee S. Glioblastoma Multiforme: A Review of its Epidemiology and Pathogenesis through Clinical Presentation and Treatment. 2017 Jan ;18(1).

38. Grochans S, Cybulska AM, Simińska D, Korbecki J, Kojder K, Chlubek D, et al. Epidemiology of Glioblastoma Multiforme–Literature Review. Cancers. 2022 May 13;14(10):2412.

39. Wilson TA, Karajannis MA, Harter DH. Glioblastoma multiforme: State of the art and future therapeutics. Surg Neurol Int. 2014;5:64.

40. Tan AC, Ashley DM, López GY, Malinzak M, Friedman HS, Khasraw M. Management of glioblastoma: State of the art and future directions. CA A Cancer J Clin. 2020 Jul;70(4):299–312.

41. Koshy M, Villano JL, Dolecek TA, Howard A, Mahmood U, Chmura SJ, et al. Improved survival time trends of glioblastoma using the SEER 17 population-based registries. J Neuro Oncol. 2012;107(1):207–12.

42. Gallego O. Nonsurgical Treatment of Recurrent Glioblastoma. Current Oncology. 2015 Aug 1;22(4):273–81.

43. Ohgaki H, Kleihues P. The Definition of Primary and Secondary Glioblastoma. Clinical Cancer Research. 2013 Feb 15;19(4):764–72.

44. Ohgaki H, Kleihues P. Genetic Pathways to Primary and Secondary Glioblastoma. The American Journal of Pathology. 2007 May;170(5):1445–53.

45. Knudsen ES, Buckmaster C, Chen TT, Feramisco JR, Wang JY. Inhibition of DNA synthesis by RB: effects on G1/S transition and S-phase progression. Genes Dev. 1998;12(15):2278-2292.

46. Johnson DG, Schneider-Broussard R. Role of E2F in cell cycle control and cancer. Front Biosci. 1998;3:d447-d448.

47. Day PJ, Cleasby A, Tickle IJ, et al. Crystal structure of human CDK4 in complex with a D-type cyclin. Proc Natl Acad Sci U S A. 2009;106(11):4166-4170.

48. Witkiewicz AK, Knudsen KE, Dicker AP, Knudsen ES. The meaning of p16(ink4a) expression in tumors: functional significance, clinical associations and future developments. Cell Cycle. 2011;10(15):2497-2503.

49. McConnell BB, Gregory FJ, Stott FJ, Hara E, Peters G. Induced expression of p16(INK4a) inhibits both CDK4- and CDK2-associated kinase activity by reassortment of cyclin-CDK-inhibitor complexes. Mol Cell Biol. 1999;19(3):1981-1989.

50. Ezhevsky SA, Nagahara H, Vocero-Akbani AM, Gius DR, Wei MC, Dowdy SF. Hypo-phosphorylation of the retinoblastoma protein (pRb) by cyclin D:Cdk4/6 complexes results in active pRb. Proc Natl Acad Sci U S A. 1997;94(20):10699-10704.

51. Narasimha AM, Kaulich M, Shapiro GS, Choi YJ, Sicinski P, Dowdy SF. Cyclin D activates the Rb tumor suppressor by mono-phosphorylation. Elife. 2014;3:e02872.

52. Masamha CP, Benbrook DM. Cyclin D1 degradation is sufficient to induce G1 cell cycle arrest despite constitutive expression of cyclin E2 in ovarian cancer cells. Cancer Res. 2009;69(16):6565-6572.

53. Kanu OO, Hughes B, Di C, et al. Glioblastoma Multiforme Oncogenomics and Signaling Pathways. Clin Med Oncol. 2009;3:39-52.

54. Strauss BE, Fontes RB, Lotfi CF, et al. Retroviral transfer of the p16INK4a cDNA inhibits C6 glioma formation in Wistar rats. Cancer Cell Int. 2002;2(1):2.

55. Singh N, Miner A, Hennis L, Mittal S. Mechanisms of temozolomide resistance in glioblastoma - a comprehensive review. Cancer Drug Resist. 2021;4(1):17-43.

56. Lahav G. Oscillations by the p53-Mdm2 Feedback Loop. Advances in Experimental Medicine and Biology .2008;641:28-38.

57. Reitman ZJ, Yan H. Isocitrate dehydrogenase 1 and 2 mutations in cancer: alterations at a crossroads of cellular metabolism. J Natl Cancer Inst. 2010;102(13):932-941.

58. Al-Khallaf H. Isocitrate dehydrogenases in physiology and cancer: biochemical and molecular insight. Cell Biosci. 2017;7:37.

59. Zhu S, Huang J, Xu R, et al. Isocitrate dehydrogenase 3b is required for spermiogenesis but dispensable for retinal viability. J Biol Chem. 2022;298(9):102387.

60. Haider AS, Ene CI, Palmisciano P, et al. Concurrent IDH1 and IDH2 mutations in glioblastoma: A case report. Front Oncol. 2023;13:1071792.

61. Reitman ZJ, Yan H. Isocitrate dehydrogenase 1 and 2 mutations in cancer: alterations at a crossroads of cellular metabolism. J Natl Cancer Inst. 2010;102(13):932-941.

62. Xu W, Yang H, Liu Y, et al. Oncometabolite 2-hydroxyglutarate is a competitive inhibitor of α-ketoglutarate-dependent dioxygenases. Cancer Cell. 2011;19(1):17-30.

63. Budanov AV. The role of tumor suppressor p53 in the antioxidant defense and metabolism. Subcell Biochem. 2014;85:337-358.

64. Ozaki T, Nakagawara A. Role of p53 in Cell Death and Human Cancers. Cancers. 2011 Mar 3;3(1):994–1013.

65. Kruse JP, Gu W. Modes of p53 Regulation. Cell. 2009 May;137(4):609–22.

66. Marine JC, Jochemsen AG. MDMX (MDM4), a Promising Target for p53 Reactivation Therapy and Beyond. Cold Spring Harb Perspect Med. 2016 Jul;6(7): a026237.

67. Dai C, Gu W. p53 post-translational modification: deregulated in tumorigenesis. Trends in Molecular Medicine. 2010 Nov;16(11):528–36.

68. Maclaine NJ, Hupp TR. The regulation of p53 by phosphorylation: a model for how distinct signals integrate into the p53 pathway. Aging. 2009 May 7;1(5):490–502.

69. Zhang Y, Hunter T. Roles of Chk1 in cell biology and cancer therapy. Int J Cancer. 2014 Mar;134(5):1013–23.

70. Ou YH, Chung PH, Sun TP, Shieh SY. p53 C-Terminal Phosphorylation by CHK1 and CHK2 Participates in the Regulation of DNA-Damage-induced C-Terminal Acetylation. MBoC. 2005 Apr;16(4):1684–95.

71. Loughery J, Cox M, Smith LM, Meek DW. Critical role for p53-serine 15 phosphorylation in stimulating transactivation at p53-responsive promoters. Nucleic Acids Research. 2014 Jul 8;42(12):7666–80.

72. Shieh SY, Ikeda M, Taya Y, Prives C. DNA Damage-Induced Phosphorylation of p53 Alleviates Inhibition by MDM2. Cell. 1997 Oct;91(3):325–34.

73. Grossman SR. p300/CBP/p53 interaction and regulation of the p53 response: p300/CBP and p53 signaling. European Journal of Biochemistry. 2001 May 15;268(10):2773–8.

74. Tang Y, Luo J, Zhang W, Gu W. Tip60-dependent acetylation of p53 modulates the decision between cell-cycle arrest and apoptosis. Mol Cell. 2006;24(6):827-839.

75. H West LE, Gozani O. Regulation of p53 function by lysine methylation. Epigenomics. 2011 Jun;3(3):361–9.

76. Shi X, Kachirskaia I, Yamaguchi H, West LE, Wen H, Wang EW, et al. Modulation of p53 Function by SET8-Mediated Methylation at Lysine 382. Molecular Cell. 2007 Aug;27(4):636–46.

77. Hu W, Feng Z, Levine AJ. The Regulation of Multiple p53 Stress Responses is Mediated through MDM2. Genes & Cancer. 2012 Mar 1;3(3–4):199–208.

78. Senitzki A, Safieh J, Sharma V, Golovenko D, Danin-Poleg Y, Inga A, & Haran TE. The complex architecture of p53 binding sites. Nucleic Acids Res. 2021;49(3):1364-1382.

79. Wang B, Xiao Z, Ren EC. Redefining the p53 response element. Proc Natl Acad Sci U S A. 2009;106(34):1 4 373-14378.

80. Vaseva AV, Marchenko ND, Moll UM. The transcription-independent mitochondrial p53 program is a major contributor to nutlin-induced apoptosis in tumor cells. Cell Cycle. 2009;8(11):1711-1719.

81. Kearns S, Lurz R, Orlova EV, Okorokov AL. Two p53 tetramers bind one consensus DNA response element. Nucleic Acids Res. 2016;44(13):6185-6199.

82. Liebl MC, Hofmann TG. The Role of p53 Signaling in Colorectal Cancer. Cancers (Basel). 2021;13(9):2125.

83. Hernández Borrero LJ, El-Deiry WS. Tumor suppressor p53: Biology, signaling pathways, and therapeutic targeting. Biochimica et Biophysica Acta (BBA) - Reviews on Cancer. 2021 Aug ;1876(1):188556.

84. Reed S, Quelle D. p53 Acetylation: Regulation and Consequences. Cancers. 2014 Dec 23;7(1):30–69.

85. Liu J, Zhang C, Wang X, Hu W, Feng Z. Tumor suppressor p53 cross-talks with TRIM family proteins. Genes & Diseases. 2020 Jul;8(4):463–74.

86. Fortin A, Cregan SP, MacLaurin JG, Kushwaha N, Hickman ES, Thompson CS, et al. APAF1 is a key transcriptional target for p53 in the regulation of neuronal cell death. Journal of Cell Biology. 2001 Oct 15;155(2):207–16.

87. He G, Zhang YW, Lee JH, Zeng SX, Wang YV, Luo Z, Dong XC, Viollet B, Wahl GM , & Lu H. AMP-Activated Protein Kinase Induces p53 by Phosphorylating MDMX and Inhibiting Its Activity. Molecular and Cellular Biology. 2014 Jan 1;34(2):148–57.

88. Vieler M, Sanyal S. p53 Isoforms and Their Implications in Cancer. Cancers. 2018 Aug 25 ; 10 (9) :288.

89. Hernández Borrero LJ, El-Deiry WS. Tumor suppressor p53: Biology, signaling pathways, and therapeutic targeting. Biochimica et Biophysica Acta (BBA) - Reviews on Cancer. 2021 Aug ;1876(1):188556.

90. Bourdon JC, Fernandes K, Murray-Zmijewski F, Liu G, Diot A, Xirodimas DP, et al. p53 isoforms can regulate p53 transcriptional activity. Genes Dev. 2005 Sep 15;19(18):2122–37.

91. Pflaum J, Schlosser S, Müller M. p53 Family and Cellular Stress Responses in Cancer. Front Oncol. 2014 Oct 21;4:285.

92. Alvarado-Ortiz E, De La Cruz-López KG, Becerril-Rico J, Sarabia-Sánchez MA, Ortiz-Sánchez E, García-Carrancá A. Mutant p53 Gain-of-Function: Role in Cancer Development, Progression, and Therapeutic Approaches. Front Cell Dev Biol. 2021 Feb 11; 8:607670.

93. Li VD, Li KH, Li JT. TP53 mutations as potential prognostic markers for specific cancers: analysis of data from The Cancer Genome Atlas and the International Agency for Research on Cancer TP53 Database. J Cancer Res Clin Oncol. 2019;145(3):625-636.

94. Raj N, Attardi LD. The Transactivation Domains of the p53 Protein. Cold Spring Harb Perspect Med. 2017;7(1):a026047.

95. Anbarasan T, Bourdon J-C. The Emerging Landscape of p53 Isoforms in Physiology, Cancer and Degenerative Diseases. International Journal of Molecular Sciences 2019;20(24):6257.

96. Baptiste N, Friedlander P, Chen X, Prives C. The proline-rich domain of p53 is required for cooperation with anti-neoplastic agents to promote apoptosis of tumor cells. Oncogene. 2002;21(1):9-21.

97. Shaulsky, G., Goldfinger, N., Ben-Ze'ev, A., & Rotter, V. Nuclear accumulation of p53 protein is mediated by several nuclear localization signals and plays a role in tumorigenesis. Molecular and cellular biology. 1990 ; 10(12), 6565–6577.

98. Harms KL, Chen X. The functional domains in p53 family proteins exhibit both common and distinct properties. Cell Death Differ. 2006;13(6):890-897.

99. Beckerman R, Prives C. Transcriptional regulation by p53. Cold Spring Harb Perspect Biol. 2010;2(8):a000935.

100. Petitjean A, Achatz MI, Borresen-Dale AL, Hainaut P, Olivier M. TP53 mutations in human cancers: functional selection and impact on cancer prognosis and outcomes. Oncogene. 2007;26(15):2157-2165.

101. Kanapathipillai M. Treating p53 Mutant Aggregation-Associated Cancer. Cancers. 2018 May 23;10(6):154.

102. Rivlin N, Brosh R, Oren M, Rotter V. Mutations in the p53 Tumor Suppressor Gene: Important Milestones at the Various Steps of Tumorigenesis. Genes & Cancer. 2011 Apr 1;2(4):466–74.

103. Kennedy MC, Lowe SW. Mutant p53: it's not all one and the same. Cell Death Differ. 2022;29(5):983-987.

104. Annor GK, Elshabassy N, Lundine D, et al. Oligomerization of Mutant p53 R273H is not Required for Gain-of-Function Chromatin Associated Activities. Front Cell Dev Biol. 2021;9:772315.

105. Joerger AC, Fersht AR. The tumor suppressor p53: from structures to drug discovery. Cold Spring Harb Perspect Biol. 2010;2(6):a000919.

106. Caron de Fromentel C, Levrero M. p53 functional loss, stemness and hepatocellular carcinoma. Hepatoma Research. 2020; 6: 80.

107. Mantovani F, Walerych D, Sal GD. Targeting mutant p53 in cancer: a long road to precision therapy. FEBS J. 2017;284(6):837-850.

108. Pilley S, Rodriguez TA, Vousden KH. Mutant p53 in cell-cell interactions. Genes Dev. 2021 Apr 1;35(7–8):433–48.

109. Kim MP, Lozano G. Mutant p53 partners in crime. Cell Death Differ. 2018 Jan;25(1):161–8.

110. Freed-Pastor WA, Prives C. Mutant p53: one name, many proteins. Genes Dev. 2012;26(12):1268-1286.

111. Lim J, Choi JH, Park EM, Choi YH. Interaction of promyelocytic leukemia/p53 affects signal transducer and activator of transcription-3 activity in response to oncostatin M. Korean J Physiol Pharmacol. 2020;24(3):203-212.

112. Girardini JE, Napoli M, Piazza S, et al. A Pin1/mutant p53 axis promotes aggressiveness in breast cancer. Cancer Cell. 2011;20(1):79-91.

113. Li, Y., Prives, C. Are interactions with p63 and p73 involved in mutant p53 gain of oncogenic function?. Oncogene.2007; 26, 2220–2225.

114. Stindt, M., Muller, P., Ludwig, R. et al. Functional interplay between MDM2, p63/p73 and mutant p53. Oncogene.2015; 34, 4300–4310.

115. Kc M, Steer CJ. A new era of gene editing for the treatment of human diseases. Swiss Med Wkly. 2019;149:w20021.

116. Adli M. The CRISPR tool kit for genome editing and beyond. Nat Commun. 2018 May 15;9(1):1911.

117. Miyaoka, Y., Berman, J., Cooper, S. et al. Systematic quantification of HDR and NHEJ reveals effects of locus, nuclease, and cell type on genome-editing. Sci Rep. 2016 ; 6, 23549.

118. Gupta D, Bhattacharjee O, Mandal D, Sen MK, Dey D, Dasgupta A, et al. CRISPR-Cas9 system: A new-fangled dawn in gene editing. Life Sciences. 2019 Sep; 232:116636.

119. Hryhorowicz M, Lipiński D, Zeyland J, Słomski R. CRISPR/Cas9 Immune System as a Tool for Genome Engineering. Arch Immunol Ther Exp. 2017 Jun;65(3):233–40.

120. Zhu Y. Advances in CRISPR/Cas9. BioMed Research International. 2022 Sep 23; 2022:1–13.

121. Modell JW, Jiang W, Marraffini LA. CRISPR-Cas systems exploit viral DNA injection to establish and maintain adaptive immunity. Nature. 2017;544(7648):101-104.

122. Nidhi S, Anand U, Oleksak P, Tripathi P, Lal JA, Thomas G, et al. Novel CRISPR–Cas Systems: An Updated Review of the Current Achievements, Applications, and Future Research Perspectives. IJMS. 2021 Mar 24;22(7):3327.

123. Zhang F, Wen Y, Guo X. CRISPR/Cas9 for genome editing: progress, implications and challenges. Hum Mol Genet. 2014;23(R1):R40-R46.

124. Sternberg, S., LaFrance, B., Kaplan, M. et al. Conformational control of DNA target cleavage by CRISPR–Cas9. Nature.2015; 527, 110–113.

125. Kozovska Z, Rajcaniova S, Munteanu P, Dzacovska S, Demkova L. CRISPR: History and perspectives to the future. Biomedicine & Pharmacotherapy. 2021 Sep; 141:111917.

126. Nishimasu H, Ran FA, Hsu PD, et al. Crystal structure of Cas9 in complex with guide RNA and target DNA. Cell. 2014;156(5):935-949.

127. Xu Y, Li Z. CRISPR-Cas systems: Overview, innovations and applications in human disease research and gene therapy. Computational and Structural Biotechnology Journal. 2020; 18:2401–15.

128. Zhang B. CRISPR/Cas gene therapy. Journal Cellular Physiology. 2021 Apr;236(4):2459–81.

129. Thakore PI, D'Ippolito AM, Song L, et al. Highly specific epigenome editing by CRISPR-Cas9 repressors for silencing of distal regulatory elements. Nat Methods. 2015;12(12):1143-1149.

130. Lei Y, Zhang X, Su J, et al. Targeted DNA methylation in vivo using an engineered dCas9-MQ1 fusion protein. Nat Commun. 2017;8:16026.

131. Park H, Shin J, Kim Y, Saito T, Saido TC, Kim J. CRISPR/dCas9-Dnmt3a-mediated targeted DNA methylation of APP rescues brain pathology in a mouse model of Alzheimer's disease. Transl Neurodegener. 2022;11(1):41.

132. Casas-Mollano JA, Zinselmeier MH, Erickson SE, Smanski MJ. CRISPR-Cas Activators for Engineering Gene Expression in Higher Eukaryotes. CRISPR J. 2020;3(5):350-364.

133. Chavez A, Tuttle M, Pruitt BW, et al. Comparison of Cas9 activators in multiple species. Nat Methods. 2016;13(7):563-567.

134. Pulecio J, Verma N, Mejía-Ramírez E, Huangfu D, Raya A. CRISPR/Cas9-Based Engineering of the Epigenome. Cell Stem Cell. 2017;21(4):431-447.

135. Chan WF, Coughlan HD, Chen Y, et al. Activation of stably silenced genes by recruitment of a synthetic de-methylating module. Nat Commun. 2022;13(1):5582.

136. Kantor A, McClements M, MacLaren RE. CRISPR-Cas9 DNA Base-Editing and Prime-Editing. IJMS. 2020 Aug 28;21(17):6240.

137. Scholefield J, Harrison PT. Prime editing - an update on the field. Gene Ther. 2021;28(7-8):396-401.

138. Hu Y, Li W. Development and Application of CRISPR-Cas Based Tools. Front Cell Dev Biol. 2022 Apr 4; 10:834646.

139. Huang Z, Fang J, Zhou M, Gong Z, Xiang T. CRISPR-Cas13: A new technology for the rapid detection of pathogenic microorganisms. Front Microbiol. 2022 Oct 28; 13:1011399.

140. Cox DBT, Gootenberg JS, Abudayyeh OO, et al. RNA editing with CRISPR-Cas13. Science. 2017;358(6366):1019-1027.

141. Abudayyeh OO, Gootenberg JS, Franklin B, et al. A cytosine deaminase for programmable single-base RNA editing. Science. 2019;365(6451):382-386.

142. Tang T, Han Y, Wang Y, Huang H, Qian P. Programmable System of Cas13-Mediated RNA Modification and Its Biological and Biomedical Applications. Front Cell Dev Biol. 2021;9:677587.

143. Liang, Y., Xu, H., Cheng, T. et al. Gene activation guided by nascent RNA-bound transcription factors. Nat Commun. 2022;13,7329.

144. Concordet JP, Haeussler M. CRISPOR: intuitive guide selection for CRISPR/Cas9 genome editing experiments and screens. Nucleic Acids Res. 2018;46(W1):W242-W245.

145. Ran FA, Hsu PD, Wright J, Agarwala V, Scott DA, Zhang F. Genome engineering using the CRISPR-Cas9 system. Nat Protoc. 2013;8(11):2281-2308.

146. Hernández Borrero LJ, El-Deiry WS. Tumor suppressor p53: Biology, signaling pathways, and therapeutic targeting. Biochim Biophys Acta Rev Cancer. 2021;1876(1):188556.

147. Zhang Y, Dube C, Gibert M, Cruickshanks N, Wang B, Coughlan M, et al. The p53 Pathway in Glioblastoma. Cancers. 2018 Sep 1;10(9):297.

148. Joung J, Ma S, Tay T, et al. A transcription factor atlas of directed differentiation. Cell. 2023;186(1):209-229.e26.

149. Mali P, Yang L, Esvelt KM, Aach J, Guell M, DiCarlo JE, et al. RNA-Guided Human Genome Engineering via Cas9. Science. 2013 Feb 15;339(6121):823–6.

150. Sander JD, Joung JK. CRISPR-Cas systems for editing, regulating and targeting genomes. Nat Biotechnol. 2014 Apr;32(4):347–55.

151. Fu Y, Sander JD, Reyon D, Cascio VM, Joung JK. Improving CRISPR-Cas nuclease specificity using truncated guide RNAs. Nat Biotechnol. 2014 Mar;32(3):279–84.

152. Hsu PD, Scott DA, Weinstein JA, Ran FA, Konermann S, Agarwala V, et al. DNA targeting specificity of RNA-guided Cas9 nucleases. Nat Biotechnol. 2013 Sep;31(9):827–32.

153. Konstantakos V, Nentidis A, Krithara A, Paliouras G. CRISPR-Cas9 gRNA efficiency prediction: an overview of predictive tools and the role of deep learning. Nucleic Acids Res. 2022;50(7):3616-3637.

154. Borst P. Ethidium DNA agarose gel electrophoresis: How it started. IUBMB Life (International Union of Biochemistry and Molecular Biology: Life). 2005 Nov 1;57(11):745–7.

155. Olmsted J, Kearns DR. Mechanism of ethidium bromide fluorescence enhancement on binding to nucleic acids. Biochemistry. 1977 Aug 9;16(16):3647–54.

156. Hayashi M, Harada Y. Direct observation of the reversible unwinding of a single DNA molecule caused by the intercalation of ethidium bromide. Nucleic Acids Research. 2007 Oct;35(19):e125.

157. Kumar A, Kaur J. Primer Based Approach for PCR Amplification of High GC Content Gene: Mycobacterium Gene as a Model. Mol Biol Int. 2014;2014:937308.

158. Livshits MA, Amosova OA, Lyubchenko YuL. Flexibility difference between double-stranded RNA and DNA as revealed by gel electrophoresis. J Biomol Struct Dyn. 1990;7(6):1237-1249.

159. Shan Q, Li S, Cao Q, Yue C, Niu M, Chen X, et al. Inhibition of chromosomal region maintenance 1 suppresses the migration and invasion of glioma cells via inactivation of the STAT3/MMP2 signaling pathway. Korean J Physiol Pharmacol. 2020 May 1;24(3):193–201.

160. De Silva T, Ye G, Liang YY, Fu G, Xu G, Peng C. Nodal Promotes Glioblastoma Cell Growth. Front Endocrin .2012;3.

161. Wang T, Meng Z, Kang Z, et al. Peptide Gene Delivery Vectors for Specific Transfection of Glioma Cells. ACS Biomater Sci Eng. 2020;6(12):6778-6789.

162. Hu KQ, Ao XS. Long non-coding RNA DLGAP1 antisense RNA 1 accelerates glioma progression via the microRNA-628-5p/DEAD-box helicase 59 pathway. Clinics (Sao Paulo). 2022;77:100002.

163. Peng X, Zhang S, Wang Y, et al. Stellettin B Sensitizes Glioblastoma to DNA-Damaging Treatments by Suppressing PI3K-Mediated Homologous Recombination Repair. Adv Sci (Weinh). 2023;10(3):e2205529.

164. Gu X, Gong H, Shen L, Gu Q. MicroRNA-129-5p inhibits human glioma cell proliferation and induces cell cycle arrest by directly targeting DNMT3A. Am J Transl Res. 2018;10(9):2834-2847.

165.Yang B, Fu X, Hao J, et al. PAXX Participates in Base Excision Repair via Interacting with Pol β and Contributes to TMZ Resistance in Glioma Cells. J Mol Neurosci. 2018;66(2):214-221.

166. Zhang T, Chai J, Chi L. Induction Of XLF And 53BP1 Expression Is Associated With Temozolomide Resistance In Glioblastoma Cells. Onco Targets Ther. 2019;12:10139-10151.

167. Wang T, Larcher L, Ma L, Veedu R. Systematic Screening of Commonly Used Commercial Transfection Reagents towards Efficient Transfection of Single-Stranded Oligonucleotides. Molecules. 2018 Oct 8;23(10):2564.

168. Breunig M, Lungwitz U, Liebl R, Goepferich A. Breaking up the correlation between efficacy and toxicity for nonviral gene delivery. Proc Natl Acad Sci U S A. 2007;104(36):14454-14459.

169. McKinnon KM. Flow Cytometry: An Overview. CP in Immunology. 2018 ;120 :5.1.1-5.1.11.

170. Takai H, Kato A, Nakamura T, Tachibana T, Sakurai T, Nanami M, et al. The importance of characterization of FITC-labeled antibodies used in tissue cross-reactivity studies. Acta Histochemica. 2011 Jul;113(4):472–6.

171. Drescher H, Weiskirchen S, Weiskirchen R. Flow Cytometry: A Blessing and a Curse. Biomedicines. 2021 Nov 4;9(11):1613.

172. Braun RK, Rudnicki MA, Sekaly RP, Filion LG. Filter selection for five color flow cytometric analysis with a single laser. Int J Lab Hematol. 2007 Oct;29(5):369–76.

173. Majewska E, Sulowska Z, Baj Z. Spontaneous apoptosis of neutrophils in whole blood and its relation to apoptosis gene proteins. Scand J Immunol. 2000;52(5):496-501.

174.Soini Y, Pääkkö P, Lehto VP. Histopathological evaluation of apoptosis in cancer. Am J Pathol. 1998;153(4):1041-1053.

175. Zhang H, Zhang H, Cao S, et al. Knockout of p53 leads to a significant increase in ALV-J replication. Poult Sci. 2021;100(10):101374.

176. Narkar A, Johnson BA, Bharne P, et al. On the role of p53 in the cellular response to aneuploidy. Cell Rep. 2021;34(12):108892.

177. Guo C, Ma X, Gao F, Guo Y. Off-target effects in CRISPR/Cas9 gene editing. Front Bioeng Biotechnol. 2023;11:1143157.

178. Engeland K. Cell cycle arrest through indirect transcriptional repression by p53: I have a DREAM. Cell Death Differ. 2018;25(1):114-132.

179. Schreiber M, Kolbus A, Piu F, et al. Control of cell cycle progression by c-Jun is p53 dependent. Genes Dev. 1999;13(5):607-619.

180. Jones SN, Sands AT, Hancock AR, et al. The tumorigenic potential and cell growth characteristics of p53-deficient cells are equivalent in the presence or absence of Mdm2. Proc Natl Acad Sci U S A. 1996;93(24):14106-14111.

181. Jaiswal SK, Raj S, DePamphilis ML. Developmental Acquisition of p53 Functions. Genes (Basel). 2021 ;12(11):1675.

182.Yan H, Solozobova V, Zhang P, et al. p53 is active in murine stem cells and alters the transcriptome in a manner that is reminiscent of mutant p53. Cell Death Dis. 2015;6(2):e1662.

183. Selli C, Erac Y, Tosun M. Effects of cell seeding density on real-time monitoring of anti-proliferative effects of transient gene silencing. J Biol Res (Thessalon). 2016;23:20.

184. Manu KA, Cao PHA, Chai TF, Casey PJ, Wang M. p21cip1/waf1 Coordinates Autophagy, Proliferation and Apoptosis in Response to Metabolic Stress. Cancers. 2019; 11(8):1112.

185. Al Bitar S, Gali-Muhtasib H. The Role of the Cyclin Dependent Kinase Inhibitor $p21^{cip1/waf1}$in Targeting Cancer: Molecular Mechanisms and Novel Therapeutics. Cancers (Basel). 2019;11(10):1475.

186. Kumari R, Jat P. Mechanisms of Cellular Senescence: Cell Cycle Arrest and Senescence Associated Secretory Phenotype. Front Cell Dev Biol. 2021;9:645593.

187. Engeland K. Cell cycle regulation: p53-p21-RB signaling. Cell Death Differ. 2022;29(5):946-960.

188. Ren D, Wang M, Guo W, et al. Wild-type p53 suppresses the epithelial-mesenchymal transition and stemness in PC-3 prostate cancer cells by modulating miR 145. Int J Oncol. 2013;42(4):1473-1481.

189. Wang B, Wang L, Mao J, et al. Mouse bone marrow mesenchymal stem cells with distinct p53 statuses display differential characteristics. Mol Med Rep. 2020;21(5):2051-2062.

190. Wu J, Zhao R, Lin J, Liu B. Integrin β4 reduces DNA damage-induced p53 activation in colorectal cancer. Oncol Rep. 2018;40(4):2183-2192.

191. Allen WL, Turkington RC, Stevenson L, Carson G, Coyle VM, Hector S, et al. Pharmacogenomic Profiling and Pathway Analyses Identify MAPK-Dependent Migration as an Acute Response to SN38 in p53 Null and p53-Mutant Colorectal Cancer Cells. Molecular Cancer Therapeutics. 2012 Aug 1;11(8):1724–34.

192. He S, Carman CV, Lee JH, Lan B, Koehler S, Atia L, et al. The tumor suppressor p53 can promote collective cellular migration. Abraham T, editor. PLoS ONE. 2019 Feb 1;14(2): e0202065.

193. Kandel R, Li SQ, Ozcelik H, Rohan T. p53 protein accumulation and mutations in normal and benign breast tissue. Int J Cancer. 2000 Jul 1;87(1):73–8.

194. Özer G, Kaygin P, DiRiCan O, Oğuztüzün S, Yilmaz Sarialtin S, Güler ŞiMşek G, et al. GSTM1, GSTP1, p53 as some probable predictors of prognosis in primary and metastatic epithelial ovarian cancer. The European Research Journal. 2023 May 4;9(3):477–83.

195. Sablina AA, Chumakov PM, Kopnin BP. Tumor Suppressor p53 and Its Homologue p73α Affect Cell Migration. Journal of Biological Chemistry. 2003 Jul;278(30):27362–71.

196. Costa RSS, Silva IFD. P53 Expression in benign Breast Disease Development: A Systematic Review. Asian Pac J Cancer Prev. 2020;21(9):2485-2491.

197. Gursan N, Sipal S, Calik M, Gundogdu C. P53, bcl-2, ki-67 li (labeling index) status in benign, proliferative, and malignant ovarian surface epithelial neoplasms. Eurasian J Med. 2009;41(1):10-14.

198. Patel A. Benign vs Malignant Tumors. JAMA Oncol. 2020;6(9):1488.

7. APPENDIX

APPENDIX A: Chemicals Used in This Project

Chemicals	Supplier Company, Catalog No
1,4-Piperazinediethanesulfonic acid	Sigma, #P6757
6x Loading Dye Purple	NEB, #B7024S
Absolute Ethanol	Sigma, #32221
Acrylamide/Bis	Sigma, #SLBM3534V
Adenosine 5′-Triphosphate (ATP)	NEB, #P0756S
Adenosine 5′-Triphosphate (ATP)	NEB, #P0756S
Agar	Sigma, #05039
Ampicillin	Neofroxx, #1728GR010
Anti- Rabbit IgG HRP linked Antibody	Cell Signaling, #7074S
Anti-Mouse HRP	Cell Signaling, #7076
Bromophenol Blue	Sigma, #B0126
Calcium Chloride	MP Biomedicals, #195088
Cell-Lytic M Cell Lysis Reagent	Sigma, #060M4117
Cloning Competent *E. Coli (*DH5α)	NEB, #C1010S
Crystal Violet	Norateks, #106092
Deoxynucleotide Solution Set	NEB, #N0446S
DimethylSulfoxide	Biomatik, #A2424
DMSO	Sigma, #SHBJ2847
Dulbecco's Phosphate-Buffered Saline	Gibco, #14190094
ECL	Thermo,#32106
Ethlyenediamine Tetraaceric Acid	Gibco, #25300054

Etidium Bromide	Sigma #e1510-10
Fetal Bovine Serum, heat inactivated	Gibco #10500064
Gelatin	Sigma, #G9391
Gene Ruler DNA Ladder Mix	Thermo Scientific,#LSG SM0331
Glacial Acetic Acid	Merck, #1.0005602500
Glucose	Sigma, #16301-1KG
Glycerol	Sigma, #15524-1L
Glycine	Bioshop, #GLN001
High Glucose Dulbecco's Modified Eagle Medium	Gibco,#419650
Isopropanol	Sigma, #24137
Isopropyl ß-D-1-thiogalactopyranoside	Fermentas, #R0392
Lipofectamine 3000	Thermo, #L3000001
Luria-Bertani Broth	Sigma, #L7659
Magnesium Chloride	NEB, #B9021S
Oligos/Primers	Sentegen Biotechnology
Opti-MEM	Gibco, #319850070
P53 Antibody	Cell Signaling, #2524
Penicillin-Streptomycin	Gibco, #15140122
Potassium Acetate	Merck, #104820
Protease Inhibitor Coktail Tablets	Roche, #11460400
Proteinase K	Macherey-Nagel, #740506
Puromycin	Sigma, #P9620
PVDF Membrane	Thermo, #B8518
RNase A	Macherey-Nagel, #740505
Skim Milk Powder	Bioshop, #SKI400

Sodium Cloride	Sigma, #13423
Sodium Dodecyl Sulfate	Sigma, #151-21-3
Sodium Hydroxide	Sigma, #06203
TE Buffer	Invitrogen, #00431008
Tris Base	BioRad, #1610716
Tris-Cl	Molekula
Trypan Blue	Sigma-Aldrich, #T8154
Trypsin-EDTA Solution	Gibco, #25300054
β-Actin (13E5) Rabbit mAb	Cell Signaling, #4970S

APPENDIX B: DNA and Protein Molecular Weight Markers

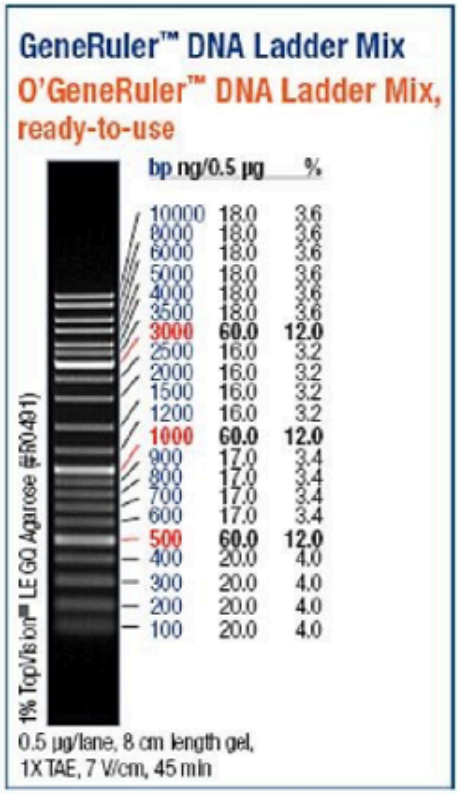

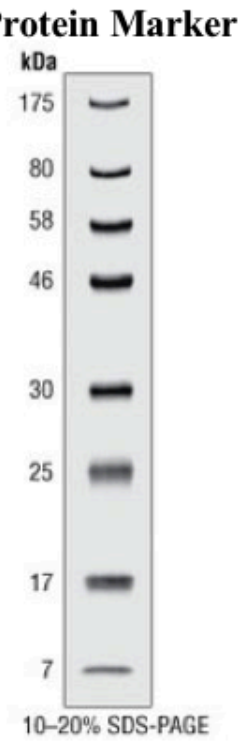

APPENDIX C: Equipment Used in This Project

Equipment	Supplier Company, Catalog No
2- Gel Tetra and Blotting Module with PowerPac HC	BioRad, #1660828EDU
Bacterial Cell Culture Incubator	Forma Steri-Cycle CO_2; Thermo Scientific, #52103030
Bacterial Shaker Incubator	Biosan, #ES-20/60
Cell and Bacterial Culture Hood	Thermo Scientific, #51026637
Cell Culture Incubator	Thermo Scientific, #51030301
Centrifuge Machine	Thermo Scientific, #SL16R
ChemiDoc Imaging System	BioRad, #1708265
Digital Shaking Dry Bath	Thermo Scientific, #88880028
Electrophoresis Apparatus	Axygen, #HGB15
Florescent Microscope	ZEIS AXIO Vert.A1
Flow Cytometry	BD FACSVerse™, #651155
Freezing container	Thermo, #N51000001
Light Microscope	ZEIS PrimoVert
Microcentrifuge Machine	Thermo Scientific, #MicroCL21R
Pipettes	Gilson, Pipetman, France
Microwave Oven	Samsung, #MW71E
Mini-PROTEAN Cell Casting Module	BioRad, #1658022EDU
Mini-PROTEAN Tetra Vertical Electrophoresis Cell	BioRad, #1658005EDU
NanoDrop One^C Microvolume UV-Vis	Thermo, #701-058112

Spectrophotometer	
Neubauer Chamber	Isolab, # LB.IS.075.03.001
pH Meter	Thermo, #12923257
T100™ Thermal Cycler	BioRad, #1861096
Varioskan Flash	ThermoScientific, MIB#5250030
Vortex	VWR, #VV3

APPENDIX D: Other Components Used in This Project

Other Components	Supplier Company, Catalog No
96-well Cell Cuture Plate	TPP, #92096
24-well Cell Cuture Plate	TPP, #92024
6-well Cell Cuture Plate	TPP, #92106
100 -mm Cell Culture Dish	TPP, #93100
T75 Flask	TPP, #Z707503
Cryovial Tube	TPP, #89012
0.2 mL PCR Tube	PCR-02-C Axygen
1.5 mL Microcentrifuge Tube	CAPP, #5101500C